TEL AVIV UNIVERSITY אוניברסיטת תל-אביב

SACKLER FACULTY OF MEDICINE

THE DR. MIRIAM AND SHELDON G. ADELSON GRADUATE SCHOOL OF MEDICINE

DEPARTMENT OF HUMAN MOLECULAR GENETICS AND BIOCHEMISTRY

MUTANT HUNTINGTIN PROTEOLYSIS REGULATION AS A POTENTIAL TREATMENT FOR HUNTINGTON'S DISEASE

THESIS SUBMITTED FOR THE DEGREE

"DOCTOR OF PHILOSOPHY"

BY

Israel Aharony

I.D. 039826854

SUBMITTED TO THE SENATE OF TEL AVIV UNIVERSITY

October 2015

THIS WORK WAS CARRIED OUT UNDER THE

SUPERVISION OF

Prof. DANIEL OFFEN

Head of the Neurosciences Laboratory, Felsenstein Medical Research Center,
Rabin Medical Center
Beilinson Campus, Sackler Faculty of Medicine,
Tel-Aviv University

אוניברסיטת תל-אביב TEL AVIV UNIVERSITY

הפקולטה לרפואה ע"ש סאקלר

המדרשה לתארים מתקדמים ע"ש מרים ושלדון ג' אדלסון

החוג לגנטיקה מולקולרית של האדם וביוכימיה

בקרה על חיתוך חלבון ההנטינגטין המוטנטי כטיפול אפשרי למחלת הנטינגטון

חיבור לשם קבלת התואר

"דוקטור לפילוסופיה"

מאת

ישראל אהרוני

ת.ז. 039826854

הוגש לסנאט של אוניברסיטת תל אביב

אוקטובר 2015

עבודה זו בוצעה בהנחייתו של

פרופ' דניאל אופן

ראש המעבדה לחקר המח
מכון פלסנשטיין למחקר רפואי,
מרכז רפואי רבין
הפקולטה לרפואה ע"ש סאקלר
אוניברסיטת ת"א

תודות

מסמך זה הוא סיכומו של מסע, שהחל עם ההחלטה לצאת מהתלם כדי לטול חלק במאמץ המשותף של המין האנושי לקדם את העולם לעבר מקום טוב יותר. אני מרגיש שזכיתי להתפתח כאדם וכחוקר, ומאושר שניתנה לי הזכות להיות חלק מעולם המדע, שחותר באופן מתמיד תחת המוסכמות ומאפשר צמיחה של תפיסות חדשות.

שותפים רבים ליוו אותי לאורך הדרך, וזה המקום לומר תודה.

בראש ובראשונה, דני. אני מאמין שהתכונה המשמעותית ביותר כמנחה היא היכולת למצוא את האיזון בין הצורך בהכוונה לבין נתינת האפשרות לצמיחה עצמאית. זכיתי למורה, מדריך וחבר שהצליח להביא את האיזון הזה לחיי היום-יום במעבדה. ידעת ליצור קרקע לצמיחה של רעיונות חדשים, קרקע שמאפשרת להתנסות, להצליח, להיכשל וללמוד. היית שם ברגעים שנזקקתי להכוונה, וגם ברגעים שנזקקתי למילה טובה.

תודה על שהכרת לי את עולם המדע דרך גישה שתמיד שמה לנגד עיניה את האנשים שמעבר למבחנות. החולים שעבורם אנו עובדים יום יום כדי לנסות ולהביא מזור לכאבם. אני שמח שזכיתי ללמוד ממך כאדם וכחוקר, ויודע שהרושם הזה ילווה אותי בהמשך דרכי המקצועית והאישית.

לכל חברי המעבדה, אתם אנשים טובים וחברים טובים. גרמתם לי להרגיש שיש לי בית שני, שתמיד אוכל למצוא בו מקום. אציין במיוחד את עדי, שנטלה חלק פעיל בפרויקט והייתה זמינה לכל בקשה לעזרה והתייעצות. וכן אציין את טלי ויעל, עמודי התווך של הידע המצטבר במעבדה. תודה על שהייתן זמינות לכל בקשת עזרה, מוכנות ללמד ולהעניק מהידע שצברתן.

לשותפים היקרים מקנדה. לפרופ' מייקל היידן, האב הרוחני של הפרויקט, שמהווה מקור השראה מקצועי ואישי ממדרגה ראשונה. לדאגמר, בעלת ידע ומקצועיות יוצאים דופן, שלוותה אותי לאורך התקופה ששהיתי במעבדה בוונקובר, והייתה שותפה בחלק גדול מהעבודה. לסוניה ושיאו-פאן שלקחו גם הן חלק פעיל בפרויקט והביאו מניסיונן. עולם המדע חוצה גבולות ותרבויות, וזכיתי להכיר חוקרים מהרמות הגבוהות ביותר, ועל כך תודתי.

תודה למשפחת קולטון, לחברת טבע ולמשרד המדע, על שתרמו מכספם להצלחת הפרויקט.

תודה למשפחתי היקרה. להוריי, על התמיכה ללא גבול, הן בתקופת לימודי הרפואה והן בזמן עריכת המחקר הרפואי. לא יכולתי לעשות זאת בלעדיכם.

לבנותיי המתוקות, שחר, אוריה והלל. אתן העדות הגדולה ביותר לנפלאות הבריאה. זכיתי לשאוב מכן כוחות להמשיך ולעבוד כדי ליצור עתיד טוב יותר עבורכן ועבור כולנו.

לאדם היקר לי מכל, שרה. כל מה ששלי, שלה הוא. תודה על שהיית שם בשבילי בכל רגע נתון. ידעת ליצור אצלי את התחושה שאני יכול, גם בזמנים מאתגרים יותר. זאת המתנה הגדולה ביותר שאדם יכול לקבל, ובזכותה הגעתי לנקודה זו.

אני מקווה שאוכל להמשיך לעמוד באחריות שניתנה לי לקדם את עולם המדע בצורה מקצועית וישרה, מתוך תחושה של שליחות.

אליק.

תוכן עניינים

תקציר

מחלת הנטינגטון היא מחלה נוירודגנרטיבית המועברת בתורשה אוטוזומלית דומיננטית. אדם הסובל ממחלת הנטינגטון יפתח הפרעה מוטורית המחמירה עם השנים, תסמינים נוירופסיכיאטריים והתדרדרות קוגניטיבית. מחלת הנטינגטון היא מחלה סופנית, כשתוחלת החיים הממוצעת היא בין עשר לחמש עשרה שנים לאחר פרוץ המחלה. היבטים נוירופתולגיים של מחלת הנטינגטון כוללים איבוד תאים מתמשך ודלדול של המח, בעיקר באיזור הסטריאטום והקורטקס הצרברלי.

המחלה נגרמת כתוצאה ממוטציה בחלבון ההנטינגטין, אשר זוהתה כהארכה של חזרות הגלוטמין בקצה ה-N טרמינלי של החלבון. בעוד ההטינגטין הנורמלי מכיל עד ל-35 חזרות של גלוטמין, ההנטינגטין המוטנטי מכיל מעל 36 חזרות. מוטציה זו מפעילה שרשרת אירועים רעילים בתאים, אשר גורמים לנזק משמעותי לתאי עצב, בעיקר לתאי עצב גבארגיים בסטריאטום וגלוטאמארגיים בקורטקס אשר מקושרים לסטריאטום.

חלבון ההנטינגטין עובר חיתוך פרוטאוליטי על ידי פרוטאזות שונות, בין השאר על ידי קבוצת הפרוטאזות הנקראים קספאזות. אחד מהאתרים העיקריים אשר נקשרו להתפתחות מחלת הנטינגטון הוא האתר המכיל חומצה אספרטית בעמדה מספר 586, אשר נחתך על ידי קספאז-6. חשיבות חיתוך ההנטינגטין המוטנטי בעמדה זו התגלתה על ידי שימוש בעכבר טרנסגני אשר מבטא חלבון הנטינגטין העמיד לחיתוך על ידי קספאז-6. עבודה זו נעשתה על ידי שותפי המחקר במעבדתו של פרופ' מייקל היידן. החוקרים גילו שמניעה גנטית של החיתוך של חלבון ההנטינגטין על ידי קספאז-6 מונעת את יצירתם של פרגמנטים רעילים ומגינה על עכברי המודל YAC128 מנוירודגנרציה ומהופעת הסימפטומים של המחלה. בעשור האחרון, מחקרים רבים נוספים גילו תפקיד משמעותי של קספאז-6 בהיווצרותה של מחלת הנטינגטון. לדוגמא,הפעלתו של הקספאז היא אירוע פתוגני מוקדם באנשים הנושאים את המוטציה. כמו כן, רמת פעילותו נמצאת בקורלציה חיובית למספר חזרות הגלוטמין ובקורלציה שלילית לגיל הופעת המחלה. בנוסף, קספאז-6 פעיל ופרגמנטים של חלבון ההנטינגטין מצויים בגרעינים של תאי עצב סטריאטליים לאחר עקה לתאים, ורמתם נמצאת בקורלציה לרעילות מוגברת.

על כן, עיכוב החיתוך של חלבון ההנטינגטין על ידי קספאז-6 הוצע כמטרה טיפולית מבטיחה, על מנת להוריד את רעילות ההנטינגטין המוטנטי ולהציל תאי עצב מניוון. בעקבות זאת, מאמצים גדולים נעשו

בעשור האחרון כדי לפתח מעכבי קספאז יעילים. לצערנו, מרבית מעכבי הקספאז הסינטטיים הם לא ספציפיים, הם בעלי חדירות נמוכה ועלולים לגרום לרעילות לא ספציפית כשניתנים בריכוזים שדרושים לעכב קספאזות תוך-תאיות.

מטרת המחקר העיקרית הינה להאיר את הפוטנציאל של עיכוב חיתוך ההנטינגטין המוטנטי על ידי קספאז-6 כאסטרטגיה טיפולית למחלת הנטינגטון. באופן ספציפי בעזרת פפטיד המעוצב מאתר החיתוך של חלבון ההנטינגטין על ידי קספאז-6, אשר יתחרה על פעילות הקספאז וכך יוריד את חיתוך החלבון המוטנטי והרעילות הנובעת מכך. סך של 11 חומצות אמינו, מסרין בעמדה 580 לאספרגין בעמדה 590 נבחרו כאתר ההכרה של קספאז-6, ורצף ה HIV-TAT (48-60) נבחר כדי לאפשר חדירה יעילה של דופן התא וכניסה לגרעין, וכן מעבר דרך מחסום דם-מח. שמו של הפפטיד הנוצר נקרא ED11.

על מנת לבחון את יכולת הפפטיד לעכב באופן ישיר את פעילות קספאז-6, נערך מבחן של פעילות הקספאז המבוסס על לומיניסנציה. נמצא שחיתוך Z-VEID-aminoluciferin על ידי קספאז-6 הורד באופן משמעותי בנוכחות ED11 בצורה תלוית מינון. בהמשך, על מנת להוכיח את הספציפיות של רצף הפפטיד, בוצעה החלפת חומצות אמינו בתוך הרצף של ED11 על ידי אלאנין. על ידי מדידת ההשפעה על יכולת העיכוב של ED11, נמצא שהחלפת חומצות אמינו מסוימות בתוך הרצף המזוהה על ידי קספאז-6 גרמו לביטול יכולת הפפטיד לעכב את קספאז-6. מכיוון שמשפחת הקספאז נושאת אתר פעיל בעל מבנה דומה, ומכיוון שישנה חשיבות רבה לעיכוב משני של קספאז-3 בעיקר בנושא הבטיחות, נבדקה ההשפעה של ED11 על פעילות קספאז-3. התגלה ש-ED11 לא משפיע על חיתוך של Z-VEID-aminoluciferin, PARP או Spectrin על ידי קספאז-3, בניגוד למעכב הקספאז הכללי zVAD-FMK, דבר המצביע על כך של-ED11 סלקטיביות רבה יותר לקספאז-6 מאשר לקספאז-3. בהמשך, הקומפטנטיות שבה ED11 משפיע על חיתוך של חלבון ההנטינגטין על ידי קספאז-6 התגלתה בעזרת מבחן רגיש המבוסס על טכנולוגיית FRET. ערכי ה-IC50 שנקבעו ל ED11 הינם 12.12nM, אשר נמצאו קרובים לערכי ה- IC50 של zVAD-FMK שנקבעו לערך 4.62nM. תוצאות אלו מצביעות על כך ש ED11 מעכב את החיתוך של חלבון ההנטינגטין על ידי קספאז-6 בפוטנטיות ראויה לציון. על מנת לבחון את האפקט הכולל של ED11 על חיתוך חלבון ההנטינגטין על ידי קספאזות שונות, קספאזות 1-10 הושרו עם החלבון ורמות החיתוך נבדקו. נמצא שאפקט העיכוב המשמעותי ביותר על ידי ED11 היה על היווצרות הפרגמנט 586 על ידי קספאז-6. אפקט

פחות נמצא על יצירת הפרגמנט 513 על ידי קספאז-1 וקספאז-10, ויצירת הפרגמנט 552 על ידי קספאז-2. בהמשך, יכולתו של ED11 לעכב את חלבון ההנטינגטין ההומני על-ידי קספאז-6 אומת בעזרת שימוש בליזאט חלבוני מסטריאטום של עכברים המבטאים חלבון זה.

לאחת שהודגמו היעילות והסלקטיביות של ED11 בניסויי ריאקציות אנזימטיות במבחנה, נבדקה ההיתכנות והבטיחות של שימוש ב-ED11 לעיכוב חיתוך ההנטינגטין המוטנטי בסביבה תוך תאית. ראשית, בעזרת שימוש בנוגדנים כנגד TAT, אומת ש ED11 מסוגל לחדור את ממברנות התא ולהיכנס לסביבה התוך תאית. בהמשך, בדיקת בטיחות השימוש ב- ED11 בסביבה תוך תאית הראתה ש-ED11 לא משפיע על חיות התא, שגשוג התאים או מצב מחזוריות התא תחת תנאים בזאליים. על מנת לבחון את יכולתו של ED11 להוריד את רמת החיתוך התוך תאי של הנטינגטין על ידי קספאז-6, קו-טרנספקציה של תאי HEK129 על יד קספאז-6 וחומצות אמינו 1-1212 של הקצה הטרמינלי של הנטינגטין בוצעה בנוכחות ED11. כימות של הפרגמנטים של 586 הראתה ש-ED11 מפחית באופן משמעותי את פעילות קספאז-6 על חלבון ההנטינגטין. ההשפעה על התוצאה הפונקציונאלית של חיתוך ההטינגטין המוטני נבדקה בעזרת בדיקת החיות ורמות השפעול של מערכת הקספאזות בתאי PC12 המבטאים חלבון הנטינגטין מוטני באופן יזום. נמצא ש-ED11 מגן על התאים גם מאיבוד החיות וגם משפעול יתר של מערכת הקספאזות אשר מושרים על ידי ביטוי ההנטינגטין המוטנטי.

על מנת לקבוע האם ED11 מסוגל להגן מפני רעילות ההנטינגטין המוטנטי בבעלי חיים, נעשה שימוש במודל עכברי של מחלת הנטינגטון הקרוי BACHD ועכברי FVB/N כביקורת. עכברי ה-BACHD מבטאים חלבון הנטינגטין מוטנטי שלם עם 97 חזרות של גלוטמין בקצה ה N-terminal. עכברים אלה מציגים חסרים מוטוריים, התנהגותיים וקוגניטיביים מתקדמים, אשר קורלטיביים לתסמינים המצויים במחלת הנטינגטון.

השלב הראשון בהערכת היתכנות הטיפול של ED11 בבעלי חיים היה להדגים את היתכנות חדירת מעבר הדם-מח. למטרה זו, הסטריאטום של עכברי FVB/N נצפה על ידי פלורוסנציה בגוף החי. הזרקה של ED11 מצומד למולקולה פלואורסנטית אפשרה ויזואליזציה של כניסה של החומר מכלי הדם לתוך פרנכימת המח, עובדה אשר מצביעה על חדירה של ED11 את האנדותליום של כלי הדם ואקסטרבזציה אל פרנכימת המח.

למחקרי יעילות הפפטיד בטיפול בבעלי חיים, הפוטנציאל הטיפולי נמדד בשתי פרדיגמות טיפול שונות, טיפול מוקדם בגיל הופעת הסימפטומים וטיפול מאוחר במצב מחלה מתקדם. לבדיקת השפעת ED11 בגיל הופעת סימפטומים, עכברי BACHD טופלו על ידי ED11 למשך חמישה חודשים, החל מגיל חמישה שבועות, על ידי משאבה תת-עורית המזריקה באופן רציף בקצב של 4 מ"ג לק"ג ליום. הטיפול על ידי ED11 גרם להפחתה של שינויי משקל הגוף, סממן המופיע גם בחולי הנטינגטון. תפקוד מוטורי, אשר פגוע באופן ניכר בחולי הנטינגטון נבדק בעכברי ה BACHD בעזרת מבחן הרוטרוד. טיפול ב-ED11 גרם לשימור משמעותי של יכולת הלמידה המוטורית, בהשוואה לעכברים המטופלים בנוזל הביקורת. יכולת מוטורית ארוכת טווח נמדדה אחת לחודש בעכברי ה-BACHD, והתגלה שטיפול ב-ED11 אפשר את שימור היכולת המוטורית ברמה הניתנת להשוואה לזו של עכברי הביקורת ללא המוטציה הגנטית. על מנת להעריך את ההשפעה על סימפטומים ניורופסיכיאטריים, התנהגות הקשורה למאפיינים דיכאוניים נמדדה במבחן השחייה הכפויה ונמצאה מופחתת בעכברים הטרנסגניים המטופלים ב-ED11 לעומת העכברים הטרנסגניים המטופלים בנוזל הביקורת. בנוסף, התנהגות הקשורה למאפיינים חרדתיים נבדקה במבחני השדה הפתוח, המבוך המורם ומבחן בחירה בין חושך לאור, ונמצאה מופחתת כתוצאה מטיפול ב-ED11. במטרה להבין את השפעת הטיפול במצב בו המחלה כבר התפרצה, עכברי BACHD טופלו החל מגיל 9 חודשים והוערכו לתפקודים מוטוריים, נוירופסיכיאטריים וקוגניטיביים. טיפול ב-ED11 גרם להתאוששות משמעותית ברמת היכולת המוטורית כפי שנמדד במבחן הרוטרוד. בנוסף, התנהגות הקשורה למאפיינים דכאוניים גם כן הופחתה בטיפול מאוחר בעכברי ה-BACHD. יתרה מכך, בחינה של יכולת מוטורית בעזרת מבוך ה- T הרטוב הראתה שעכברי BACHD המטופלים ב- ED11 מראים יכולת קוגניטיבית וגמישות בקבלת החלטות בצורה משמעותית טוב יותר מאשר עכברי BACHD המטופלים בנוזל הביקורת.

על מנת לבחון את הקורלציה בין ההשפעה ההתנהגותית של טיפול ב-ED11 למאפיינים נוירופתולוגיים, אטרופיה של המח נמדדה בעזרת דימות תהודה מגנטית (MRI). כימות של המידע הראה שביטוי גן ההנטינגטין המוטנטי לא גרם לאטרופיה סטריאטלית, קורטיקלית או היפוקמפלית בעכברי ה-BACHD, ולכן לא ניתן היה להסיק על השפעת הטיפול על אטרופיה של המח. בנוסף, בעזרת המרקר DARPP-32 לתאי עצב גבארגיים, לא זיהינו הפחתה בעכברי ה-BACHD בהשוואה לעכברי הביקורת ללא השינוי הטרנסגני. היווצרות אגרגטים נבדקה בעזרת אימונופלואורוסנציה ומבחני אגרגציה בעזרת פילטרציה.

התגלה שהטיפול ב-ED11 לא השפיע בצורה משמעותית על היווצרות האגרגציות. לבסוף, נבדקה השפעת ED11 על פרוטאוליזה של ההנטינגטין המוטנטי על ידי קספאז-6 בגוף החי. בעקבות הימצאות מתחת לסף דטקציה של פרגמנט 586 בגוף החי, לא זוהו הפרגמנטים בעכברי ה-BACHD, ולכן לא ניתן היה לכמת את השפעת הטיפול על היווצרותם בגוף החי.

למסקנה, המחקר המוצג בעבודה זו מדגים ששימוש בפפטידים המבוססים על רצפים טבעיים היא גישה ברת ביצוע לעיכוב חיתוך חלבונים על ידי קספאזות, ובעלת פוטנציאל לשימוש למטרות טיפוליות. עבודות נוספות צריכות להתבצע על מנת לתרגם את ממצאנו ממודלים בבעלי חיים לחולים במחלת הנטינגטון. בנוסף, ממצאים אלו עשויים להיות ישימים במחלות נוירודגנרטיביות או נוירולוגיות אחרות אשר בהן ישנה מעורבות של קספאז-6 בתהליך יצירת הפתולוגיה. אנו מקווים שבעתיד, המידע שהתגלה במחקר זה יוביל להקלה בסבלם של החולים במחלה.

Table of contents

List of figures

List of tables

Abbreviations

HD	Huntington's disease
MSN	Medium-sized spiny neurons
MRI	Magnetic Resonance Imaging
Htt	Huntingtin
PolyQ	Poly-glutamine
Caspase	Cysteine-dependent aspartate-specific proteases
SATB1	Special AT-rich sequence-binding protein-1
APP	Amyloid precursor protein
CNS	Central nervous system
C6R	Caspase-6 resistant
YAC	Yeast artificial chromosome
NMDA	N-methyl-D-aspartate
CMK	Chloromethylketone
DMK	Diazomethylketone
AOMK	Acyloxymethylketone
FMK	Fluoromethylketone
Oph	Phenoxymethylketone
3-NP	3-Nitropropionic acid
ROS	Reactive oxygen species
BDNF	Brain-derived neurotrophic factor
IPSC	Induced pluripotent cells
MPTP	1-methyl-4-phenyl-1,2,3,6-tetrahydropyridine
C.elegans	Caenorhabditis elegans
BAC	Bacterial artificial chromosome
IGF-1	Insulin-like growth factor 1
EPM	Elevated plus maze
OF	Open field

FST	Forced swim test
SPT	Sucrose preference test
TAT	Trans-activator of transcription
FITC	Fluorescein isothiocyanate
DMSO	Dimethyl sulfoxide
DOC	Deoxycholic acid
DTT	Dithiothreitol
EDTA	Ethylenediamine-tetra-acetic acid
HEPES	4-(2-hydroxyethyl)-1-piperazineethanesulfonic acid
NP-40	Nonyl phenoxypolyethoxylethanol
TRIS	Trimethylsilyl
SDS	Sodium dodecyl sulfate
PBS	Phosphate-buffered saline
PVDF	polyvinylidene difluoride
BrdU	5-Bromo-2′-deoxyuridine
DMEM	Dulbecco’s Modified Eagle’s Medium
FCS	Fetal calf serum (FCS)
FLICA	Fluorescent Labeled Inhibitor of Caspases
PSN	Penicillin-Streptomycin-Nystatin
PI	Propidium iodide
DAPI	4',6-diamidino-2-phenylindole
DAB	Di-amino-benzidine
PCR	Polymerase chain reaction
DARPP32	Dopamine- and cAMP-regulated phosphoprotein
PARP	Poly [ADP-ribose] polymerase
MHtt	Mutant Huntingtin
MEF	Mouse embryonic fibroblasts
IL2	Interleukin-2
FRET	Fluorescence Resonance Energy Transfer

PA	Ponasterone a
LDH	Lactate dehydrogenase
FAM	Fluorescein
RPM	Rounds per minute
PFA	Paraformaldehyde
RLU	Relative light units
SEM	Standard error of the mean

1. Abstract

Huntington's disease (HD) is a neurodegenerative disease with an autosomal dominant inheritance pattern. A person who suffers from HD symptoms will develop progressive motor dysfunction, neuropsychiatric symptoms, and cognitive decline. HD is fatal, as life expectancy is approximately 10-15 years after the age of onset. Neuropathological aspects of HD include progressive cell loss and atrophy, primarily in the striatum and the cerebral cortex.

The disease is caused by a mutation in the Huntingtin (Htt) protein, which was found to be an extension of glutamine residues repeatnear the N-terminal end of the protein. While wild-type Htt contains up to 35 glutamine repeats, mutant Htt contains above 36 glutamine repeats. This mutation triggers events that cause diverse toxic pathways to be activated, resulting in significant damage to GABAergic medium spiny striatal neurons (MSN) as well as glutamatergic cortical neurons that project to the striatum.

Htt is a subject of proteolytic cleavage by various cysteine-dependent aspartate-specific proteases (caspases). One of the main cleavage sites associated with the development of HD is the Asp586, which is cleaved by caspase-6. The importance of mutant Htt proteolysis at Asp586 was revealed in a mouse model to express caspase-6 resistant mutant Htt by our research collaborator Professor Michael Hayden and his group. They discovered that genetic prevention of caspase-6 cleavage of mutant Htt prevents the generation of toxic N-terminal fragments and protects the YAC128 mouse model of HD from neurodegeneration and appearance of disease symptoms. Over the past decade, numerous other studies have uncovered a significant role of caspase-6 in HD

pathogenesis. For example, its activation is an early pathogenic event in HD mutation carriers, and the level of activation is directly correlated with CAG repeat length and inversely correlated with age of onset. In addition, activated caspase-6 and cleaved fragments of Htt are found in the nuclei of striatal neurons after the initiation of cellular stress, which correlates with increased toxicity.

Therefore, inhibiting mutant Htt proteolysis by caspase-6 was suggested as a promising therapeutic target for reducing mutant Htt toxicity and rescuing neuronal cells from degeneration. Consequently, extensive efforts have been exerted over the past decade to develop efficient caspase inhibitors. Unfortunately, most synthetic caspase inhibitors are non-specific, lack sufficient permeability, and might cause nonspecific toxic effects when added at concentrations that are required to inhibit intracellular caspases.

The primary research goal was to elucidate the potential of targeting mutant Htt proteolysis by caspase-6 as a therapeutic strategy for HD, using the concept of compound based enzyme inhibition approach. Specifically with the design of an Htt caspase-6 cleavage site based peptide that will compete on caspases-6 activity and by thus reducing mutant Htt proteolysis and subsequent toxicity. A total 11 amino acids of the Htt protein, from Ser580 to Asn590 were selected as the proposed inhibitor caspase-6 recognition site, and the HIV-TAT (48-60) was selected to facilitate efficient cellular and nuclear penetration, and transportation through the Blood-brain barrier. The peptide created was designated as ED11.

In order to test the ability of the designed peptide to directly inhibit caspase-6 activity, a luminescence-based caspase activity assays was conducted. It was found that the cleavage of Z-VEID-aminoluciferin was significantly reduced in the presence of ED11 in

a dose-dependent manner, which provides the substantial proof that ED11 directly inhibit caspase-6 activity. Next, to provide evidence of the specificity of the designed peptide sequence, an alanine substitution of different amino acids of ED11 was made. By measuring the effect on ED11 inhibition ability, it was found that the replacement of amino acids that include the recognition site of caspase-6 resulted in the elimination of ED11 ability to inhibit caspase-6. Due to caspase family active site similarity and the significance of cross-reactivity with caspase-3 in terms of safety, the influence of ED11 on caspase-3 activity was tested. It was revealed that ED11 did not influence cleavage of Z-VEID-aminolucifern, PARP or Specterin by caspase-3, in contrast to the pan-caspase inhibitor zVAD-FMK, indicating ED11 has selectivity for caspase-6 over caspase-3. Next, the competency by which ED11 influence Htt proteolysis by caspase-6 was revealed by using a sensitive Htt cleavage FRET-based assay. The IC50 determined for ED11 is 12.12nM, comparable to the IC50 of the covalently binding synthetic inhibitor zVAD-FMK that was found to be 4.62nM. These results Indicate ED11 inhibits Htt cleavage by Caspase-6 with marked competency. To elucidate the overall effect on Htt caspase cleavage by ED11, Htt protein cleavage by caspases 1–10 was conducted. It was found that the inhibitory effect of ED11 was most pronounced for the generation of the 586 fragment by caspase-6. A lesser effect of the inhibitor was found on caspase-1 and caspase-10 mediated generation of the 513 fragment and caspase-2 mediated generation of the 552 fragment. Next, the ability of ED11 to inhibit human mutant Htt cleavage by caspase-6 was verified by the use of protein lysate from the striatum of human mutant Htt expressing HD mouse model.

After demonstrating the efficacy and selectivity of ED11 in an in-vitro enzymatic reaction studies, the feasibility and safety of ED11 in inhibiting caspase cleavage of mutant Htt in the intra-cellular environment was tested. First, using anti-TAT antibodies, it was verified that ED11 can penetrate cellular membranes and enter cells. Next, the intra-cellular safety evaluation of ED11 has shown that ED11 does not influence cell viability, proliferation or cell cycle status under basal conditions. To evaluate the ability of ED11 to reduce intracellular Htt cleavage by caspase-6, co-transfection of HEK293 cells with caspase-6 and the N-terminal 1212 amino acids of 15Q-Htt was conducted in the presence of ED11. Quantification of Htt 586 fragments showed that ED11 significantly inhibited the intra-cellular caspase-6 activity. The influence on the functional outcome of mutant Htt cleavage was tested by measuring the viability and caspase activation of inducible 145Q-mHtt expressing PC12 cells after treatment with ED11. ED11 was found to protect the cells both from viability loss and excess caspase activation induced by mutant Htt expression.

To determine ED11 ability to protect from mutant Htt toxicity in-vivo, the HD mouse model BACHD and control background FVB/N were used. BACHD mice express full-length mutant Htt with 97 glutamine repeats at the N-terminal and demonstrate progressive motor, behavioral and cognitive deficits which correlate to symptoms present in HD.

The first step in evaluating the in-vivo feasibility of ED11 treatment was to demonstrate the blood-brain penetration ability. For this goal, FVB/N mice striatum was monitored by in-vivo fluorescence. The injection of FITC conjugated ED11 enabled visualization of the

entry from the blood vessels into the brain parenchyma, indicating ED11 penetrated the blood vessel endothelium and extravagated into the brain parenchyma.

For efficacy studies in-vivo, the therapeutic potential was measured in two main treatment paradigms, early treatment at the age of symptoms appearance and late treatment at an advanced disease state. For the evaluation of ED11 effect in an early disease state, BACHD mice were treated with ED11 for five months starting at the age of five weeks, by a subcutaneous implanted mini-pump, injecting continuously at the rate of 4mg/kg/day. ED11 treatment was shown to attenuate body weight alterations, a feature also found in HD patients. Motor function, which is markedly impaired in HD was tested in the BACHD mice using the Rotarod test. Treatment with ED11 in BACHD mice resulted with marked preservation of the motor learning skill, as compared to the vehicle-treated BACHD mice. The long-term motor function was monitored monthly in the BACHD mice, and it was discovered that ED11 enabled the preservation of motor function at a level comparable to that of the wild-type mice. For evaluation of Neuropsychiatric symptoms, depression-related behavior in the Forced swim test (FST) and was found to be significantly reduced by the treatment with ED11. In addition, anxiety-related behavior in the open-field, Elevated plus maze (EPM) and dark-light choice tests was attenuated in the presence of ED11 treatment.

It is imperative to understand the effect of treatment in a state in which the disease symptoms have already appeared. For this goal, BACHD mice commenced treatment at the age of 9 months and evaluated for the motor, neuropsychiatric and cognitive impairments. ED11 treatment resulted in a significant motor performance recovery as measured by the Rotarod test. In addition, depressive related behavior was attenuated also

in the late treated BACHD mice. Furthermore, the evaluation of cognitive performance by the swimming T-maze test revealed that ED11 treated mice as well as the wild-type mice, superior to the vehicle treated BACHD mice.

To examine the correlation of ED11 influence on behavior with neuropathology, brain atrophy was evaluated using Magnetic Resonance Imaging (MRI). Quantification revealed that No striatal, cortical or hippocampal atrophy was evidenced in the BACHD mice used in this study. In addition, using DARPP-32 as a marker for MSN, we did not detect any reduction in the BACHD mice compared to controls. Aggregates formation was quantified using immunofluorescence and filter trap assays. In this aspect ED11 treatment did not influence aggregate formation in a significant matter. Lastly, The impact of ED11 on mutant Htt proteolysis by caspase-6 in-vivo was tested. Unfortunately, due to the low abundance of mutant Htt caspase-6 fragments in-vivo we were unable to detect a corresponding fragment in the BACHD animals used in the current study.

In conclusion, our study demonstrates that the use of substrate-based peptides is a feasible concept for inhibition of caspase-mediated protein cleavage for therapeutic purposes. Further studies should be performed to translate our findings from animal models to HD patients. In addition, our findings might be applicable in other neurodegenerative or neurological diseases where caspase-6 activity plays a part in the pathogenic process. We truly hope that in the future, the data generated in this research study will eventually help to ease the suffering of HD patients.

2. Introduction

2.1. Huntington's disease characteristics

2.1.1. Clinical presentation

Huntington's disease (HD) is a fatal neurodegenerative disease with an autosomal dominant inheritance pattern. The prevalence of HD is averaged as 4–10 cases per 100,000 worldwide. The peak age of onset is between 35 and 50 years[1]. Symptoms of HD include progressive motor dysfunction, neuropsychiatric symptoms, and cognitive decline. Progressive motor disturbances involve changes in coordination, involuntary movements, restlessness, twitching and muscle spasms. As time passes, a dystonia appears, balance and walking are impaired, progressive chorea movements are evident and swallowing problems occur. At final stages, inability to walk or speak, severe rigidity and serious weight loss are evident. In parallel with motor disturbances, there is a gradual impairment of the mental processes involved in comprehension, reasoning, judgment, and memory[2,3]. Other Commonly reported early symptoms in HD include progressive weight loss, alterations in sexual behavior and disturbances in the wake-sleep cycle that occur very early in the course of the disease[4]. Eventually, people affected with HD become unable to care for themselves, therefore require long-term institutional care. Life-threatening complications may result from injuries related to serious falls, poor nutrition, infection, choking, and inflammation. Life expectancy of HD is approximately 10-15 years after the age of onset. Most HD patients eventually lose their lives due to aspiration pneumonia because of swallowing difficulties, or as a result of cardio-vascular

complications[2]. An additional HD sub-type existed, which is termed juvenile HD. In this form, the symptoms occur earlier in life, they are generally more severe and a more rapid disease progression is observed[5].

2.1.2. Neuropathology

HD pathology is most prominent brain related, as progressive cell loss and atrophy in the striatum is evident[6]. HD pathological state is classified as five different severity grades, based on post-mortem brains gross and histological examination. Grade 0 is not different from normal brains at a gross examination, but histological examination will reveal 30-40% neuronal loss in the head of the caudate. In grade 1, atrophy, neuronal loss and astrogliosis are evident in the tail and body of the caudate nucleus. At grades 2 and 3, progressive gross striatal atrophy can be observed, while grade 4 includes massive striatal atrophy and up to 95% neuronal loss in histological examination. Among the neurons affected in HD, the most prominent degeneration occurs in GABAergic medium-sized spiny neurons (MSN)[7,8]. In addition, striatal neurons projections to other areas in the brain are depleted in the advanced stage of HD, along with different neuron types. Furthermore, it is now well known that the cerebral cortex, diffuse white matter, the cerebellum, globus pallidus, thalamus, subthalamic nucleus, substantia nigra and hypothalamus can undergo significant atrophy[4,9,10]. The observation of wide-spread brain atrophy has been confirmed in living patients using Magnetic Resonance Imaging (MRI)[11]. Later observations demonstrated that the atrophic process in evident even before symptoms onset[12-14]. Nowadays, research on MRI-derived disease development bio-markers is continuously conducted around the world[15].

2.1.3. Pathogenesis

HD is caused by a mutation in the HTT gene, which is found on chromosome 4 in location 4p16.3. The mutation was found to be an unstable expansion of CAG repeats within the coding region of the HTT gene[16]. The protein encoded from this gene is called Huntingtin (Htt), which is a large (340-350 kD, 3144 A.A) protein that has a prominent role in a variety of cellular functions. These include but not limited to transcription, gastrulation, neurogenesis, neurotransmission, axonal transport, neural positioning, and apoptosis[17,18]. The mutation in the HTT gene in HD patients leads to an elongation of glutamine residues repetitions near the N-terminal end of the protein. While wild-type Htt contains up to 35 glutamine repeats, Mutant Htt contains 36-55 repeats in adult HD patients and >60 repeats in juvenile HD patients. This single mutation triggers events that cause diverse toxic pathways to be activated, resulting in significant damage to GABAergic MSN as well as glutamatergic cortical neurons that project to the striatum[19]. The loss of the GABAergic MSN results in a lack of inhibitory signals from the striatum to the globus pallidus and the substantia nigra, and therefore induces excitatory signals to the neocortex. This disequilibrium is considered to be the cause for the involuntary movement symptom of the disease.

There are several proposed mechanisms for the neuronal dysfunction resulting from mutant Htt expression: Formation of mutant Htt aggregates and inclusions[20,21], the altered conformation of mutant Htt leading to transcriptional dysregulation[22], excessive stimulation of glutamate receptors leading to excitotoxic neuronal damage[23] , and induction of apoptosis[24]. Plus, the fact that there is a reduction in normal Htt activity may also contribute to disease manifestation, due to the important role of Htt in cellular

activity, and the fact that wild-type Htt plays an important role in neuronal protection and survival[25,26].

Extensive research has found a variety of underlying molecular dysfunctions resulting from mutant Htt expression. Therefore, an efficient therapeutic intervention needs to be directed at an early process in the pathogenesis of HD.

2.2. Caspase involvement in Huntington's disease

2.2.1. Caspase cleavage of Huntingtin

Htt is a subject of proteolytic cleavage by various caspases. Caspases (cysteine-dependent aspartate-specific proteases) are a family of cysteine proteases that are highly conserved in multicellular organisms and function as central regulators of apoptosis. They function as endoproteases, by hydrolysis of a peptide bond only after conserved tetra-peptide domains (Marked as P4-P3-P2-P1) within the target protein. These tetra-peptide domains end with an aspartic acid residue at position P1, and the cleavage occurs between P1 and the subsequent residue. The amino acids at position P2-P4 facilitate the specificity for different caspases[27-29]. This caspase-mediated process results in either substrate inactivation, or it may generate active signaling molecules that participate in ordered processes such as apoptosis and inflammation. Over the past decades, various caspases have been discovered, and were broadly classified by their known roles in apoptosis (caspase-3, -6, -7, -8, and -9 in mammals), and in inflammation (caspase-1, -4, -5, -12 in humans and caspase-1, -11, and -12 in mice). The functions of caspase-2, -10, and -14 are less easily categorized. Caspases involved in apoptosis have been sub classified by their

mechanism of action and are either initiator caspases (caspase-8 and -9) or executioner caspases (caspase-3, -6, and -7)[30].

In 1996, Htt was found to be a substrate for caspase cleavage, as it is cleaved by caspase-3 at amino acids Asp513 and Asp552, caspase-2 at amino acid Asp552, and caspase-6 at amino acid Asp586[31]. The role of caspase cleavage of Htt was a subject for extensive research in past years. Due to the fact that cellular toxicity was increased in cells expressing Htt fragments, a hypothesis named "the toxic fragments theory" was developed (Fig. 1). According to this theory, a strong link is found between caspase proteolysis of Htt and cellular toxicity evident in HD. Proteolytic cleavage of Htt, which is more evident in the mutant form of the protein, leads to a generation of toxic fragments, which leads to the activation of different toxic pathways, which in turn leads to neuronal dysfunction including an additional activation of caspases. This results in a vicious cycle, which results in disease symptoms and neuronal death[32]. The toxic fragments theory was reinforced in numerous studies. Although the cleavage occurs both in normal and mutant Htt, the mutant form is more susceptible to proteolysis. The cleavage generates N-terminus fragments that aggregate in the cytoplasm and nucleus of HD patients brain cells. The fragments aggregate particularly in the cerebral cortex of patients with low-grade neuropathology, even when striatal atrophy is still in its early stages[33-35]. N-terminus Htt aggregates also form when mutant Htt is expressed in vitro, in neuronal and nonneuronal cells[36]. Furthermore, mutant Htt fragments accumulate both in

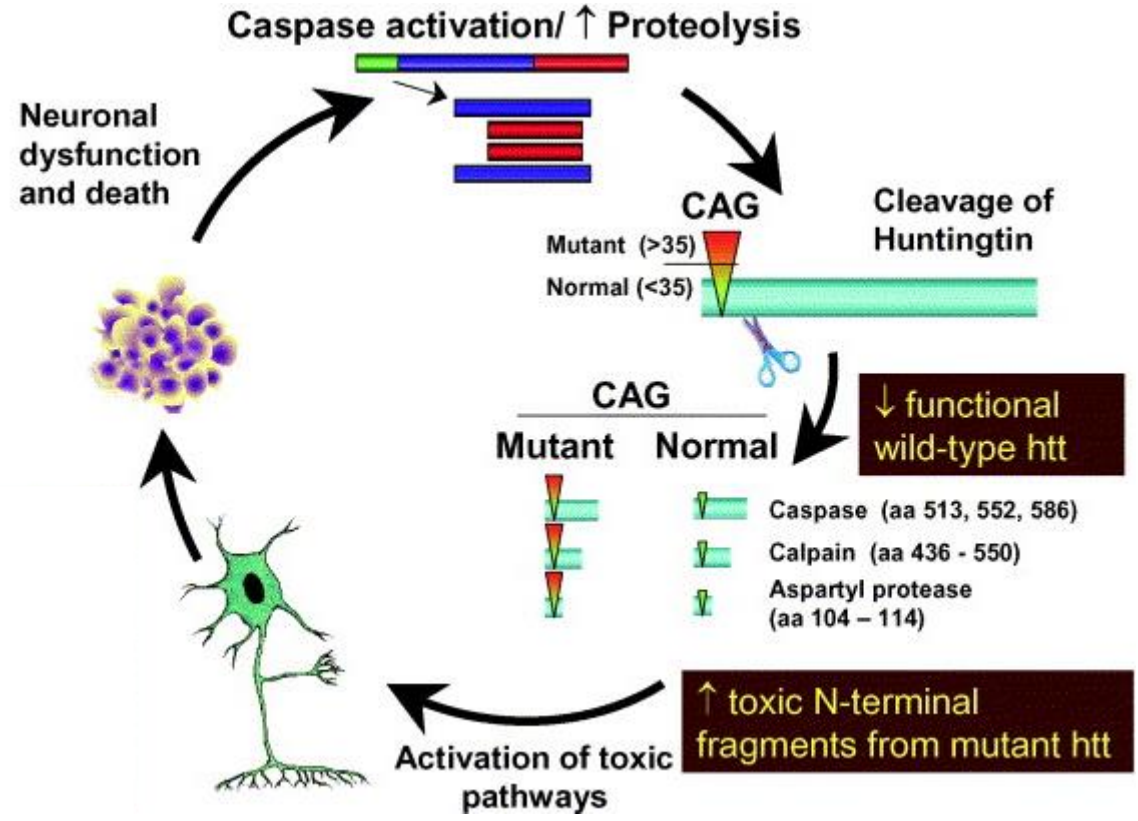

Figure 1: The toxic fragment hypothesis (modified from Wellington et al.[37])

Cleavage of Htt generates toxic N-terminal fragments that, when containing expanded polyglutamine tracts, fail to be efficiently degraded and accumulate within cells. The resulting fragments initiate activation of a variety of toxic pathways. In addition, Htt proteolysis results in the loss of neuroprotective functions of intact Htt. Together, these effects result in increased neuronal stress and decreased neuronal function. Excess activation of cell death pathways including caspases and calpains results in additional cleavage of Htt and a spiral of toxicity that ultimately causes neuronal death

the nucleus and in the cytoplasm and create a toxic effect that eventually leads to cell death[33,38-41]. It has been shown that the toxic fragments cause additional activation of caspases 3 and 6[42], thus creating a positive feedback cycle of caspase activation and induction of apoptosis. The significance of caspases proteolysis of mutant Htt is manifested in the fact that inhibiting caspase cleavage of Htt reduces toxicity and

aggregate formation in neuronal and non-neuronal cells[43]. Moreover, experiments in animal models for HD have demonstrated that preventing caspase cleavage of Htt has a prominent beneficial effect on HD related phenotypes. These studies and their importance for understanding caspases role in HD will be further elucidated later.

2.2.2. Caspase-6 role in Huntington's disease pathogenesis

Caspase-6 was first discovered in 1995 as a participant in apoptotic pathways[44]. In contrast to caspase-3 and caspase-7, which target tetrapepide sequences with aspartate at their P4 position, caspase-6 targets sequences with either leucine or valine at the P4 position[45]. This distinctive feature enables caspase-6 to cleave unique substrates such as Lamin A/C[46,47], SATB1[48], APP[49], presenilin-1[50], DJ-1[51], And as mentioned, Htt. Recently, a number of novel caspase-6 substrates were found using proteomic approach, and research in underway to further uncover caspase-6 role in health and disease[52]. Although Caspase-6 was previously regarded to as a part of the executioner caspases, the reality is more complex. Caspase-6 can be activated by caspase-3 and caspsae-7, and can inversely activate these caspases as well[53,54]. Furthermore, caspases-6 has a role as an initiator caspase, as it process other initiators caspases such as caspase-8 and caspase-10[53,55]. These findings suggest a more important role of caspase-6 as and upstream regulator in physiological or pathological pathways.

Over the past 10 years, numerous studies have uncovered a significant role of caspase-6 in HD pathogenesis: its activation is an early pathogenic event in HD mutation carriers, and the level of activation is directly correlated with CAG repeat length and inversely correlated with age of onset[42]. In addition, activated caspase-6 and cleaved fragments of

Htt are found in the nuclei of striatal neurons after the initiation of cellular stress, which correlate with increased toxicity[56]. Recent evidence shows that caspase-6 activity induced by mutant Htt is not restricted to the central nervous system (CNS), but can be found in muscle tissue from HD patients and in HD mouse models[57], suggesting that caspase-6 might be involved in central as well as peripheral features of HD. The importance of mutant Htt proteolysis at Asp586 was revealed in a mouse model genetically engineered to express Caspase-6 resistant (C6R) human mutant Htt. The researchers have targeted two sites of human mutant Htt in the YAC128 mouse model of HD where caspase-3 or caspase-6 mediated proteolysis occurs. They discovered that mice expressing C6R human mutant Htt do not develop striatal neurodegeneration and are protected from motor deficits and the depressive phenotype seen in HD mouse models. Furthermore, these mice are protected from neurotoxicity induced by multiple stressors including NMDA, quinolinic acid and staurosporine, demonstrating the protective effects of C6R mutant Htt expression. These observations were evident in mice expressing caspase-6 resistant human mutant Htt but not in mice expressing caspase-3 resistant human mutant Htt[58]. In a complementary study, transgenic mice expressing the 586 amino acid N-terminal fragment of human mutant Htt demonstrated severe neurologic abnormalities and aggregate formation[59]. These observations imply that inhibition of human mutant Htt proteolysis by caspase-6 would both reduce the load of toxic N-terminal fragments and maintain the neuroprotective function of wild-type Htt. Therefore, the specific inhibition of caspase-6 was suggested as a disease-modifying therapeutic strategy. The importance of caspase-6 in mutant Htt pathogenesis has recently been challenged in studies that crossed caspase-6 deficient mice and HD mouse models[60,61]. These reports have

demonstrated the continued presence of 586 amino acid human mutant Htt fragments in the absence of caspase-6, suggesting that additional proteases are involved in mutant Htt fragmentation at this site. Nonetheless, caspase-6 deficiency provided significant beneficial effects including a decrease of full-length human mutant Htt and human mutant Htt fragments and a significant reduction in aggregate formation. Furthermore, body weight levels and motor deficits were attenuated. In contrast to the genetic ablation of caspase-6, compound based inhibition of caspase-6 activity in adulthood may be more efficient in providing protection from mutant Htt toxicity in vivo.

2.3. Caspase inhibition as a therapeutic approach

Ever since the discovery of caspases as a major component of mammalian cell death pathway[62], they have been subjected to an extensive research addressing their contribution to a variety of physiologic and pathologic processes. Genetic manipulations and compound based alteration of caspase activity have created a growing body of evidence, establishing a prominent role of caspases in the pathogenesis of diseases from different medical fields. These include oncology[63], neurology[64-69], endocrinology[70], infectious diseases[71], cardiology[72], rheumatology[73] and others. The establishment of caspases as a major player in disease pathogenesis has made caspase inhibition a leading therapeutic necessity, resulting in the necessity to create safe and efficient caspase inhibitors.

When addressing the safety of caspase inhibitors as a therapeutic tool, a few concerns are typically raised. First of all, since caspases play a major role in inducing apoptosis, the question of cancer formation resulting from caspase inhibition is raised. In order to

address this question, a number of studies have been conducted in basic and clinical research. It has been found that although caspases has a prominent role in apoptosis, the lack of activity of a single caspase, with the exception of caspase-8, is compensated by different caspase-dependent and caspase-independent signaling pathways in order to assure the apoptotic process. Moreover, none of the caspase knockout mice tested to this date has been subjected to a higher cancer appearance rate[74]. Clearly, these observations need to be reinforced over the course of time. A few studies have been published recently that addresses the question whether caspase-6 causes tumorigenesis. One study discovered that Inflammation-induced tumorigenesis in mouse colon is caspase-6 independent, revealing that caspase-6 deficient mice did not demonstrate a change in colonic tumor multiplicity, burden or distribution[75]. Nevertheless, other studies have revealed that caspase-6 inhibition may cause resistance to certain cancer targeted drugs[76,77], emphasizing the notion that in populations who are in need of medical treatment for cancer, caspase-6 inhibition as a therapeutic strategy needs to be strongly evaluated.

Another important issue to address regarding caspase inhibition safety will be the effect on normal apoptotic functions, which may result in organ dysfunction. For this goal, numerous tests have been made in different caspase knockout mice. Caspases 3, 8, and 9 knockouts have been found to be incompatible with life, as their knockout does not permit live mouse newborns to be delivered[78-80]. Other caspase knockout has a certain influence on apoptotic pathways. For example, caspase-1 knockout has been shown to down regulate processing and secretion of different cytokines and to cause resistance to septic shock[81] and caspase-2 knockout has been shown to cause certain defects in

apoptosis induction by chemotherapeutic drugs in oocytes[82]. Studies in caspase-6 knockout mice have revealed that there is an age-dependent increase in cortical and striatal volume. In addition, these mice show a hypoactive phenotype and display learning deficits[83]. It is important to note that genetic knockout of caspase-6 have influence on brain development in the embryonic stage, as caspase-6 has as prominent role in neuronal pruning process and development[84] in this stage. This observation highlights the limited insights that can be achieved from studies in caspase knockout mice, in contrast to compound based caspase inhibition or conditional knockout in the adult life. The safety of caspase-6 inhibition may be demonstrated by the fact that in a healthy adult life basal state, caspase-6 is found mainly in its inactivated form, and is mostly activated only during aging and in pathological states[42,85,86].

For achieving the goal of inhibiting caspase activity, a variety of caspase inhibitors were developed over the years. There are mainly two types of caspase inhibitors, peptidomimetics and small molecule based caspase inhibitors. The peptide based caspase inhibitors contain a tetrapeptide that corresponds to the tetrapeptide motif found on caspase substrates as mentioned earlier. This tetrapeptide is typically conjugated to an affinity increasing molecule in the C-terminal. The nature of the inhibitor depends on the conjugated molecule. When an aldehyde group is conjugated the inhibitor is considered to be a reversible inhibitor, while conjugation of chloromethylketone (CMK), diazomethylketone (DMK), acyloxymethylketone (AOMK), fluoromethylketone (FMK) or phenoxymethylketone (Oph), creates a covalently binding irreversible inhibitor[87,88]. Experience with these caspase inhibitors over the years has presented three main issues that have been preventing the use of these compounds as therapeutic substrates. The first

is the lack of selectivity, as studies have shown that classic caspase inhibitors demonstrate significant cross-reactivity towards non-target caspases[89-91]. This cause cross inhibition of various caspases, and thus inflict undesired effect on uninvolved caspases. The second issue to be addressed is the penetration of the blood-brain barrier. As most of the peptide based caspase inhibitors lack the ability to enter the CNS through the blood-brain barrier, the use of these inhibitors in neurodegenerative disease is highly limited[92-94]. The third issue to be addressed, which can be a result of the previously mentioned disadvantages of earlier caspase inhibitors, is the toxicity related to the use of these inhibitors[95]. For example, the use of zVAD-FMK as a therapeutic compound was halted due to extensive liver toxicity in dog trials[96]. Over the years, the search for a safer, more specific and CNS-penetrating caspase inhibitors has yielded a few promising compounds[97-100], which are currently pending clinical or in the process of clinical trials. Unfortunately, none of these inhibitors are specific for a particular caspase, and none are aimed towards inhibiting caspase-6 or intended for the treatment of HD. Taking into account the limitations current caspase inhibitors have, the search for a specific, safe and effective caspase-6 inhibitor is crucial and is significant for the advancement of caspase-6 inhibition as a therapeutic approach for HD.

2.4. Research models of Huntington's disease

Modeling HD has been an immense point of interest since the discovery of the Htt gene. Over the years, numerous in-vitro and in-vivo models have been developed. These models have been effectively used to elucidate pathological pathways, molecular targets and therapeutic interventions. In the following sections, methods of modeling HD will be discussed, with emphasis on models used in the presented research study.

2.4.1. In-vitro models

Earlier in-vitro models relied on different stressors that mimicked the toxic environment in which human mutant Htt expressing cells were exposed to in the living brain. Such models generally include the use of glutamate, 3-Nitropropionic acid (3-NP), L-Homocysteic acid and other various toxins to induce cellular damage[101-105]. At a later stage, after the discovery of the Htt gene, human mutant Htt expressing cell-lines were developed, and were shown to recapitulate several HD related phenotypes. Such phenotypes include aggregate formation[106,107], increased caspase activation[39,108], and sensitivity to different toxic substrates such as glutamate, 3-NP and staurosporine2[109,110]. In addition, stressful environments, such as serum-deprived culture media, cause cell death in a time-dependent manner, including an increase in reactive oxygen species (ROS) levels and cytochrome C release[111]. As was elaborated earlier, the use of human mutant Htt expressing cells enabled the elaboration of the significance of human Mutant Htt proteolysis. For example, passive nuclear transportation of N-terminal fragments of Htt was found, which indicated proteolysis is a necessary step for nuclear entry of Htt[38]. Furthermore, the introduction of a short N-terminal EXON1 fragment of human mutant Htt by plasmid transfection, resulted in rapid cell death, and was used to model the effect of short mutant Htt fragment on cellular function[112,113]. In addition to the ability to enable the further understanding of HD pathogenic pathways, these cell models enabled researchers to test therapeutic compound potential. Different compounds were tested in terms of protection from cytotoxicity[114], Caspase activation[43,115], mitochondrial dysfunction[116], decreased brain-derived neurotrophic factor (BDNF) expression[117] and more. It is important to note that cells that hold the ability to use the inducible expression

of human wild-type or human mutant Htt have been useful for the further understanding disease mechanisms and evaluating therapeutic approaches for HD[108,118,119], as they are able to recapitulate time-dependent human mutant Htt influence on cells. As genetic reprogramming methods were developed, induced pluripotent cells (IPSC) based model strategy was created. In this method, cells derived from a variety of tissues from HD patients, have been subject to reprogramming and were further developed as cellular models of HD[120-123].

2.4.2. In-vivo models

The in-vivo models for HD are based on a few main approaches. Before the identification of the HTT gene, HD in-vivo modeling mainly relied on chemical injection of neurotoxins to the striatum of rodents and primates. The substrates injected include quinolinic acid, kainic acid, MPTP and 3-NP[124-126]. Studies have shown that by injecting neurotoxins into the striatum, HD pathologic features are evident in the animal models. These include the regional selectivity of neuronal damage with axonal sparing, mitochondrial dysfunction, oxidative damage and caspase activation[125,127-129]. In addition, behavioral impairments are also evident in these chemical models, including impaired locomotor activity and memory performance[130-132]. Although the use of these models does not recapitulate the human mutant Htt induced neuronal damage, they still remain good models to study neuroprotection and neuro-restorative therapies in HD. The next step in HD in-vivo modeling was available after the discovery of the HTT gene in 1996. Since then, a wide variety of HD models that expressed expanded glutamine repeats containing human mutant Htt have been developed. This concept was used in different species such as C.elegans, Drosophila, mice and primates[133-135]. The most commonly

used model is the mouse model, due to its efficiency, economy, handling capability, reproducibility and ease of genetic manipulation. The first transgenic mouse model is the R6/2. It was generated by inserting the exon-1 of human mutant Htt with 144 glutamine repeats under the control of the human Htt promoter[136]. As evident in the cellular model that expresses N-terminal mutant Htt, the R6/2 mice present severe phenotype, with a life span of 13 weeks and severe progressive motor deficits as early as 5-6 weeks. This severe phenotype indicates the acute toxicity of the N-terminal fragment of human mutant Htt[137]. In addition to the clinical manifestations, these mice exhibit similar pathologic features as HD patients, such as Neuroanatomical abnormalities[138], aggregate formation[34], Mithochondrial damage[139], skeletal muscle atrophy[140] and caspase activation[141]. Over the years, other N-terminal human mutant Htt expressing transgenic mice were developed, that reinforced the severity of N-terminal mutant Htt induced neurotoxicity. These include the N171-82Q transgenic HD mice, which express the first 171 N-terminal amino acids of mutant Htt, and the N586-82Q transgenic mice expressing the N-terminal 586 amino acids of human Htt[142,143]. In recent years, the most extensively studied mouse models are the full-length mutant Htt expressing HD mouse models. The two leading models in this aspect are the YAC128 carrying 128 CAG repeats and the BACHD mice carrying 97 CAG/CAA mixed repeats[144,145]. The full-length human mutant is expressed under the human Htt promoter, which enables a relatively reliable study using the human genomic regulatory elements and protein content. BACHD and YAC128 recapitulate behavioral and pathological aspects of HD, which develops gradually over several months. In this study, the BACHD mice were used due to their more robust behavioral phenotype. Therefore, the BACHD mice will be thoroughly presented.

BACHD mice were created on FVB/N background, using bacterial artificial chromosome (BAC)-mediated transgenic approach. A 240 kb RP11-866L6 BAC containing 170 kb human Htt locus with 97 glutamine repeats was used as the transplanted DNA. Several pathological features of HD are recapitulated in the BACHD mice. They exhibit late-onset and relatively selective neuropathology in the cortex and striatum with no change in the cerebellum. In addition neuronal synaptic dysfunction is evident in these mice[146,147]. In terms of aggregation, the BACHD mice revealed that the slowly progressive and selective pathogenic process in HD mouse brains can occur without early and diffuse nuclear accumulation of aggregated mutant Htt. It indicates that a relatively steady-state level of predominantly full-length mutant Htt and a small amount of mutant Htt N-terminal fragments are sufficient to elicit the disease process[145]. BACHD mice exhibit excessive body weight gain. This is not a clinical feature of HD because HD patients often exhibit weight loss after disease onset. However, overexpression of both human mutant and wild-type Htt in the YAC models also result in weight gain as in BACHD mice[148]. Therefore, the weight gain phenotype in these mice is likely attributable to the dose-dependent increase of Htt function. In addition, the body weight changes are considered to be modulated by Full-length Htt levels by influencing Insulin-like growth factor 1 (IGF-1) expression[149]. BACHD mice demonstrate other pathological attributes such as disruption of hypothalamic neurocircuits[150] and dysfunction of the circadian behavior and physiology[151]. Concerning behavioral changes, BACHD mice recapitulate many features of HD, as they address motor, cognitive and neuropsychiatric-like symptoms. The Motor deficit starts at around 9 weeks of age, and is evidenced by subjecting the mice to the Rotarod, rearing and climbing and beam crossing tests[145,152].

Neuropsychiatric-like symptoms include anxiety and depression. Anxiety is demonstrated in the elevated plus maze (EPM) test, open field test (OF), fear conditioning and startle response[153-155]. Depressive-like behavior can be found in the forced swim test (FST) and sucrose preference test (SPT)[156,157]. Lastly, cognitive impairments can be detected in the motor learning task, strategy shifting tasks and object recognition tests[154,155,158]. Taken together the features of BACHD as a mouse model for HD, it can be concluded that they are suitable for use as a model for testing human mutant Htt proteolysis regulation as a potential treatment for HD.

3. Research aim

The primary goal of the research study is to assess the potential of targeting mutant Htt proteolysis by caspase-6 as a therapeutic strategy for HD and to establish the use of substrate-based peptides as a feasible concept for inhibition of caspase-mediated protein cleavage for therapeutic purposes. Specifically, adopting the enzyme inhibition approach, this research aimed to develop a peptide sequence design that would reduce caspase-6 activity thereby providing protection from mutant Htt induced toxicity. To confirm the efficient and safe therapeutic potential of the peptide, the following steps are to be completed, which serves as the minor objectives:

1. Show the ability of the designed peptide to directly inhibit caspase-6 activity.
2. Provide evidence of the specificity, selectivity, and competency of the designed peptide sequence and its influence over Htt proteolysis by caspase-6.
3. Establish the safety properties of the designed peptide.
4. Ascertain in-vitro efficacy of the designed peptide: its ability to penetrate cell membrane, influence the intra-cellular caspase-6 cleavage of mutant Htt and protect cells from mutant Htt toxicity.
5. Ascertain in-vivo efficacy of the designed peptide: its ability to enter the CNS and to improve behavioral outcomes in an in-vivo HD mouse model at both early and late treatment paradigms.
6. Assess the peptide influence on neuropathology that is produced by mutant Htt expression in-vivo.

4. Materials and methods

4.1. Materials

Table 1. List of Peptides

Peptide	Sequence	Manufacturer	Web site
ED11	GRKKRRQRRRPPQSSEIVLDGTDN	China-peptides	www.Chinapeptides.org
TAT-only	GRKKRRQRRRPPQ		
I4A	GRKKRRQRRRPPQSSEAVLDGTDN		
D7A	GRKKRRQRRRPPQSSEIVLAGTDN		
D10A	GRKKRRQRRRPPQSSEIVLDGTAN		
ED11-FITC	GRKKRRQRRRPPQSSEIVLDGTDNK-FITC		
ED11-No TAT-FITC	SSEIVLDGTDNK-FITC		
TAT-FITC	YGRKKRRK-FITC		

Table 2. In-vitro enzymatic reaction experiments materials

Material	Manufacturer	Web-site	Catalog #
Caspase-Glo® 6 assay	Promega	www.worldwide.promega.com	G0971
Complete protease inhibitors	Roche	www.lifescience.roche.com	11836153001
Dimethyl sulfoxide (DMSO)	Sigma-Aldreich	www.sigmaaldrich.com	D5879
Deoxycholic acid (DOC)	Sigma-Aldreich	www.sigmaaldrich.com	D2510
Dithiothreitol (DTT)	Life-technologies	www.lifetechnologies.com	P2325

Ethylenediamine-tetra-acetic acid (EDTA)	Biological Industries	www.bioind.com	03-015-1
Glycerol	Sigma-Aldreich	www.sigmaaldrich.com	G5516
HEPES buffer	Biological Industries	www.bioind.com	03-025-1
NaCl	Sigma-Aldreich	www.sigmaaldrich.com	S7653
Nitro-cellulose membranes 0.45µM	Life-technologies	www.lifetechnologies.com	LC2006
NP-40	Life-technologies	www.lifetechnologies.com	85125
Nupage TRIS acetate SDS-page 3-8%	Life-technologies	www.lifetechnologies.com	WG1603BOX
Phosphate-buffered saline (PBS)	Biological Industries	www.bioind.com	02-020-1A
Pierce BCA Protein Assay Kit	Life-technologies	www.lifetechnologies.com	23225
PVDF membranes 0.45µm	Life-technologies	www.lifetechnologies.com	88518
Recombinant human caspase-1	Enzo life-science	www.enzolifesciences.com	BML-SE168-5000
Recombinant human caspase-2	Enzo life-science	www.enzolifesciences.com	BML-SE175-5000
Recombinant human caspase-3	Enzo life-science	www.enzolifesciences.com	BML-SE169-5000
Recombinant human caspase-4	Enzo life-science	www.enzolifesciences.com	BML-SE176-5000
Recombinant human caspase-5	Enzo life-science	www.enzolifesciences.com	BML-SE171-5000
Recombinant human caspase-6	Enzo life-science	www.enzolifesciences.com	BML-SE170-5000
Recombinant human caspase-7	Enzo life-science	www.enzolifesciences.com	BML-SE177-5000
Recombinant human	Enzo life-science	www.enzolifesciences.com	BML-SE172-

caspase-8			5000
Recombinant human caspase-9	Enzo life-science	www.enzolifesciences.com	BML-SE173-5000
Recombinant human caspase-10	Enzo life-science	www.enzolifesciences.com	BML-SE174-5000
Saline	Teva	www.tevagenerics.com	AWB1324
Sodium fluoride (NaF)	Sigma-Aldreich	www.sigmaaldrich.com	S7920
Water, Cell culture grade	Biological Industries	www.bioind.com	03-055-1A
zVAD-FMK	Enzo life-science	www.enzolifesciences.com	ALX-260-020-M005
Z-VEID aminoluciferin	Promega	www.worldwide.promega.com	G0971

Table 3. Cellular in-vitro experiments materials

Material	**Manufacturer**	**Web-site**	**Catalog #**
5-Bromo-2′-deoxyuridine (BrdU)	Sigma-Aldreich	www.sigmaaldrich.com	B5002
Alamar-blue dye	AbD serotec	www.abdserotec.com	BUF012A
Cell culture flasks	Corning	www.corning.com	3290
Cell culture plates	Greiner	www.gbo.com	657185
CHAPS hydrate	Sigma-Aldreich	www.sigmaaldrich.com	C9426
Dulbecco's Modified Eagle's Medium (DMEM)	Biological Industries	www.bioind.com	01-050-1
Fetal calf serum (FCS)	Biological Industries	www.bioind.com	04-121-1
FLAG-tagged human caspase-6 plasmid	Prof. Michael Hayden laboratory	Prof. Michael Hayden laboratory	In house

FLICA caspase-6 activity assay	ICT	www.immunochemistry.com	95
G418 antibiotic	Life-technologies	www.lifetechnologies.com	11811-031
Hoechst stain	ICT	www.immunochemistry.com	639
Horse serum	Biological Industries	www.bioind.com	04-124-1A
Htt 15Q 1-586 plasmid	Prof. Michael Hayden laboratory	Prof. Michael Hayden laboratory	In house
LDH Cytotoxicity Detection Kit	Clontech	www.clontech.com	MK401
L-glutamine	Biological Industries	www.bioind.com	41-218-25
Paraformaldehyde	Sigma-Aldreich	www.sigmaaldrich.com	P6148
Penicillin-Streptomycin-Nystatin (PSN) antibiotics	Biological Industries	www.bioind.com	03-032-1
Plasmid 3949-15Q-HTT	Prof. Michael Hayden laboratory	Prof. Michael Hayden laboratory	In house
Ponasterone a	Life-technologies	www.lifetechnologies.com	H101-01
Propidium iodide (PI)	Sigma-Aldreich	www.sigmaaldrich.com	P4864
Tris buffer pH8	Sigma-Aldreich	www.sigmaaldrich.com	03268-100ML-F
Xtreme gene 9 transfection reagent	Roche	www.lifescience.roche.com	06365787001
Zeocin	Life-technologies	www.lifetechnologies.com	R25005

Table 4. In-vivo experiments materials

Material	**Manufacturer**	**Web-site**	**Catalog #**
2-methly-butylene	Sigma-Aldreich	www.sigmaaldrich.com	86262
70% ethanol	Gadot	www.gadot.com	830107411
Agarose gel	Lonza	www.lonza.com/	50002

Albumin- FITC conjugated	Sigma-Aldreich	www.sigmaaldrich.com	A9771
Alzet mini-pump model 1004	Alzet osmotic pumps	www.alzet.com	1004
DAPI	Sigma-Aldreich	www.sigmaaldrich.com	D9542
Di-amino-benzidine (DAB)	Life-technologies	www.lifetechnologies.com	34002
Gel-red nucleic stain	Biotium	www.biotium.com	41003
Gotaq green PCR mix	Promega	www.worldwide.promega.com	M7122
Ketamine	Kepro	www.kepro.nl	46
Proteinase K	Roche	www.lifescience.roche.com	03115879001
Sodium Azide	Sigma-Aldreich	www.sigmaaldrich.com	S2002
Sucrose	Bio-lab	www.biolab-chemicals.com	192205
Tissue-TEK O.C.T	Sakura	www.sakura.eu	4583
Xylazine	Dechra veterinary	www.dechra-export.com	Xylaz

Table 5. Antibodies

Antibody	**Dilution**	**Manufacturer**	**Web-site**	**Catalog #**
BKP1	1/1000	Prof. Michael Hayden laboratory	Prof. Michael Hayden laboratory	In house
D2-labeled NeoHtt586	360 ng/ml	Prof. Michael Hayden laboratory	Prof. Michael Hayden laboratory	In house
IRDye 680RD Goat anti-Mouse	1/15000	Licor	www.licor.com	925-68070
IRDye 800CW Goat anti-rabbit	1/15000	Licor	www.licor.com	925-32211
Mouse anti 2166	1/2000	Millipore	www.merckmillipore.com	MAB2166

Mouse anti Spectrin	1/1000	Enzo life-sciences	www.enzolifesciences.com/	BML-FG6090-0100
Mouse anti TAT (47-58)	1/250	Abcam	www.abcam .com	ab63957
Mouse anti β-Actin	1/10000	Sigma	www.sigmaaldrich.com	A5441
Mouse anti-DARPP32	1/1000	Millipore	www.merckmillipore.com	AB1656
Rabbit anti Calnexin	1/250	Abcam	www.abcam .com	ab22595
Rabbit anti Htt 4-19	1/1000	CHDI	www.catalog.coriell.org	CH00146
Rabbit anti PARP	1/1000	Cell signaling technology	www.cellsignal.com/	9542
Tb-labelled BKP1 antibody	36 ng/ml	Prof. Michael Hayden laboratory	Prof. Michael Hayden laboratory	In house

Table 6. Cells

Cell type	**Manufacturer**	**Web-site**	**Catalog #**
145Q-MHtt expressing PC12 cells	CHDI	www.catalog.coriell.org	CH00288
COS-7	ATCC	www.atcc.org	CRL-1651
HEK cells	Life-technologies	www.lifetechnologies.com	K1538
Mouse embryonic fibroblasts (MEF)	Prof. Michael Hayden laboratory	Prof. Michael Hayden laboratory	In house
SH-SY5Y	ATCC	www.atcc.org	CRL-2266

Table 7. Primers

Primer	Sequence	Manufacturer	Web-site
BACHD forward	5’ GAG CCA TGA TTG TGC TAT CG 3’	Hy-labs	www.hylabs.co.il
BACHD reverse	5’ CAC GGT CTT TCT TGG TAG CTG 3’		
IL2 forward	5’ CTA GGC CAC AGA ATT GAA AGA TCT 3’		
IL2 reverse	5’ GTA GGT GGA AAT TCT AGC ATC ATC C 3’		

Table 8. Equipment and software

Instrumentation/ Software	Manufacturer	Web-site
-80oC RevcoFreezer	Thermo Fisher Scientific	www.thermofisher.com
BX52TF normal & fluorescent light source microscope	Olympus	www.olympusmicro.com
Cellvizio	Mauna Kea Technologies	www.maunakeatech.com
Centrifuge 5403 or 5417C or 5810R	Ohermle Z 360 K	www.hermle-labortechnik.de
Centrifuge RC5C plus	Ohermle Z 360 K	www.hermle-labortechnik.de
DP50-CU microscope digital camera	Olympus	www.olympusmicro.com
Electrophoresis power supply model 3000Xi	BioRad	www.bio-rad.com
Elevated plus maze test apparatus	Polycryl	www.polycryl.co.il
FACS-Caliber flow cytometer	BD biosciences	www.bdbiosciences.com
Forced swim test	Polycryl	www.polycryl.co.il

apparatus		
Gel box for Electrophoresis	BioRad	www.bio-rad.com
GraphPad prism version 6.0	Graphpad	www.graphpad.com
Ice machine	Scotsman AF-10	www.scotsman-ice.com
Imaris X64 7.3.0 software	Bitplane	www.bitplane.com
Incubator	Tuttnauer	www.tuttnauer.com
Laminar hood – Class II	Tuttnauer	www.tuttnauer.com
Light dark choice test apparatus	Polycryl	www.polycryl.co.il
Light-microscope BH-2	Olympus	www.olympusmicro.com
MetaMorph software version 6.3	Molecular devices	www.moleculardevices.com
Odyssey	LI-COR	www.licor.com
Odyssey 2.1 software	LI-COR	www.licor.com
Odyssey Infrared Imager , 9120	LI-COR	www.licor.com
Open field test apparatus	Polycryl	www.polycryl.co.il
PCR device	Applied biosystems	www.lifetechnologies.com
pH Meter MP220	BIO-TEK instruments	www.biotek.com
Rotarod	San Diego instruments	www.sandiegoinstruments.com
Stereotaxic device	N.B.T.	www.nbtltd.com
Surgical Staple System	Fine science tools (FST)	www.finescience.com
Swimming T-maze apparatus	Polycryl	www.polycryl.co.il
Synergy HT micro-plate reader	BIO-TEK instruments	www.biotek.com
xenon lamp Victor Plate Reader	Perkin Elmer	www.perkinelmer.com

4.2. Methods

4.2.1. Peptide synthesis and dissolution

ED11 (GRKKRRQRRRPPQSSEIVLDGTDN), TAT-only (GRKKRRQRRRPPQ), ED11-FITC (GRKKRRQRRRPPQSSEIVLDGTDNK-FITC), ED11-No TAT-FITC (SSEIVLDGTDNK-FITC), TAT-FITC (YGRKKRRK-FITC), I4A (GRKKRRQRRRPPQSSEAVLDGTDN), D7A (GRKKRRQRRRPPQSSEIVLAGTDN) and D10A (GRKKRRQRRRPPQSSEIVLDGTAN) were synthesized by China-Peptides Ltd. (Shanghai, China) with a purification level at over 95%. For the purified caspase activity assays, peptides were dissolved in DMSO (Sigma, USA). For the cell culture involved experiments, peptides were initially dissolved in cell-culture grade H_2O (Biological industries, Israel, 20% of total solution), and further diluted with phosphate-buffered saline (PBS, Biological industries, Israel, 80% of total solution) to the desired concentrations. For in-vivo studies, peptides were initially dissolved in cell-culture grade H_2O (20% of total solution) and further diluted by 0.9% saline (Teva, Israel, 80% of total solution).

4.2.2. In-vitro enzymatic reaction experiments

4.2.2.1. In-vitro direct caspase-6 inhibition

To determine caspase inhibition by ED11, the Caspase-Glo® 6 assay (Promega, USA) was carried out according to the manufacturer's instructions. 0.1U/ml Purified caspase-6 (Enzo Life Sciences, USA) or caspase-3 (Abcam, UK) was incubated with 5µM Z-VEID-aminoluciferin with the tested compounds. A control sample containing the Z-VEID-

aminoluciferin substrate without caspase-6 was used as background and subtracted from the tested samples readings. The luminescent signal of released aminoluciferin was detected using a Synergy HT multi-mode micro-plate reader (Bio-Tek, USA).

4.2.2.2. PARP and Spectrin cleavage by caspase-3

HEK cells were lysed in MCB buffer (50 mM HEPES pH 7.4, 100 mM NaCl, 1% Igepal, 1 mM EDTA, 10% Glycerol, Roche complete protease inhibitors), and DTT was added to 10 mM after the protein concentration was measured in cleared lysates. 50 U Caspase-3 enzyme was mixed with ED11 or zVAD-FMK in MCB buffer supplemented with 10 mM DTT in a total volume of 5 ul and incubated at room temperature for 1h. Then, 40 ug of HEK lysate (adjusted to 2 ug/ul) were added and the samples were incubated at 37°C for 1h. SDS-PAGE loading dye was added, samples were denatured and run on a 3-8% Tris-Acetate SDS-PAGE gel (Life technologies). After transfer to PVDF membranes, the blots were probed with spectrin (1/1000, Enzo life-science, USA), PARP (1/1000, Cell signaling Technology) and Actin (1/10000, Millipore) antibodies in the Li-cor system.

4.2.2.3. FRET assay for caspase-6 activity

The N-terminal 1212 amino acids of Htt with 15Q and the 4c mutations (D513A, D552A, D530A, D589A)[56] were transiently transfected and overexpressed in COS-7 cells. Cells were lysed in SDP buffer (50 mM Tris pH8, 150 mM NaCl, 1% Igepal, 1x Roche complete protease inhibitor) and cleared lysates were used as a substrate for the activity assay. Caspase-6 enzyme (Enzo life-science) was diluted to 0.125 U/ul in FRET buffer (10 mM HEPES pH7.4, 100 mM NaCl, 0.05% gelatin, 0.1% CHAPS, 2 mM DTT) and mixed with different concentrations of ED11 in a final volume of 22 ul in a white

384well plate. Samples were incubated for 1h at room temperature, then 28 ul of a mix of COS-7 lysate containing Htt protein (90 ng/ul), Tb-labelled BKP1 antibody (36 ng/ml) and D2-labeled monoclonal 586 neo-epitope antibody (360 ng/ml)[56] in FRET buffer were added. The plate was incubated at 37°C for 6h, and then stored for an additional 18h at 4°C. Plates were measured with a xenon lamp Victor Plate Reader (Perkin Elmer) after excitation at 340 nm (time delay 50 us, window 200 ms). The signal measured at 615 nm resulted from the emission of the terbium-labeled antibody and was used for normalization of potential signal artifacts. The cleaved htt-specific signal at 665 nm resulted from emission of the D2-labeled neo-epitope antibody antibody after time-delayed excitation by the terbium. Caspase-6 activity was measured by the amount of cleaved Htt generated and represented by the 665/615-nm ratio.

4.2.2.4. Cleavage of Huntingtin by caspases 1-10

COS7 cells were transiently transfected with the 3949-15Q-HTT construct[56] using the Xtreme gene 9 transfection reagent (Roche Applied Science, Canada), according to the manufacturer's protocol. Twenty-four hours post-transfection, cells were harvested and lysed. Fifty units of purified active human caspase-1 through 10 each (Enzo Life Sciences) were mixed with 10 μM ED11 in caspase buffer (100 mM HEPES pH 7.4, 200 mM NaCl, 0.2% CHAPS, 2mM EDTA, 20% glycerol and 10 mM DTT) and incubated for 30min at room temperature. About 40 μg of total protein from cell lysates were added, and the reaction was incubated for 1 h at 37°C. A human Htt 15Q fragment truncated at amino acid 586 was overexpressed in COS7 cells and used as a size control on the western blot. SDS–PAGE loading dye was added, and samples were denatured and run on a 10% Tris-Glycine SDS–PAGE gel. After transfer to PVDF membranes, the blots

were probed with the polyclonal antibody BKP1[159] directed against amino acids 1-17 of Htt. Membranes were scanned and quantified using the Li-Cor system.

4.2.2.5. Caspase-6 cleavage of human mutant huntingtin in striatal lysates

For brain lysate preparation, FVB/N BACHD mice and their wild-type littermates were euthanized by de-capitation. Striata were dissected and placed in lysis buffer (200mM HEPES, 150mM NaCl, 1mM Na3Vo4, 5mM EDTA, 1% NP-40, 0.5% DOC, 50mM NaF) with protease inhibitors (Roche) for 1 hour on ice. Tissue debris was removed by centrifugation at 20,000 × g for 15 min at 4°C. Protein concentration was determined by the BCA method (Pierce). 50µg of lysate proteins were exposed to 100U/ml recombinant active human caspase-6 for 45 minutes at 37°C in the present of 10µM ED11 or DMSO as vehicle control. Lysates were subsequently loaded on 7.5% SDS-PAGE gels and transferred to 0.45µM nitro-cellulose membranes. The membranes were probed with rabbit anti-Htt 4-19 (1:1000, CHDI, USA), and mouse anti β-actin (1:10000, Sigma, USA). Secondary antibodies used were IRDye 800CW Goat anti-rabbit IgG and IRDye 680RD Goat anti-Mouse IgG (Licor, USA), respectively. Fluorescent signal was read using the Li-cor Odyssey imaging system.

4.2.3. In vitro cell based experiments

4.2.3.1. Cell culture

Human neuroblastoma cells SH-SY5Y cells (ATCC), COS cells and MEF cells were grown on tissue culture plates (Greiner, Germany) in Dulbecco's Modified Eagle's

Medium (DMEM, Biological Industries, Israel), supplemented with 10% fetal calf serum (FCS, Biological Industries, Israel), 1% L-glutamine and 1% PSN antibiotics (Biological Industries, Israel). Inducible 145Q-MHtt expressing PC12 cells were obtained from CHDI (by Coriell institute, USA). Cells were grown in suspension in 75cm^3 culture flasks (Corning, USA) DMEM, supplemented with 15% Horse-serum (Biological industries, Israel), 2.5% FCS, 0.1mg/ml G418 (Life-technologies, USA), 0.1mg/ml Zeocin (Life-technologies, USA), 1% L-glutamine and 1% SPN antibiotics (Biological Industries Israel). all cell types were incubated at 37ºC in a humidified atmosphere with 5% CO2, and passaged twice a week.

4.2.3.2. Intra-cellular anti-TAT staining for ED11 detection

Mouse embryonic fibroblasts (MEFs) derived from FVB/N wt mice[160] were treated with different amounts of ED11 in the media for 16 hours. Cells were washed with PBS, fixed with 4% paraformaldehyde in PBS for 30min at room temperature and processed for immunofluorescence with an anti-TAT antibody (1/250, Abcam, USA), Alexa-488 labeled secondary antibody (Life-technologies, USA) and Hoechst nuclear counterstaining (Sigma, USA)

4.2.3.3. Cell proliferation and cell cycle analysis

For cell proliferation and cell cycle analysis, SH-SY5Y cells were pre-incubated with 25µM ED11 for one hour. Then, 10µM 5-bromo-2-deoxyuridine (BrdU, Sigma, USA) was added for 2 hours. Medium was discarded and cells were fixed with 70% ethanol. DNA denaturation was conducted with 1.5M HCl exposure for 30 min. FITC conjugated anti-BrdU antibody was used to mark incorporated BrdU, and DNA Staining was done by

propidium iodide (PI, Sigma, USA). 15,000 cells per sample were read using FACS-Calibur flow cytometer, and cell-cycle analysis was conducted after doublet discrimination.

4.2.3.4. Huntingtin caspase-6 co-transfection

COS-7 cells were transiently co-transfected with equal amounts of FLAG-tagged human caspase-6 and the N-terminal 1212 amino acids of human Htt with 15Q[56] using the X-treme Gene reagent (Roche) according to manufacturer's instructions. 1 hour after transfection, ED11 peptide was added to the growth medium. Cells were harvested by scraping in the medium 24 hours after transfection and the presence of cleaved Htt was assessed by Western blotting using the mouse anti-Htt antibody 2166 (Millipore, USA) or the neo-epitope antibody against Htt cleaved at Asp586[56]. Signals were normalized to calnexin as a loading control.

4.2.3.5. Mutant Huntingtin induced toxicity

To induce mHtt expression, Inducible human 145Q-mHtt expressing PC12 cells were incubated with 25µM ponasterone a (PA, Life-technologies) for the indicated time periods, in the presence of 25µM ED11 or vehicle as control. For viability assessment, the medium was depleted and washed twice with PBS, and Alamar-blue dye (1/10 in the culture medium, AbD serotec, UK) was added to the cells, as instructed by the manufacturer. Fluorescence was monitored at 530-560nm excitation wavelength and 590nm emission wavelength, and viability was calculated as the percentage of untreated control. LDH release was measured by the LDH Cytotoxicity Detection Kit (Clonetech), following manufacturer's instructions. Briefly, PC12 cells were grown on a 6-well plate

at a density of 7×10^5 cells/ml, and samples were taken at the indicated time points. Subsequently, samples were centrifuged, transferred to a 96 well plate and were incubated with the reaction mixture for 30 min in the dark. The plate was read at 492 nm and 690 nm as reference in Synergy HT multi-mode micro-plate reader, and calculations were done in reference to a none-induced control.

4.2.3.6. Intra-cellular caspase activity assay

For FLICA caspase-6 assay, cells were adjusted to 1.5×10^6 cells/ml and were incubated with FAM-VEID-FMK for 1 hour at 37°C as described. Hoechst stain (ICT, USA) was used as nucleus counterstaining. The images were recorded with a fluorescence microscope (OLYMPUS, USA) at 40X magnification and image analysis was made by the Image-J software.

4.2.4. In-vivo efficacy studies

4.2.4.1. Animal care

All animal-related procedures were approved by Tel-Aviv University Committee of Animal Use for Research and Education, under protocols M-13-024, M-13-061 and M-13-110. BACHD mice were obtained from Jackson laboratory. The mice were placed under 12 hour light/dark conditions and housed in individually ventilated cages with ad libitum access to food and water.

4.2.4.2. BACHD mice genotyping

BACHD mice are heterozygous for transgenic human mutant Htt gene with 97 glutamine repeats. For identification of the transgenic mice from each litter, the PCR reaction was

carried out. DNA was extracted by tail clipping and placing the tail in tail lysis buffer (Viagen, Israel) and proteinase K (Roche-diagnostics). The primers used for PCR reaction were 5' GAG CCA TGA TTG TGC TAT CG 3' as a forward primer and 5' CAC GGT CTT TCT TGG TAG CTG 3'. IL2 primers 5' CTA GGC CAC AGA ATT GAA AGA TCT 3' (Forward) and 5' GTA GGT GGA AAT TCT AGC ATC ATC C 3' (Reverse) were used as positive control. PCR reaction mix included ddH2O, Primers (Hylabs, Israel), Gotaq green PCR mix (Taq DNA polymerase, dNTPs, MgCl2 and reaction buffers, Promega, USA) and DMSO (Sigma-Aldrich, USA). After PCR reaction finished, the reaction products were placed into electrophoresis 2% agarose gel (Lonza, USA) with Gelred nucleic acid stain (Biotium). The gels were then subjected to an electric field of 120 Waltz. Using Ultraviolet reading method, positive DNA band for BACHD detection was found at 359bp and for IL2 control at 324bp.

4.2.4.3. Assessment of blood-brain barrier penetration in-vivo

To assess ED11's ability to penetrate the BBB and enter the brain parenchyma, a modified in vivo brain delivery detection method was used. A previously reported two photon-based brain delivery detection method[161] was adjusted to an endoscopic microscopy probe-based method[162] to enable deep brain detection. FVB/N mice (n = 2) were injected IV with one of the following compounds: FITC-conjugated albumin, a marker of intact blood vessels (10 mg in 200 µl of saline), FITC-conjugated TAT, as a positive control for extravasation from the blood vessels, FITC-conjugated ED11 lacking the TAT cell-penetrating sequence (50 mg/kg) and FITC-conjugated ED11 (50 mg/kg). Twenty minutes after compound injection, the mice were anesthetized with a mixture of ketamine (100 mg/kg) and xylazine (8 mg/kg). The mice were then placed in a

stereotaxic device, and a 0.3 mm fluorescence detection probe was inserted into the central caudate–putamen. Coordinates with respect to the bregma used were: anterior-posterior +0.5, medial-lateral +2, dorsal-ventral −2.7. 40 minutes after compound injection, fluorescence was monitored using a 488 nm excitation laser.

4.2.4.4. ED11 in-vivo efficacy trials

To evaluate ED11 ability to provide protection from mutant Htt toxicity in-vivo, the HD mouse model BACHD[145] and their FVB/N wild-type littermates were used. Mice were assigned to the different groups according to littermates in order to minimize inherent variability. Mice were housed in mixed genotype and treatment cages, and researcher was blinded as regards to mouse genotype and treatment throughout all of the behavioral tests. Delivery of the tested compound was done by a subcutaneously implanted mini-pump alzet model 1004 (DURECT) according to the manufacturer's instructions. The pumps infuse continuously for 28 days, at a dose of 4mg/kg/day. Replacement with freshly prepared pumps was conducted every 28 days until experiment completion. The behavioral tests were separated by a minimum of one week between each trial and at least a week after implantations to allow mice recovery. For the evaluation of ED11 effect in an early disease state, BACHD mice were treated with ED11 starting at the age of 5 weeks. Three treatment groups were tested –Wild-type mice treated with vehicle (20% ddH20, 80% saline), BACHD mice treated with vehicle, and BACHD mice treated with ED11. n=10-12 males and n=10-12 females per group. In order to evaluate the ED11 effect on mutant Htt toxicity in an advanced disease state, BACHD mice were treated with ED11 starting at the age of 36 weeks. Three treatment groups were tested – Wild

type mice treated with vehicle (20% ddH20, 80% saline), BACHD mice treated with vehicle, and BACHD mice treated with ED11. n=10-12 males per group.

4.2.4.4.1. Rotarod test

Motor coordination and strength were assessed using the accelerating Rotarod according to an adapted previously reported protocol[145]. During the training period, mice were placed on an accelerating rod (0-21 RPM in 4 min), and latency to fall from the rod was recorded. The mice were tested three times per day with a two hours inter-trial rest for three consecutive days. For the Rotarod test, Mice were placed on the accelerating rod (0 to 21 RPM in 4 minutes) for 3 consecutive trials with a 5 minutes inter-trial rest, and the average score was taken for analysis .

4.2.4.4.2. Forced swim test

The forced swim test was conducted as previously described[163] with minor modifications. The mice were placed in a 15cm diameter 40cm height cylinder, filled with water (23-25 °C) to a depth of 20cm. Animals behavior was recorded by a side camera for 6 minutes. For mobility analysis, the animal mobility state in the last 4 minutes was evaluated using the Noldus ethovision video tracking software.

4.2.4.4.3. Climbing test

Climbing behavior is used to assess motor movement and coordination. A Mouse was placed on a flat surface and a closed-top wire mesh cylinder 15 cm x 20 cm tall was placed over the mouse. The animal's behavior was videotaped and measured over a 5

minute period. The time from when a mouse's fourth foot left the tabletop to the time when the first foot was replaced on the tabletop was scored as time spent climbing.

4.2.4.4.4. Elevated plus maze test

The elevated plus maze is generally used for the assessment of anxiety-related behavior. A plus-shaped maze containing two dark and enclosed arms and two open and lit arms, elevated 100 cm above ground, was used. The arms were 30 × 5 cm with a 5 × 5 cm center area, and the walls of the closed arms were 40 cm high. Mice were placed in the center of the maze, tracked for 5 min with a video camera, and then returned to their home cage. Time spent in the open arms, the numbers of entries to the open arms, and latency to enter the open arms were scored using Ethovision video tracking system.

4.2.4.4.5. Open field test

For the open field test, an unfamiliar open field (50 × 50 cm) was used. Mice were placed in one corner of the arena and their behavior was recorded for 20 min and scored with the Ethovision video tracking system. Total distance traveled, total time spent in the center and the number of entries to the center were measured.

4.2.4.4.6. Light dark choice test

The light dark choice test was conducted as previously described[164]. The arena consisted of two compartments, a dark compartment (14 × 27 × 26 cm) and a compartment illuminated by 1050 lux (30 × 27 × 26 cm), connected by a small passage. Mice were placed in the light compartment to initiate a 5-min test session. The time spent in the dark compartment, the number of entries to the dark compartment and the latency of entering

the dark zone were measured. The indices collected in these tests were quantified using Ethovision video tracking system.

4.2.4.4.7. Swimming T-maze strategy shifting test

The swimming T-maze strategy shifting test was conducted as previously described[165]. The apparatus consisted of 3 arms (9 × 50cm each) filled with water to a depth of 15cm. On the first three days, the mice were subjected to a learning period. In the learning period, a transparent platform is hidden at the end of the right arm. The mouse is placed at the stern of the T-maze 4 times a day with a 45 minutes interval between trials. On the fourth day, the strategy shift paradigm was initiated, as the platform was relocated to the left arm, and the mice were placed at the stern 4 times with a 45 minutes interval between trials. Time to reach hidden platform was recorded and analyzed using Ethovision video tracking system.

4.2.5. Neuropathology studies

4.2.5.1. Brain preparation for neuropathology studies

Mice were injected with a mixture of Ketamine (85mg/kg) and xylazine (8mg/kg) IP. Then, using an electric pump through a syringe, they were intracardially perfused with PBS followed by ice-cold 4% paraformaldehyde (PFA) in PBS. The brains were removed and post-fixed in 4% PFA at 4°C for 24 hours, and then cryopreserved in 30% sucrose. Subsequently, brains were quickly frozen by -80°C cold 2-methly-butylene (Sigma, USA), mounted with Tissue-TEK O.C.T. and sectioned by a cryostat (Leica

CM1850, Germany) into 10µm coronal sections. Sections were then stored in PBS with 0.08% sodium azide (Sigma,USA) at 4°C until immunohistochemical processing.

4.2.5.2. MRI protocol and analysis

MRI scanning and analysis were performed by BioImage (Haifa, Israel). MRI was performed with a 7 T MRI scanner (Bruker, Billerica, MA, USA) with a 30 cm bore and a gradient strength of up to 400mT/m, using a quadrature head coil. The mice were anesthetized with 1–2% isoflurane and oxygen, and were maintained at 37°C. Animal breathing was monitored with a breathing sensor. T2-weighted imaging was performed with the following parameters: multi-slice multi-echo sequence, repetition time 2000ms, 10 different echo times (ms):10, 20, 30, 40, 50, 60, 70, 80, 90, 100and spatial resolution: 0.07 × 0.07 × 0.8mm3. For image analysis, T2-relaxation maps were calculated using BioImage software was written in Matlab (Mathworks©), using least-squares algorithm.For volumetric analysis, the images were rotated and cropped, and the regions of interest were outlined manually. A trained operator manually segmented the caudate–putamen, cortex, frontal cortex, motor cortex and hippocampus to evaluate volume changes.

4.2.5.3. Medium sized spiny neurons immunostaining

Free-floating sections were incubated in primary mouse anti-DARPP32 (1/1000, Millipore, USA) overnight at room temperature. Sections incubated without primary antibody served as controls. Sections were washed and incubated with horseradish peroxidase-conjugated secondary antibody (1:500, Jackson ImmunoResearch Laboratories) for 2 hours at room temperature. Staining was visualized using DAB (3-3’

diaminobenzidine). Sections were photo-graphed using a Zeiss Axioplan 2 microscope and Coolsnap HQ Digital CCD camera (Photometrics). The amount of DARPP32 was determined using MetaMorph software version 6.3 (Universal Imaging Corporation). Labeling was identified using constant threshold levels for all images and analyzed using integrated morphometry. Relative levels of staining were calculated as the sum of the integrated optical density of each image divided by the area of the region selected then multiplied by the sampling interval and section thickness (25mm). No staining was observed in a negative control without primary antibody

4.2.5.4. Brain aggregates detection

For polyclonal aggregate antibody S830 single labeling (1/750, an in-house antibody in Prof. Michael's Hayden laboratory, Canada) was used. Antigen retrieval was performed by microwaving four times for 5 min each time at 40% power in 10 mM citrate buffer and then treating with 20μg/ml Proteinase K (Eastman Kodak Scientific, USA) for 10 min at 37°C. Duplicate photos were taken from the same area of cortex and striatum at identical magnification and exposure settings. Aggregates and DAPI-stained nuclei were quantified using Imaris X64 7.3.0 software. The Aggregate number was normalized to the number of DAPI-stained nuclei in the field.

4.2.5.5. In-vivo mutant Huntingtin fragmentation

For brain lysate preparation, FVB/N BACHD mice and their wild-type littermates were euthanized by de-capitation. Striata were dissected and placed in lysis buffer (200mM HEPES, 150mM NaCl, 1mM Na3Vo4, 5mM EDTA, 1% NP-40, 0.5% DOC, 50mM NaF) with protease inhibitors (Roche, USA) for 1 hour on ice. Tissue debris was

removed by centrifugation at 20,000 × g for 15 min at 4°C. Protein concentration was determined by the BCA method (Pierce). 50µg of lysate proteins were subsequently loaded on 7.5% SDS-PAGE gels and transferred to 0.45µM nitro-cellulose membranes. The membranes were probed with 1C2 antibody (1/1000, Millipore, USA) and mouse anti β-actin (1:10000, Sigma, USA) as a loading control. Secondary antibodies used were IRDye 800CW Goat anti-rabbit IgG and IRDye 680RD Goat anti-Mouse IgG (1/15000, Licor Ltd.), respectively. The fluorescent signal was read using the Odyssey imaging system.

4.2.6. Statistical analysis

Statistical analysis was performed using GraphPad prism version 6.0. Statistical significance of differences between two groups was evaluated by Student's unpaired t-test. When three groups were addressed, statistical evaluation was made by one-way ANOVA followed by Tukey's multiple comparison post hoc test. When addressing time point-dependent alterations, area under the curve (AUC) was calculated and comparison between treatments was done using one-way ANOVA followed by Tukey's multiple comparison post hoc test. Data is presented as mean ± SEM, and the level of $P < 0.05$ was accepted as statistically significant.

5. Results

5.1. Peptide-based caspase-6 inhibitor concept and design

For investigating the feasibility of capase-6 inhibition as a potential treatment for HD, the native Htt caspase-6 cleavage site sequence was selected to act as a modulator of caspase-6 activity. In human Htt, the cleavage occurs between amino acids Asp586 and Gly587 (**Fig. 2**). Due to the understanding that amino acids surrounding the cleavage site have a role in determining the affinity and specificity of caspase cleavage in this site[166], 11 amino acids from Ser580 to Asn590 were selected as the proposed inhibitor caspase-6 recognition site. The complexity of cell and blood-barrier penetration was addressed by utilized a cell penetrating peptide sequence. Among the recognizable cell penetrating peptides sequences, the HIV-TAT (amino acids Gly48-Gln60) was selected. This HIV-TAT sequence has been proven in the past to facilitate efficient cellular and nuclear penetration, and transportation through the Blood-brain barrier, without causing apparent toxic effects[167-169]. These considerations led to the peptide sequence GRKKRRQRRRPPQSSEIVLDGTDN (**Fig. 2**), designated as ED11. The hypothesis presented is that by administrating ED11 in-vitro and in-vivo, caspase-6 activity will be reduced, and protection from mutant Htt induced toxicity will be provided.

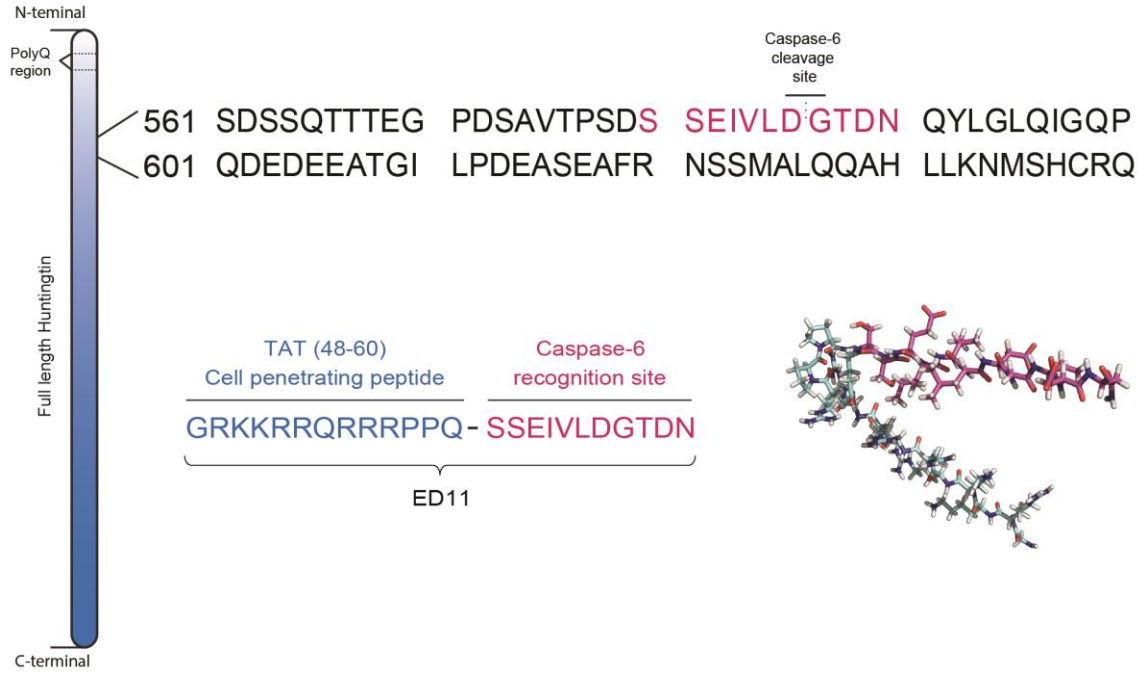

Figure 2: Structural representation of the concept and design of ED11.

The native Htt caspase-6 cleavage site sequence (aa 580-590, marked in pink) is presented. ED11 caspase-6 recognition site correlates to Htt caspase-6 cleavage site. In the N-terminal, ED11 contains a TAT (48-60) cell penetrating peptide sequence, which enables it to penetrate the cellular membrane and the blood-brain barrier (marked in blue). The structural figure was created using PyMol software (http://www.pymol.org/).

5.2. In-vitro evaluation of caspase-6 inhibition by ED11

After designing ED11 peptide sequence, it was essential to elucidate whether it can directly impact caspase-6 activity. In order to determine the potency and specificity of caspase-6 inhibition by ED11, a series of in-vitro enzymatic reaction experiments have been conducted and are presented in the following sections.

5.2.1. Direct inhibition of caspase-6 activity by ED11

For detecting direct interference with caspase-6 activity, a luminescence-based probe was used. The probe is composed of the tetra-peptide VEID conjugated to aminoluciferin (Z-VEID-aminoluciferin). Upon cleavage by caspase-6, the molecule emits light which is quantified by photometer as Relative Light Units (RLU) (**Fig. 3A**). Purified active caspase-6 was incubated with Z-VEID-aminoluciferin in the presence of ED11 or the isolated TAT peptide as a negative control. It was found that while Z-VEID-aminoluciferin cleavage was significantly inhibited by 10µM ED11 (AUC 66494± 193.5 vs. 103456±2035, $P<0.001$) the control peptide containing 10µM TAT (48-60) sequence alone did not influence the reaction (103130±450) (**Fig. 3B**). Furthermore, the effect of ED11 was found to be dose-dependent ($P<0.05$) (**Fig. 3C**). Taken together, these findings provide the substantial proof that ED11 directly inhibit caspase-6 activity.

5.2.2. ED11 sequence specificity

In the aim of further elucidating the specificity of the ED11 amino acid sequence to inhibit caspase-6, an alanine substitution of different amino acids of ED11 was conducted as illustrated in **fig. 4A**. The effect of this modification on caspase-6 activity was determined by measuring RLU after incubation of caspase-6, Z-VEID-aminoluciferin and 10µM from each peptide (**Fig. 4B**). As was observed, the replacement of amino acid Isoleucine at position 4 or Aspartic acid at position 7 of ED11 has resulted in the elimination of ED11 ability to inhibit caspase-6 (as % of control: I4A 103.8±2.086, D7A 100.8±4.066, ED11 66.6±5.230, $P<0.01$). This observation was not found when replacement of the Aspartic acid at position 10 was made (D10A 77.62±3.038). These

results indicate that ED11 caspase-6 inhibition is mediated by specific amino acids, which supports the hypothesis that a natural substrate based peptide can effectively compete on caspase-6 active site.

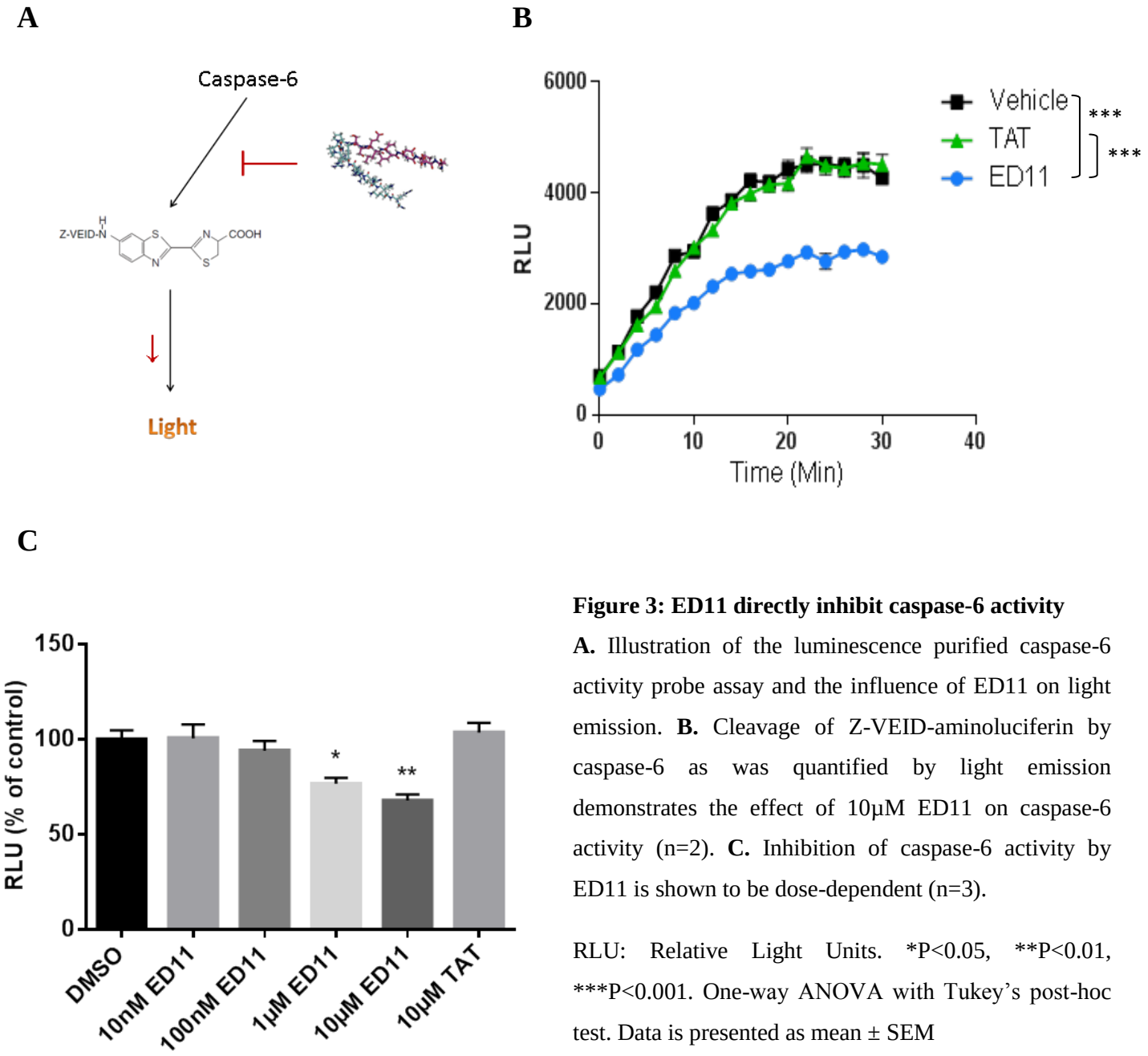

Figure 3: ED11 directly inhibit caspase-6 activity

A. Illustration of the luminescence purified caspase-6 activity probe assay and the influence of ED11 on light emission. **B.** Cleavage of Z-VEID-aminoluciferin by caspase-6 as was quantified by light emission demonstrates the effect of 10µM ED11 on caspase-6 activity (n=2). **C.** Inhibition of caspase-6 activity by ED11 is shown to be dose-dependent (n=3).

RLU: Relative Light Units. *P<0.05, **P<0.01, ***P<0.001. One-way ANOVA with Tukey's post-hoc test. Data is presented as mean ± SEM

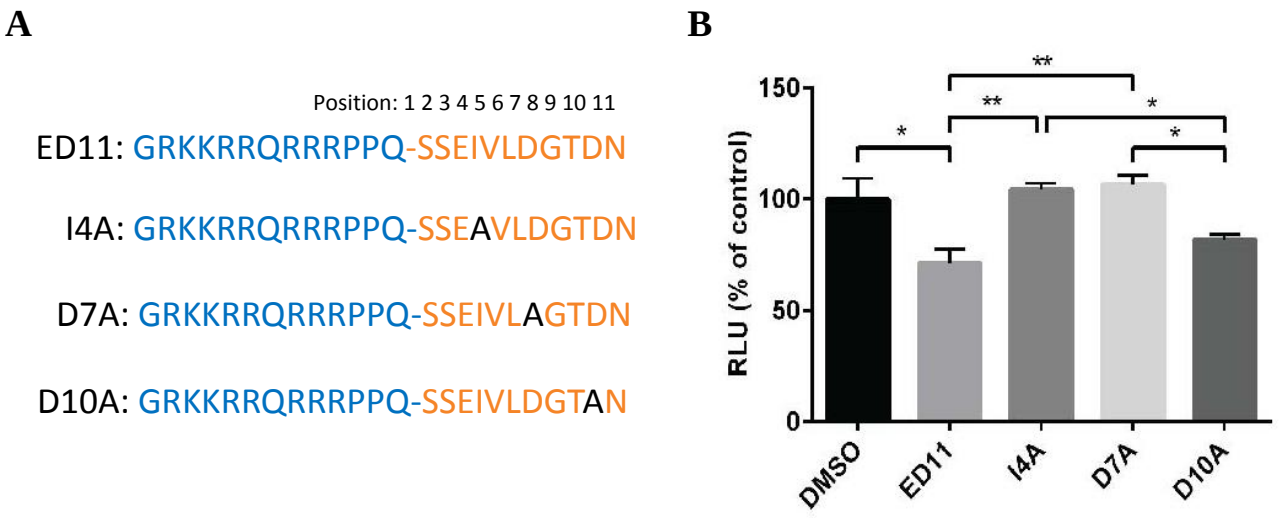

Figure 4: Identification of the amino acids essential for the inhibitory activity of ED11

A. For evaluation of specific amino acids role in caspase-6 inhibition, Isoleucine at position 4m Aspartic acid at position 7 or Aspartic acid at position 10 were substituted by Alanine. **B.** I4A and D7A variations of ED11 lack the ability to inhibit capase-6, while replacement of Aspartic acid at position 10 did not have the same effect (n=3).

RLU: Relative Light Units. *P<0.05, **P<0.01. One-way ANOVA with Tukey's post-hoc test. Data is presented as mean ± SEM.

5.2.3. Caspase-6 inhibition selectivity

As was thoroughly discussed in the introduction section, the selectivity of caspase inhibitor to a specific caspase is of great importance. Therefore, it is imperative to test ED11's effect on the activity of other members of the caspase family. To this goal, the effect of ED11 was tested firstly on caspase-3, which shares a similar active site to caspase-6. In addition, caspase-3 has an important role in the physiological function and the lack of caspase-3 activity is considered to be toxic to normal cell function[170-173]. Caspase-6 specificity over caspase-3 was first tested by incubating caspase-3 or caspase-

6 with Z-VEID-aminoluciferin in the presence of ED11 or the synthetic pan-caspase inhibitor zVAD-FMK as a control. When monitoring the influence on caspase-6 activity, both ED11 and zVAD-FMK inhibit the proteolytic process (AUC 251930±10245, 228554±5902 vs. 346153±16499, respectively, $P<0.05$). However, when addressing caspase-3 activity, no influence of ED11 on Z-VEID-aminoluciferin cleavage by caspase-3 was recorded (1177000±46000 vs. 1333000±45500), while zVAD-FMK inhibited also caspase-3 activity (701329±33639, $P<0.01$) (**Fig. 5A-B**). This indicates ED11 is selective to caspase-6 but not caspase-3 in blocking Z-VAID-aminoluciferin proteolysis. Next goal was to examine the impact of ED11 on cellular protein lysate cleavage by caspase-3. For this purpose, Caspase-3 was incubated with HEK cell-line lysate, in the presence of ED11 or zVAD-FMK in different concentrations. The cleavage level of PARP and Spectrin, two endogenous Caspase-3 targets, was detected using the western blot technique (**Fig. 5C**). As was observed, ED11 did not influence Spectrin or PARP cleavage by Caspase-3, in contrast to the pan-caspase inhibitor zVAD-FMK ($P<0.01$) (**Fig. 5D**). These results indicate ED11 does not directly interfere with caspase-3 mediated proteolysis in the concentrations tested.

5.2.4. Inhibition of caspase-6 cleavage of human Huntingtin by ED11

After providing proof of the ability of ED11 to directly inhibit caspase-6, the efficacy of ED11 inhibition of caspase-6 cleavage of Htt was evaluated. To achieve this goal, human Htt protein was overexpressed in COS7 cells, and cell lysate was incubated with active caspase-6. This was done in the presence of the detection antibodies Tb-BKP1 in the N-terminus and D2-neo-586 which binds only to the Caspase-6 cleaved Htt. Fragmentation levels were quantified using FRET technique, at an excitation wavelength of 340 nm and

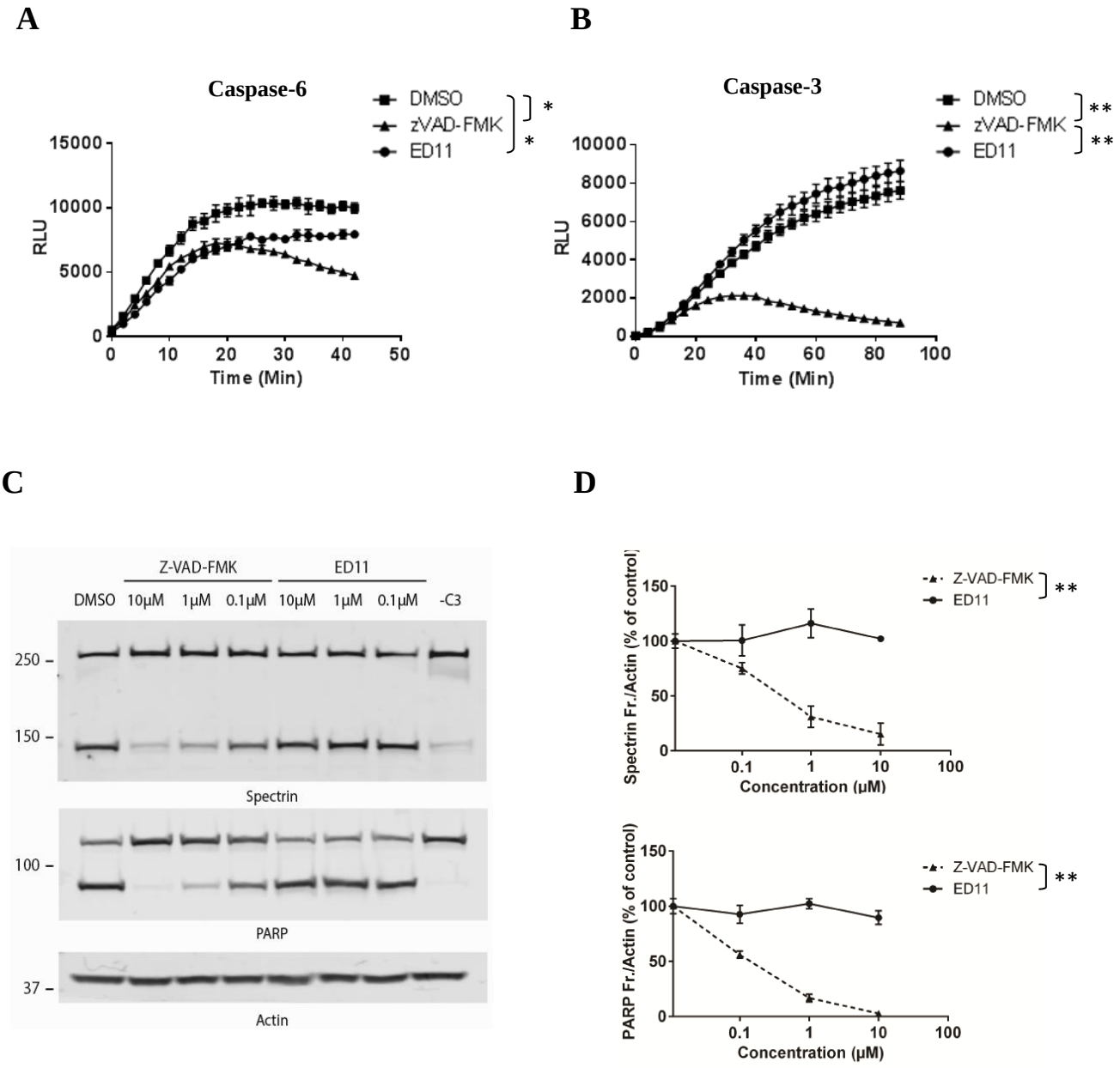

Figure 5: ED11 selectively inhibits purified caspase-6 cleavage of Z-VEID-aminoluciferin

To test the ED11 selectivity of caspase-6 over caspase-3, a purified caspase cleavage assay was conducted. **A.** When addressing proteolytic cleavage of Z-VEID-aminoluciferin by caspase-6, Both ED11 and zVAD-FMK control inhibit caspase-6 proteolytic activity. **B.** ED11 does not influence caspase-3 cleavage of Z-VEID-aminoluciferin, while zVAD-FMK significantly inhibit the reaction. **C-D.** Evalutaion of the influence of ED11 on caspase-3 protein cleavage in HEK cell-line lysate demonstrates ED11 did not influence Spectrin or PARP cleavage by Caspase-3, in contrast to the pan-caspase inhibitor zVAD-FMK.

RLU: Relative Light Units. *P<0.05, **P<0.01. Two-way ANOVA with Tukey's post-hoc test Data is presented as mean ± SEM.

an emission wavelength of 665 nm (**Fig. 6A**). The effect of ED11 or zVAD-FMK presence on fragment formation was plotted as a function of concentration to detect IC50 values. The IC50 determined for ED11 is 12.12nM, and IC50 for the zVAD-FMK control was 4.62nM (**Fig 6B**). These results indicate ED11 inhibit human Htt cleavage by Caspase-6 with competency comparable to that of a covalently binding synthetic inhibitor.

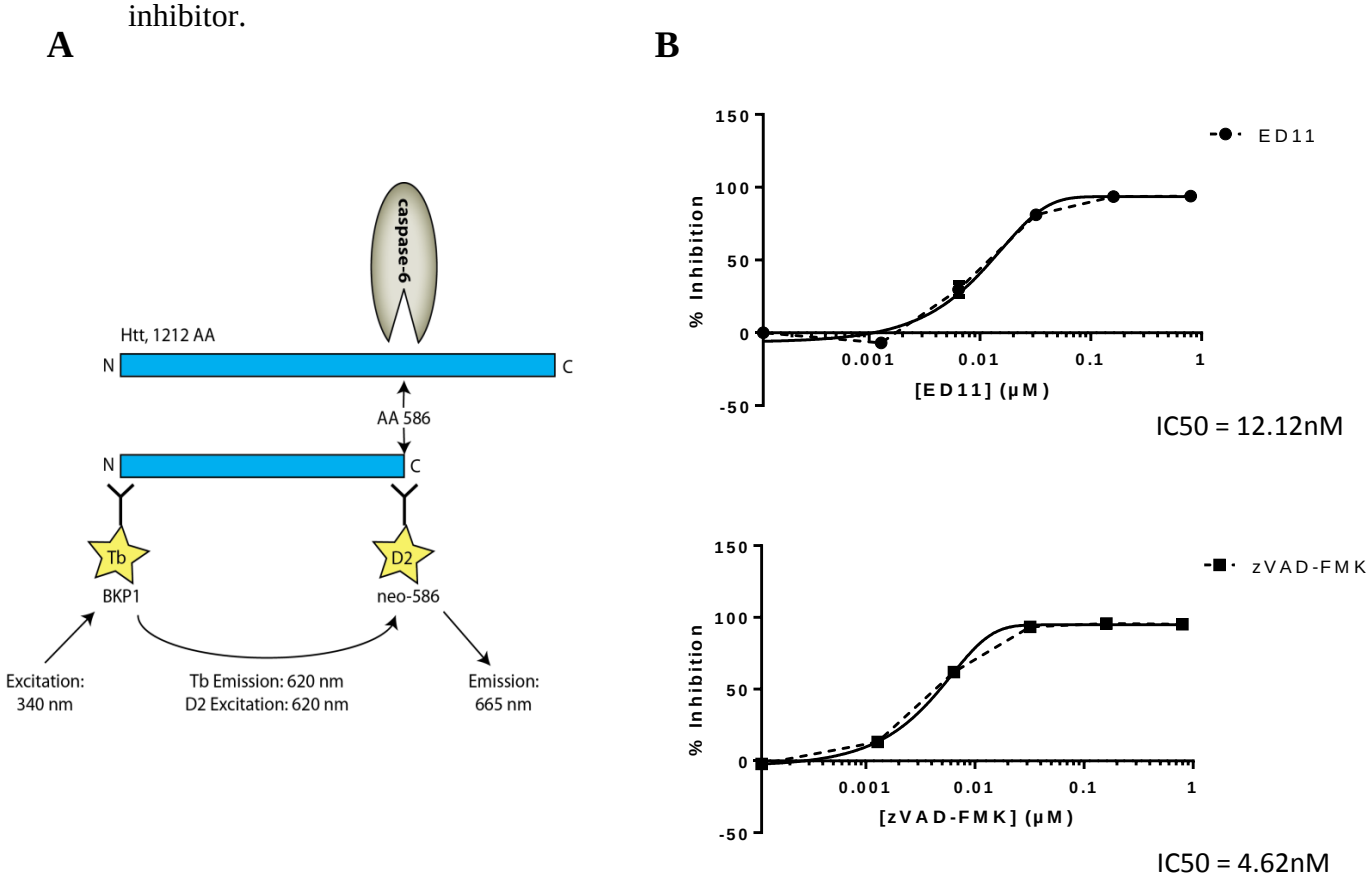

Figure 6: Evaluation of ED11 effect on caspase-6 mediated Huntingtin proteolysis

To test ED11 efficacy in preventing caspase-6 proteolysis of Htt, a sensitive FRET-based assay was conducted and IC50 values determined. **A.** The Tb-BKP1 antibody detects the N-terminal of Htt and D2-neo-586 detects caspase-6 cleavage generated neo-epitope at aa586. An excitation wavelength of 340 nm and an emission wavelength of 665 nm is used to detect caspase-6 generated Htt fragments. **B.** Non-linear regression analysis of ED11 and zVAD-FMK influence on Htt cleavage reveals IC50 values as 12.12nM for ED11 and 4.62nM for zVAD-FMK (n=2).

Data is presented as fitted data after non-linear regression analysis.

5.2.5. ED11 overall effect on caspase cleavage of human Huntingtin

In order to test the inhibitory effect of ED11 on a wider range of caspases, human Htt protein cleavage by caspases 1–10 was conducted. It was recently demonstrated that these caspases can cleave Htt at different sites[174]. The effect of 50nM ED11 on fragment generation was quantified using western blot with the anti-BKP1 antibody. After incubation of the different caspases with Huntingtin, western blot staining by BKP1 antibody demonstrated that the inhibitory effect of ED11 was most pronounced for the generation of the 586 fragment by caspase-6 (68.58±15.6%, $P<0.01$). A lesser effect of the inhibitor was found on caspase-1 and caspase-10 mediated generation of the 513 fragment (78.48±4.02%, 77.47±8.56%, respectively, $P<0.05$) and caspase-2 mediated generation of the 552 fragment (81.9±4.84%, $P<0.05$) (**Fig. 7**). In addition, the 513 fragment generation by caspase-5 was up-regulated (185.7±20.19%, $P<0.01$)

5.2.6. ED11 effect on human mutant Huntingtin cleavage

Next, the ability of ED11 to inhibit human mutant Htt cleavage by caspase-6 was determined. To this goal, striatal extracts from BACHD mice, which expresses human mutant Htt with 97 glutamine repeats, were incubated with caspase-6 in the presence of ED11. Western blots staining with antibodies Htt 4-19 provide qualitative evidence that the addition of 10 μM ED11 abolished proteolysis of the human mutant Htt transgene by caspase-6 (**Fig. 8**).

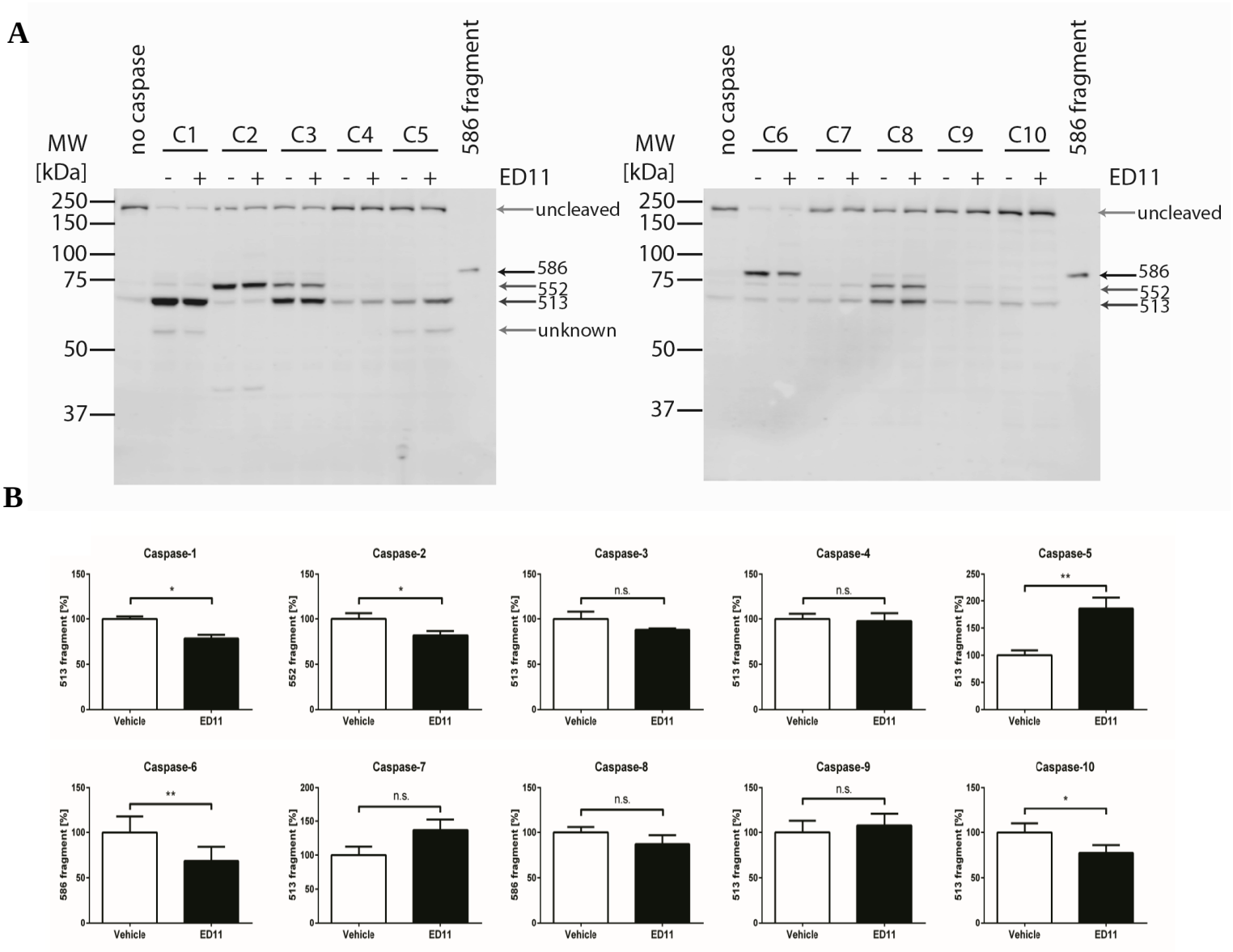

Figure 7: ED11 effect on caspase mediated Htt cleavage

A. To test the overall effect of 50nM ED11 on caspase cleavage of Htt, Htt protein cleavage by caspases 1-10 was conducted and evaluation of the effect of ED11 on fragment generation was visualized using western blot stained with the anti-BKP1 antibody (n=4). **B.** Quantification demonstrated that the most pronounced effect of ED11 is the reduction of cleavage at Asp586 by caspase-6. A weaker inhibition of caspase-1 and -10 cleavage at Asp513 and caspase-2 cleavage at Asp552 was also observed, as well as an increase of caspase-5 cleavage at Asp513. Other caspases cleavage was not significantly altered. *P<0.05, **P<0.01. Two-tailed Student's T-test. Data is expressed as mean ± SEM.

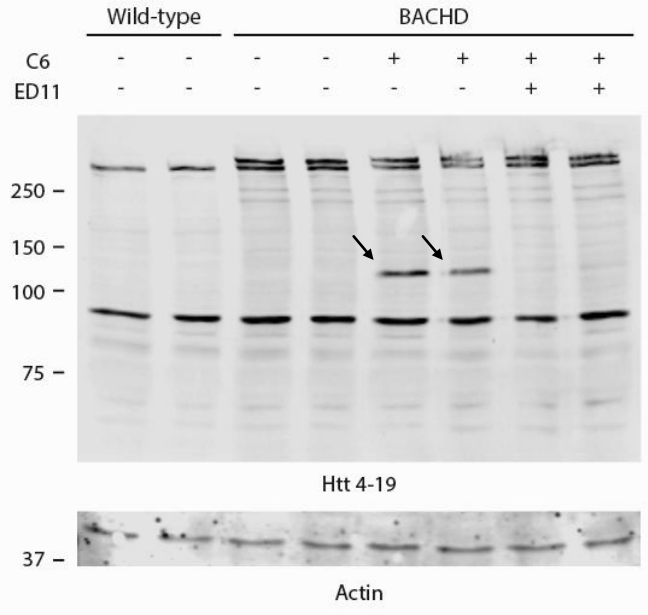

Figure 8: ED11 reduces human mutant Htt caspase-6 proteolysis

BACHD striata protein extracts were incubated with caspase-6 for 45 minutes at 37°C and proteins were assayed using standard western blot assay. Incubation with Anti-Htt 4-19 antibodies showed caspase-6 fragmentation of human mutant Htt is blocked in the presence of ED11. Arrows indicate caspase-6 generated fragment of mutant Htt.

5.3. Evaluation of the Intra-cellular caspase-6 inhibition by ED11

After demonstrating the efficacy and selectivity of ED11 in an in-vitro enzymatic reaction studies, the feasibility and safety of ED11 in inhibiting caspase cleavage of human mutant Htt in the cellular environment was tested.

5.3.1. Penetration of the cellular membranes

One of the fundamental issues to address for therapeutic purposes is the ability of a compound to penetrate cellular membranes. In order to confirm ED11 ability to penetrate cellular membranes and enter cells, different concentration of the peptide were incubated with mouse embryonic fibroblast (MEF) cells for 1 hour. Immunofluorescence Staining with an anti-TAT antibody and DAPI counterstaining demonstrated the dose-dependent accumulation of ED11 (**Fig. 9**), indicating its presence within the cell.

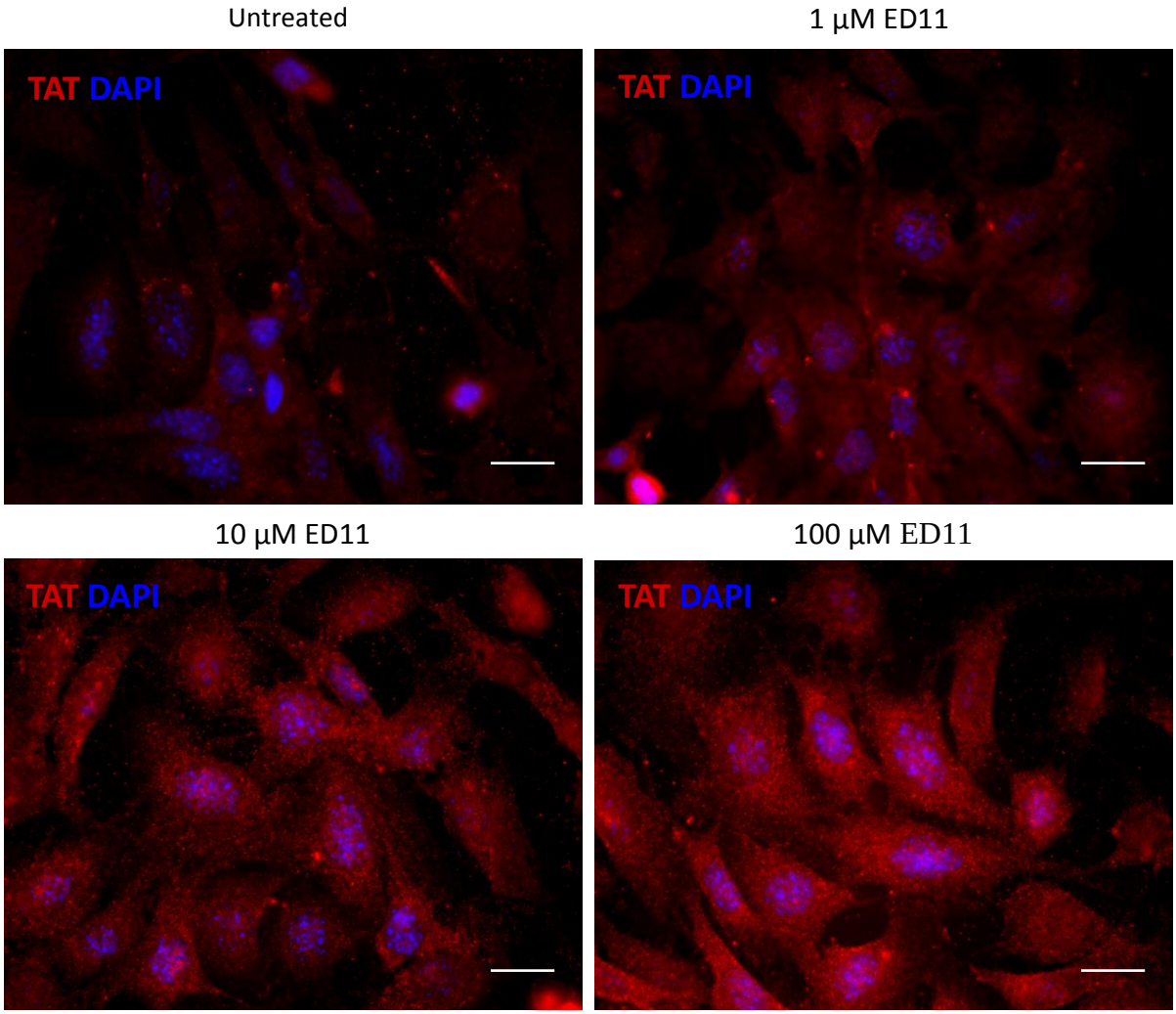

Figure 9: ED11 penetrates the cell membrane

Representative images of MEF cells incubated with the indicated concentrations of ED11 and labeled with DAPI and anti-TAT antibody. Scale bars indicate 50µm.

5.3.2. ED11 impact on cell properties in basal conditions

In order to verify ED11 does not induce cellular toxicity as part of safety evaluation, the influence on cell viability was examined. For this purpose, SH-SY5Y cells were incubated for 48 hours with 25µM ED11, and viability was measured using Alamar blue assay. Quantification revealed that no reduction in cell viability was evident (3003±334.9 vs. 2957±177.5) (**Fig. 10A**). Next, using BrdU proliferation assay, it was verified that

ED11 does not cause a proliferative effect on cells. As was observed (**Fig 10B**), the proliferative cells percentage was scarcely affected by 24 hours ED11 treatment compared to vehicle (47.52±0.485% vs. 48.15±1.25). Since it was previously shown that caspase-3 and caspase-7 inhibitors cause cell cycle arrest, ED11 alteration of cell cycle status was examined. The results confirm that ED11 did not alter cell cycle status in basal conditions (**Fig. 10C**). Overall, the results presented here support the notion that ED11 may be safe for intra-cellular administration since it does not alter the mentioned normal cellular properties.

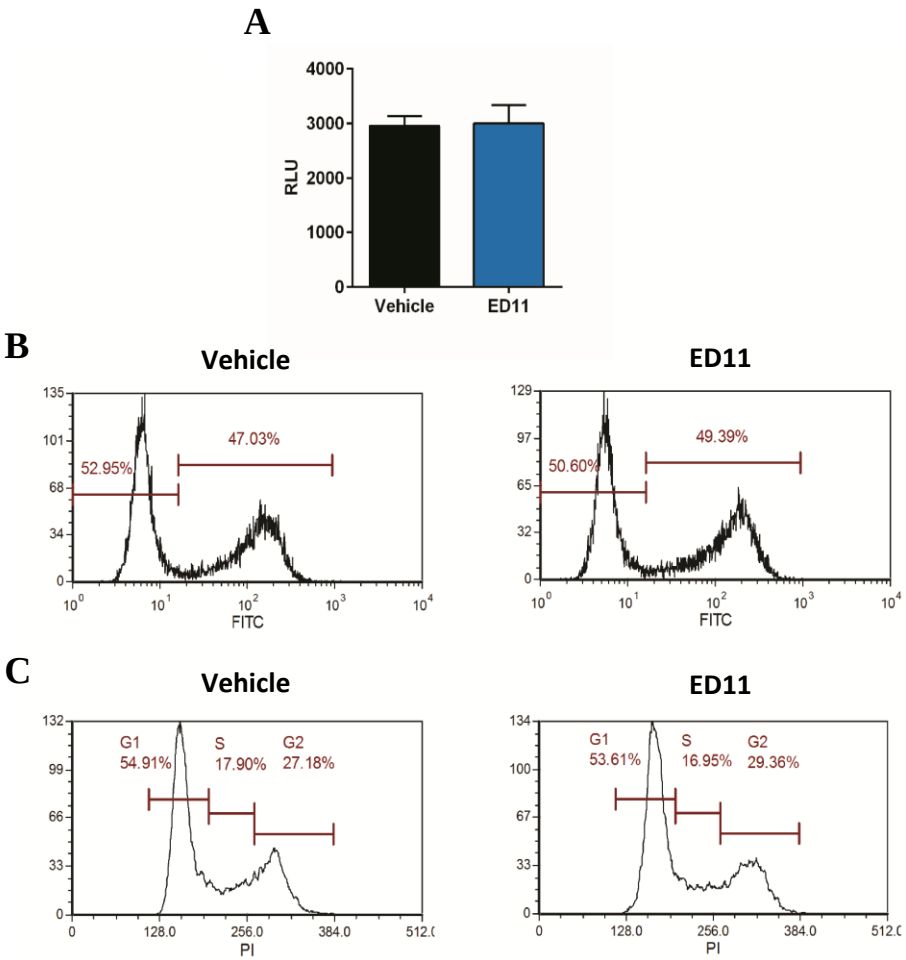

Figure 10: ED11 does not influence cell viability, proliferation or cell cycle status under basal conditions.

A. No ED11 dependent reduction in cell viability was observed in an Alamar blue cell viability assay after 24 hours incubation (n=3). **B.** Cytometer readings of incorporated BrdU as a proliferation marker demonstrating that the proliferative cells percentage was scarcely affected by ED11 compared to vehicle (n=2). **C.** Analysis of the cell cycle status revealed no effect of ED11 treatment on the cell cycle under basal condition (n=2). Two-tailed Student's T-test. Data is presented as mean ± SEM.

5.3.3. Influence on the intra-cellular caspase-6 cleavage of Huntingtin

To evaluate the ability of ED11 to reduce intracellular Htt cleavage by caspase-6, co-transfection of HEK293 cells with caspase-6 and the N-terminal 1212 amino acids of human 15Q-Htt was conducted in the presence of ED11. Human Htt 586 fragment levels were quantified 24 hours after transfection using anti-Htt (mab2166) and anti-Htt586 neo-epitope antibodies (**Fig. 11A**). Treatment with ED11 resulted in a significant reduction of the 586 fragment resulting from caspase-6 cleavage (41.26±5.16%, $P<0.01$) (**Fig. 11B-C**), whereas no effect on the auto-activation of caspase-6 was observed. The cell-permeable pan-caspase inhibitor control Q-VD-OPh, however, inhibited both caspase-6 auto-activation and Htt cleavage (**Fig. 11A**). These findings suggest that ED11 is able to block the intracellular cleavage of human Htt by active caspase-6.

5.3.4. Effect on human mutant Huntingtin toxicity in a cell-based model of Huntington's disease

In order to evaluate ED11 ability to protect cells from mutant Htt toxicity, PC12 cells harboring an inducible human 145Q-mHtt expressing vector were placed under chronic serum deprivation stress and induced to express human mutant Htt for 72 hours. Cell viability measurements indicate that human 145Q-mHtt expression gradually decreased viability compared to uninduced PC12 cells as a control (43.45±9.75%, $P<0.05$). Treatment by ED11 resulted in the preservation of cell viability (88.59±19.5, $P<0.05$) (**Fig 12A**). Next, cell death was addressed by measuring LDH release. As was observed, ED11 treatment resulted in an attenuation of LDH release that was evident after 72 hours of human 145Q-mHtt expression (9.77±2.72% vs. 17.84±1.54%) (**Fig 12B**). These

findings show that cellular human mutant Htt toxicity can be attenuated by ED11 treatment.

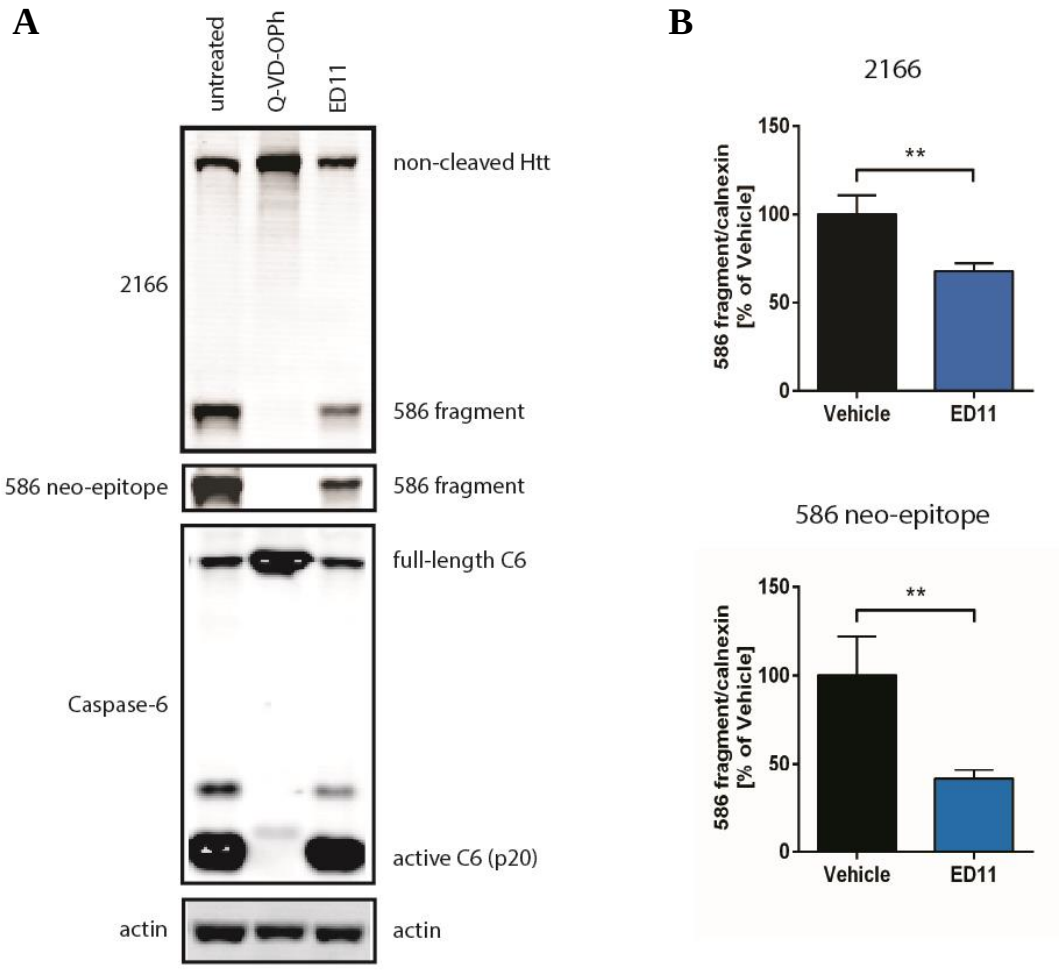

Figure 11: ED11 inhibits the intra-cellular caspase-6 cleavage of human Huntingtin

HEK293 cells were co-transfected with caspase-6 and N-terminal 15QHtt for 24 hours in the presence of ED11. **A.** Western blots of cell lysate stained with mab2166 and 586 neo-epitope antibodies demonstrate the generation of 586 fragment of human Htt after caspase-6 cleavage, and the influence of ED11 and Q-VD-Oph on their level. Lower panel demonstrates the evidence of full-length caspase-6 and active caspase-6 (p20) presence. **B.** Quantification of the Htt fragment generated by caspase-6 that was detected by mab2166 and 586 neo-epitope antibodies demonstrate a significant reduction of the intra-cellular caspase-6 cleavage by ED11 (n=4-8). **P<0.01. Two-tailed Student's T-test. Data is presented as mean ± SEM.

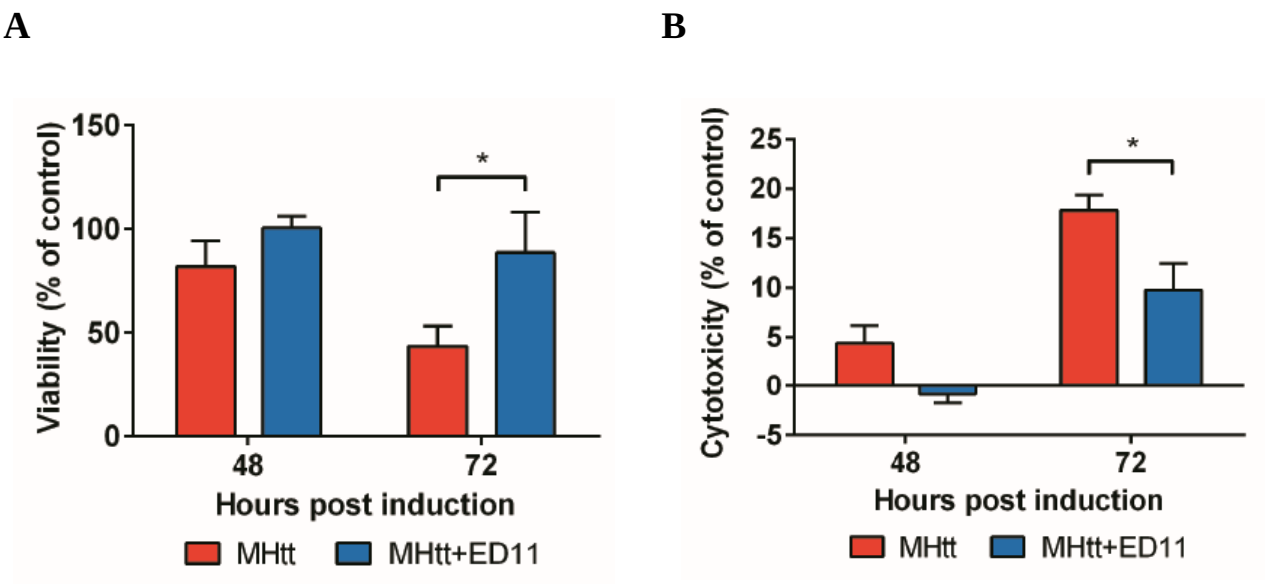

Figure 12: ED11 protects human 145Q-MHtt expressing cell from viability loss and cell death

PC12 cells harboring an inducible human 145Q-mHtt expressing vector were placed under chronic serum deprivation stress and induced to express mutant Htt for 72 hours. **A.** Viability measurement by Alamar blue viability assay indicates a decline in cell viability after 72 hours, which was normalized in the presence of ED11 (n=5). **B.** Cell death measurement by LDH release indicated that the cellular toxicity induced by mutant Htt expression was reduced by ED11 treatment (n=5).

*P<0.05. Two-tailed Student's T-test. Data is presented as mean ± SEM.

5.3.5. Effect on caspase activity in human mutant huntingtin expressing cells

Caspase activation is known to be aggravated in HD patients and in HD models. Since this process is considered to be mediated by mutant Htt toxicity, the influence of ED11 on caspase activation was measured. PC12 cells were induced to express human 145Q-mutant Htt and were put under serum deprivation conditions for 48 hours. The cell permeable pan-caspase activity fluorescence indicator FAM-VEID-FMK was introduced

to the cells at the end point, and cells were subjected to microscopy examination (**Fig. 13A**). The positive signal area was then quantified and normalized to Hoechst stain (**Fig. 13B**). Quantification reveals that inducement of human 145Q-mutant Htt significantly increased caspase activity compared to uninduced PC12 cells as a control (13.63±2.45 vs. 5.572±2.121, $P<0.05$), which was normalized by the treatment of ED11 (4.777±1.063, $P<0.01$).

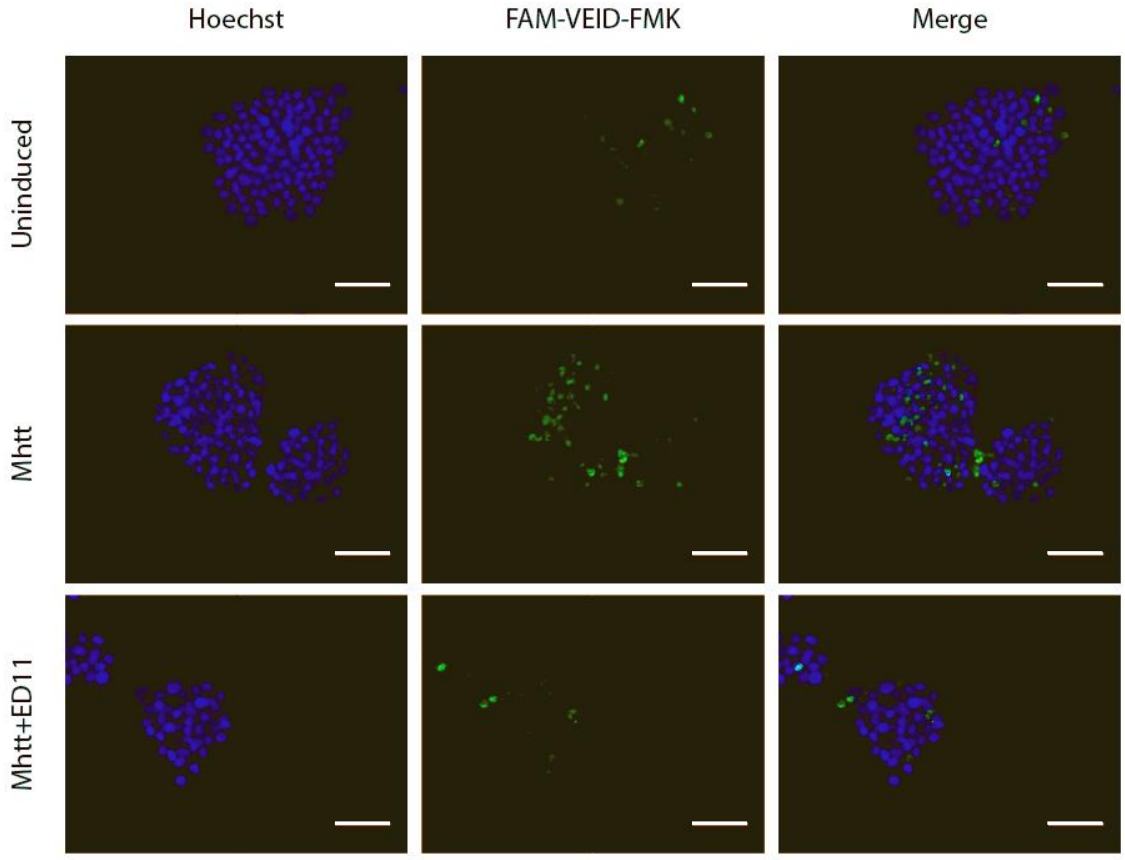

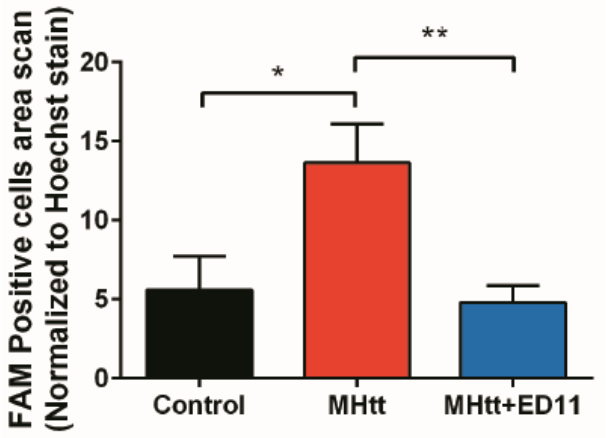

Figure 13: ED11 inhibits the intra-cellular caspase activity

Mutant human Htt expressing PC12 were put under serum deprivation for 48 hours and caspase activity was detected using FAM-VEID-FMK. **A.** Representative microscopy pictures show a positive signal of FAM on Hoechst stain background. **B.** Area scan quantification of FAM demonstrates human mutant Htt expression caused increased caspase activity compared to the uninduced PC12 cells. This activation was inhibited by ED11 treatment (n=7).

Scale bars indicate 50µm. MHtt: mutant Htt. *P<0.05 **P<0.01. One-way ANOVA with Tukey's post hoc test. Data is presented as mean ± SEM.

5.4. In-vivo evaluation of caspase-6 inhibition by ED11

To determine ED11 ability to protect from mutant Htt toxicity in-vivo, the HD mouse model BACHD and control background FVB/N were used. As was elaborated in the introduction, BACHD mice express full-length mutant Htt with 97 glutamine repeats at the N-terminal. These mice demonstrate progressive motor, behavioral and cognitive deficits and therefore are suitable for evaluating HD treatment modalities. First, the blood-brain barrier penetration ability of ED11 was tested. Next, for efficacy studies, the therapeutic potential was measured in two main treatment paradigms, early treatment at the age of symptoms appearance and late treatment at an advanced disease state.

5.4.1. Penetration of the blood brain barrier

To monitor the ability of ED11 to penetrate the blood-brain barrier (BBB) in vivo, the CellVizio system which enables detection of fluorescence in blood vessels and its accumulation in the brain parenchyma was used. FVB/N Mice were injected IV with one of the following compounds: FITC conjugated albumin, a marker of intact blood vessels. FITC conjugated TAT (48-60), as a positive control for extravasation from the blood vessels (TAT-FITC). FITC conjugated ED11 lacking the TAT (48-60) cell penetrating sequence (ED11 TAT^{-}-FITC) and FITC conjugated ED11 (ED11-FITC) (**Fig.14**). The mice were placed in a stereotaxic device, and a fluorescence detection probe was inserted to the central caudate-putamen. 40 min after compound injection, fluorescence was monitored using a 488nm excitation laser. As was observed, while FITC conjugated Albumin and ED11 lacking the cell penetrating sequence TAT (48-60) remained confound to the blood vessels, FITC conjugated TAT (48-60) and ED11 penetrated the

blood vessel endothelium and extravagated into the brain parenchyma (Fig. 1C). These results support the hypothesis that TAT (48-60) enables ED11 to penetrate the blood-brain barrier and enter the CNS.

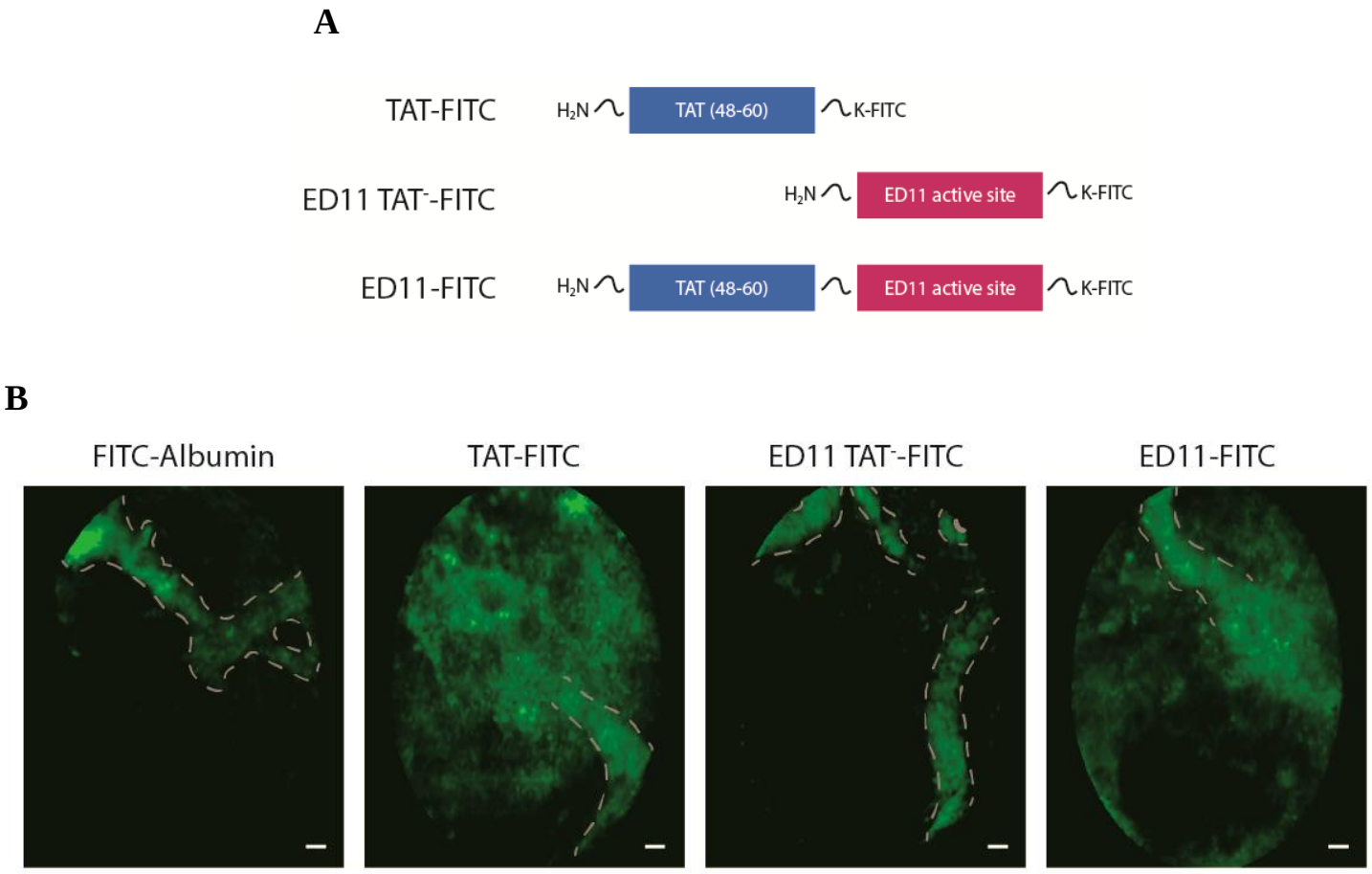

Figure 14: ED11 extravagates into the brain parenchyma in-vivo

In-vivo CNS penetration of the mentioned compounds was monitored by detecting fluorescence signal extravasation out of the blood vessels and into the brain parenchyma. **A.** Tested compounds composition is illustrated: FITC conjugated TAT (TAT-FITC), FITC conjugated ED11 lacking the TAT cell penetrating sequence (ED11 TAT—FITC) and FITC conjugated ED11 (ED11-FITC). **B.** FITC conjugated albumin as a marker of blood vessels and ED11 TAT--FITC does not penetrate blood vessels. In contrast, TAT-FITC as a positive control and ED11-FITC displays extravasation into the brain parenchyma. Scale bars indicate 20µM. Dashed lines represent blood vessels contour.

5.4.2. The efficacy of ED11 treatment in-vivo in an early disease state

For the evaluation of ED11 effect in an early disease state, BACHD mice were treated with ED11 starting at the age of 5 weeks, by a subcutaneously implanted mini-pump, injecting continuously at the rate of 4mg/kg/day. Three treatment groups were tested – Wild type mice treated with vehicle (20% ddH20, 80% saline), BACHD mice treated with vehicle, and BACHD mice treated with ED11. Motor and behavioral performances were evaluated throughout the treatment, and the mice were sacrificed at the age of 25 weeks. Experimental timeline is presented in the following diagram (**Fig. 15**)

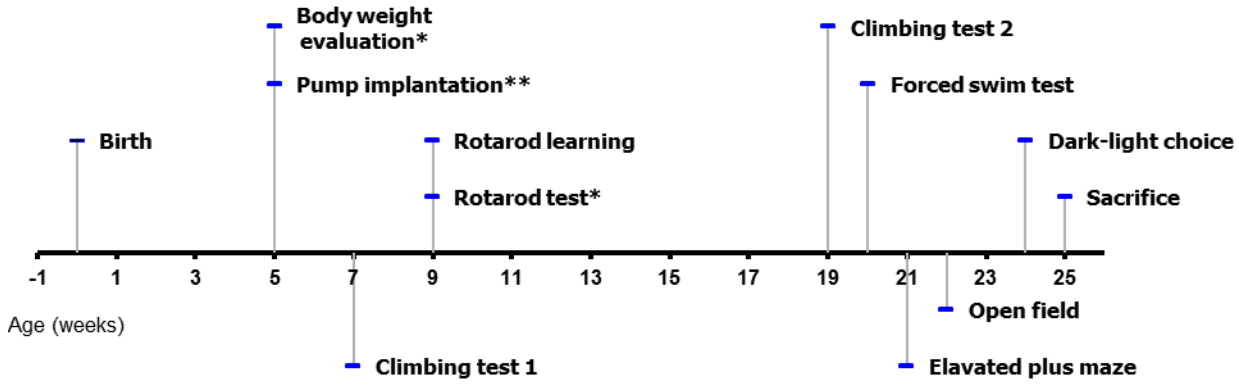

* Repeated every 2 weeks
** Repeated every 4 weeks

Figure 15: Early treatment paradigm experimental time-line

5.4.2.1. Attenuation of body weight alterations

Huntington's disease patients demonstrate a decrease in body weight throughout their illness[175]. In contrary, different mouse models for HD demonstrates an increase in body weight, including the YAC128 and BACHD mice. This discrepancy was explained by the modulation of weight gain by human Htt and human mutant Htt in different tissues[148,149]. In order to address the influence of ED11 on body weight gain of the BACHD mice, which was reported to be up-regulated due to human mutant Htt over-expression, we monitored the mice body weight throughout the study. As demonstrated in **Fig.16**, treatment with ED11 attenuated body weight gain of the BACHD male mice (36.74±0.80gr vs. 40.63±1.59gr, P<0.01). This data indicates ED11 influence human mutant Htt expression mediated body weight alterations. The difference in the females group did not show statistical significance.

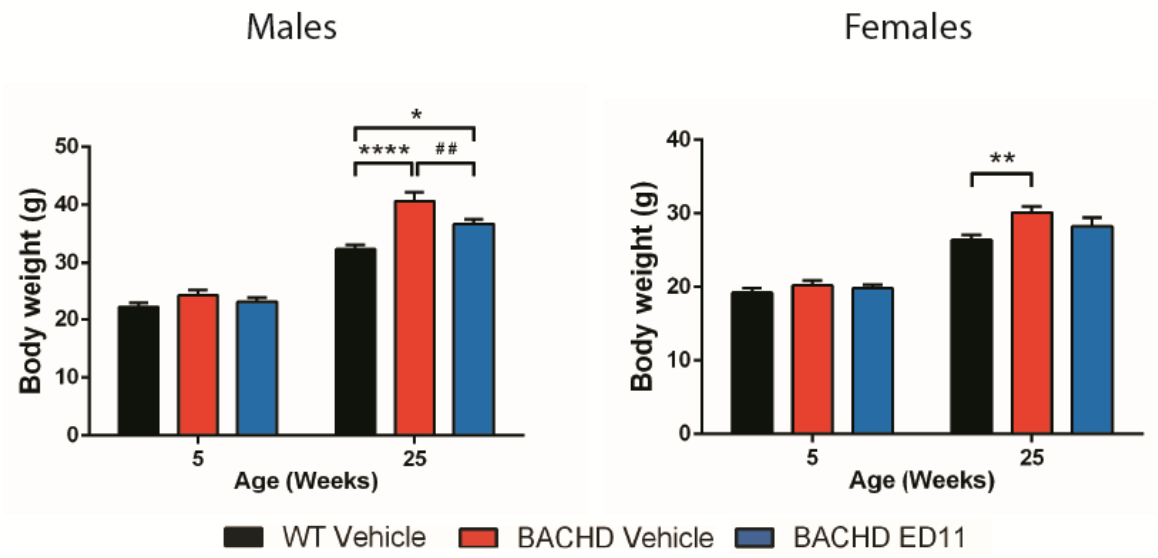

Figure 16: Body weight measurements of pre-treatment and post-treatment BACHD mice

Measurements of body weight at age 25 weeks indicates mutant Htt caused excess body weight gain in vehicle treated BACHD mice, while treatment with ED11 was able to attenuate this phenotypic weight alteration (n=10-12). *P<0.05, **P<0.01, ****P<0.0001. One-way ANOVA with Tukey's post-hoc test. Data is presented as mean ± SEM.

5.4.2.2. Preservation of motor learning skill

HD patients demonstrate a deficit in motor learning skill[176]. Therefore, the motor learning skill of the BACHD mice was tested at the age of 8 weeks, 21 days after treatment commencement. During the training period, mice were placed on an accelerating rod, and latency to fall from the rod was recorded. The mice were tested three times per day for three consecutive days. During these training sessions, BACHD mice treated with ED11 demonstrated higher motor learning capabilities than the vehicle-treated BACHD mice in the male group (80.73±7.00 vs. 52.30±9.051, P<0.05). The female group showed a trend toward motor skill learning improvement (124.0±15.65 vs. 129.8±9.218, P=0.081). The effect of ED11 is more prominent in day 2 and 3, as the training progresses (**Fig. 17**).

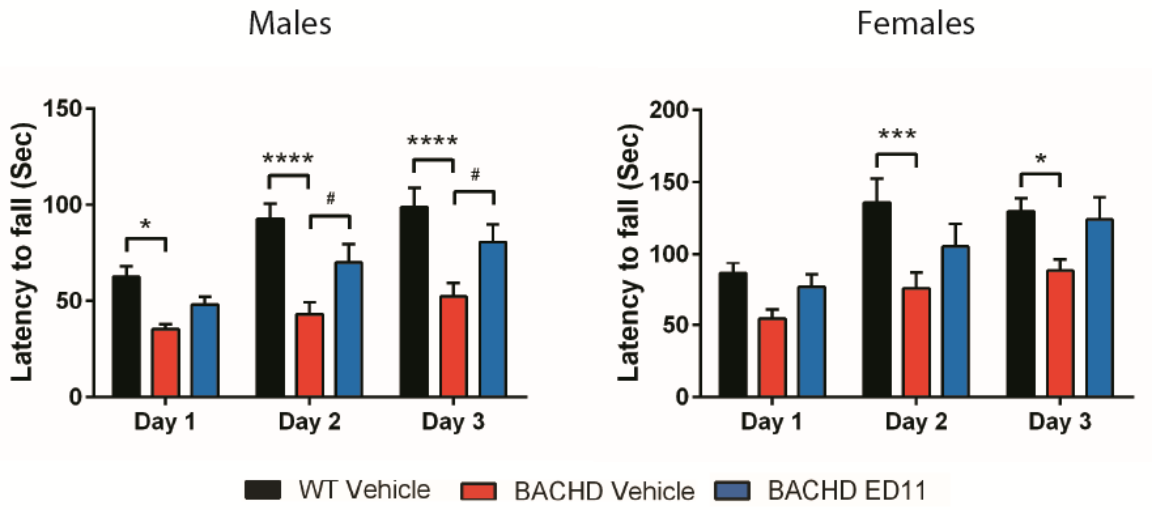

Figure 17: ED11 Influence on motor learning skill

Rotarod training performance was measured by latency to fall from an accelerating rod 3 weeks after treatment commencement for 3 consecutive days, three trials per day. While vehicle treated BACHD mice demonstrated marked impairments, ED11 treated mice impairment was significantly milder (n=10-12).

*P<0.05, ***P<0.001, ****P<0.0001. One-way ANOVA with Tukey's post-hoc test. Data is presented as mean ± SEM.

5.4.2.3. Preservation of long-term motor performance

To test ED11 influence on long-term motor performance deficit, a hallmark of HD manifestation, we tested the influence of ED11 on the long-term motor performance of the BACHD mice. To this goal, we examined the mice in the Rotarod test every 4 weeks starting at the age of 9 weeks. The results indicate that while the vehicle-treated BACHD mice performed significantly lower than the wild-type mice (60.32±9.48 vs. 105.4±10.68, $P<0.001$), ED11 treated BACHD mice remained longer on the accelerating rod, their performance comparable to the wild-type mice (102.3±10.85, $P<0.01$ compared to vehicle-treated BACHD). This effect was observed mainly in the male group. However, in the female group, a similar pattern was observed, although the differences did not reach statistical significance (**Fig 18A**). Since body weight differences were observed, it is important to verify that the beneficial effects of ED11 were not weight dependent. To this aim, we matched male subjects with the same body weight and compared their Rotarod performance. Body weight matching indicated that the beneficial effect of ED11 cannot be attributed to the lower body weight of the ED11 treated mice, as the beneficial effect remained statistically significant (135.36±13.02 vs. 76.33±7.15, $P<0.01$) (**Fig. 18B**). Overall, these results show that ED11 early treatment can help preserve motor function impairment caused by human mutant Htt expression in the BACHD mouse model.

A

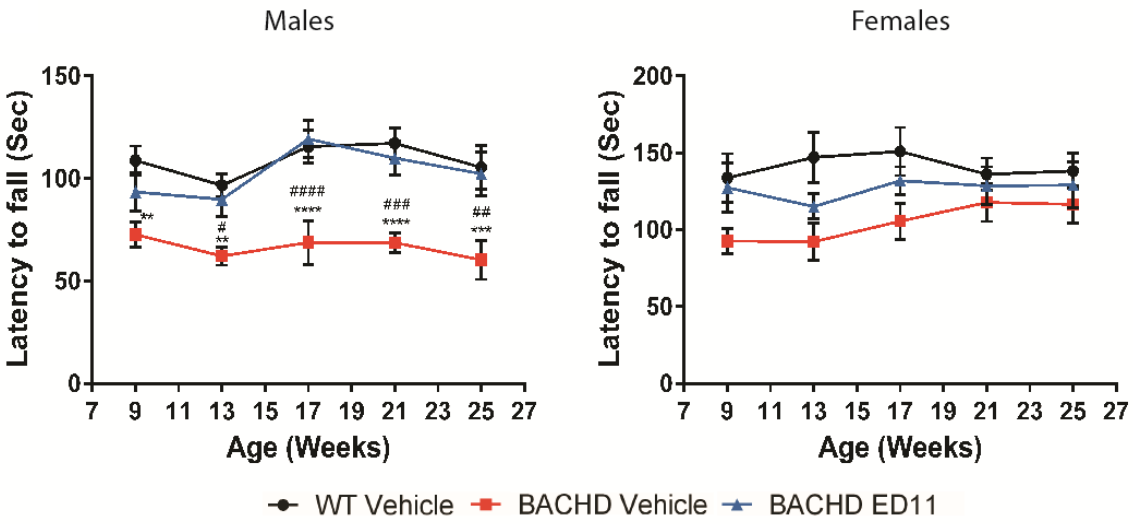

B

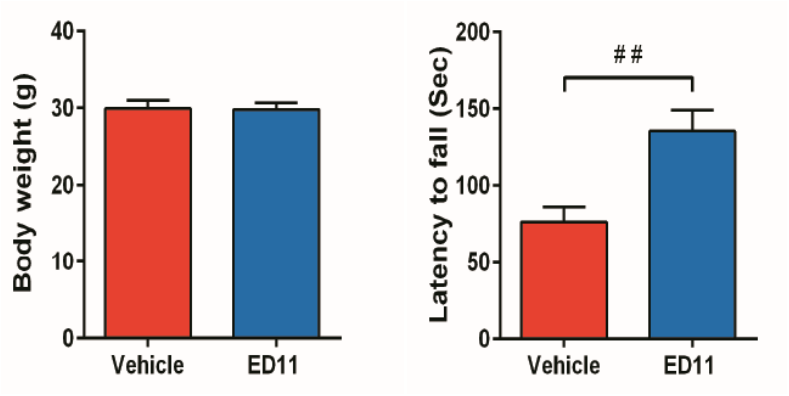

Figure 18: ED11 Influence on of long-term motor performance

Long-term rotarod performance was measured by latency to fall from an accelerating rod every 4 weeks. **A.** Male BACHD mice treated with ED11 showed preserved motor performance compared with WT mice. The same trend was detected in the female group, which did not show a significant motor impairment in our cohort (n=10-12). **B.** Matching according to body weight supports the fact that the beneficial effect of ED11 cannot be attributed to the lower body weight of the ED11-treated mice (n=6).

*: Statistical difference from the WT group

#: Statistical difference from the ED11 group

**P<0.01, ***P<0.001, ****P<0.0001, #P<0.05, ##P<0.01, ###P<0.001, ####P<0.0001. One-way ANOVA followed by Tukey's post-hoc test. Data is presented as mean ± SEM.

5.4.2.4. Protection from depression-related behavior

Depression is considered to be a manifestation strongly associated with HD[177]. In order to evaluate the influence of ED11 on the depression-related behavior of the BACHD mice, the forced swim test (FST) was conducted at 20 weeks of age. ED11-treated mice did not exhibit the increased immobility observed in the vehicle-treated BACHD mice (44.89±5.22 vs. 27.56±5.35, P<0.05) (**Fig. 19**), indicating that ED11 protects against the depression-related phenotype. No correlation was found between motor performance in the rotarod test and time spent immobile in the FST (Pearson correlation coefficient r = 0.057, P-value = 0.83, two-tailed Student's t-test), confirming that the protective effect of ED11 was not directly related to motor ability.

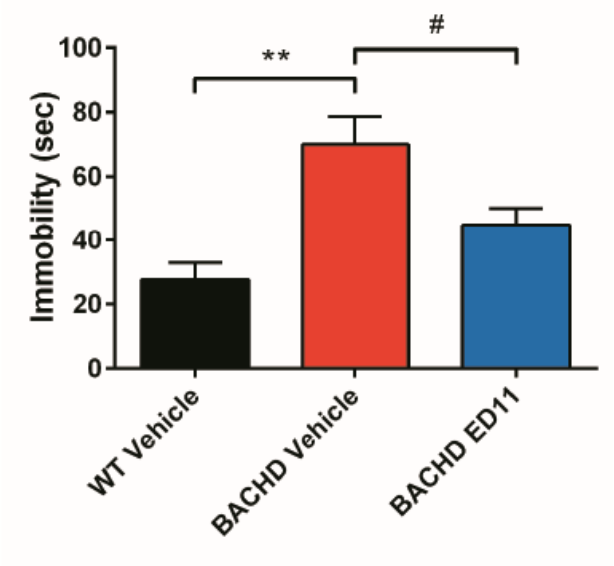

Figure 19: Influence of ED11 on depression-related behavior of BACHD mice

Depression-related behavior was measured by time spent immobile in the FST .Vehicle treated BACHD mice were significantly less mobile than their wild-type littermates, indicating a depressive-like state of these mice. Treatment with ED11 significantly decreased the time spent immobile, indicating a reduction of the depression-related phenotype in the BACHD mice (n=20-23).

*P<0.05, **P<0.01. One-way ANOVA followed by Tukey's post-hoc test. Data is presented as mean ± SEM.

5.4.2.5. Influence on climbing behavior

Climbing behavior was used to assess motor movement and coordination. BACHD mice were placed on a flat surface and a closed-top wire mesh cylinder is placed over the mouse. The animal's behavior is videotaped and measured over a 5 minute period and time spent climbing was measured. The first test was conducted at the age of 7 weeks (**Fig. 20A**), and the second test at the age of 19 weeks (**Fig. 20B**). A trend toward lower time spent climbing in the vehicle-treated BACHD mice was observed, while the ED11 treated mice show a trend toward higher time spent climbing, similar to the wild-type mice.

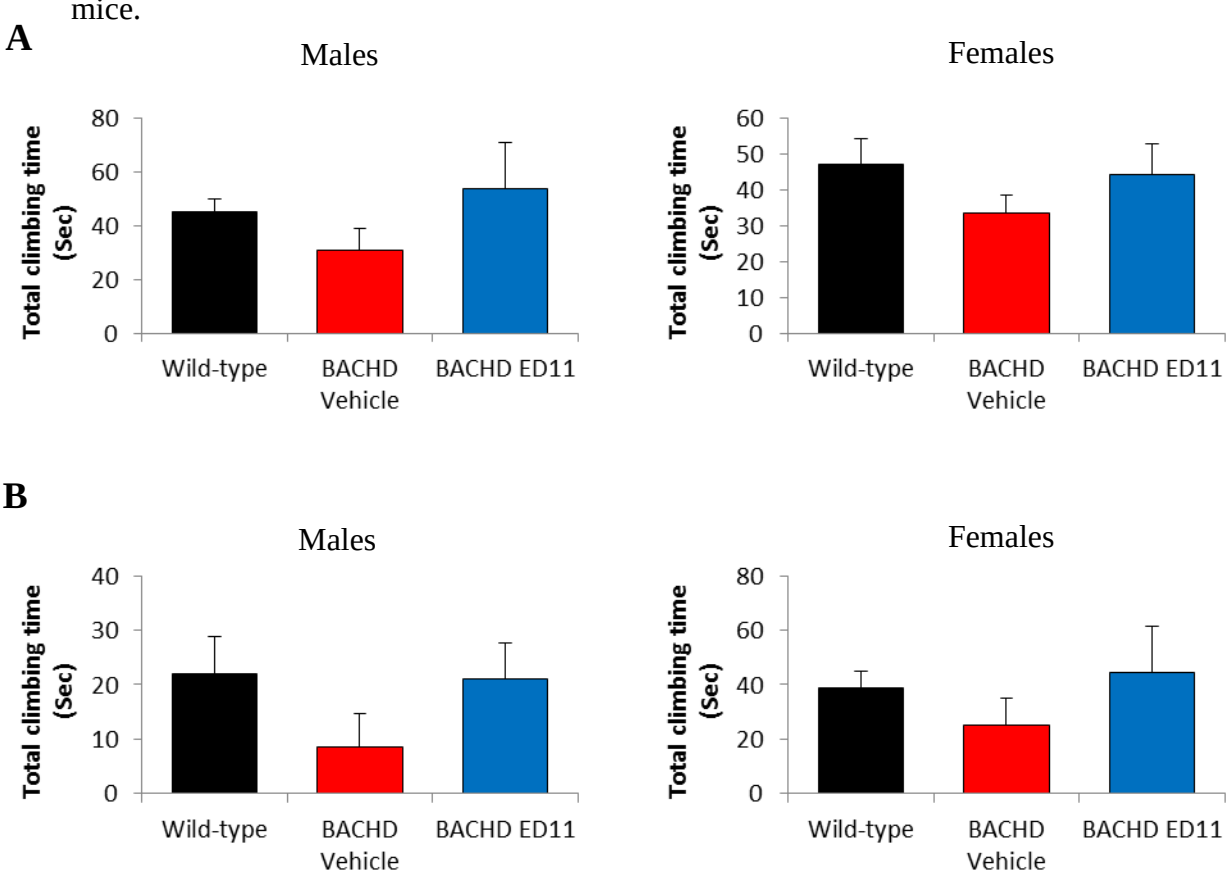

Figure 20: Determination of climbing ability in the cylinder climbing test

The climbing test was conducted at the age of 7 weeks (**A**) and at the age of 19 weeks (**B**). Vehicle treated BACHD displayed a trend toward less time spent climbing compared to wild-type mice, while the ED11 treated mice displayed similar performance to the wild-type mice (n=10-12). Data is presented as mean ± SEM.

5.4.2.6. Influence on anxiety-related behavior

Anxiety-related behavior is commonly observed also in HD patients[178]. Therefore, the effect of ED11 on anxiety-related behavior was tested in a number of behavioral tests in the BACHD mice. First, basal locomotor activity, exploratory activity and anxiety-related behavior were measured in the open field test. 22 weeks age BACH mice were placed in one corner of the arena and their behavior was recorded for 20 min. Total distance traveled, total time spent in the center and the number of entries to the center was measured. Since no significant difference was observed between male and female performance, the analysis was united for both genders. No significant differences in total distance traveled were observed between the treatments groups, indicating that basal locomotor activity was unchanged (**Fig. 21A**). Exploratory activity and anxiety-related behavior were measured by quantification of the time spent in the center and number of transitions to the center. Whereas BACHD mice show decreased exploratory and increased anxiety-related behavior, the ED11-treatedmice showed more transitions to the center (8.31±0.84 vs. 5.10±0.62, $P<0.05$) and a trend toward increased time spent in the center compared with vehicle-treated BACHD mice (38.71±3.12 vs. 50.90±, $P=0.075$), indicating lower anxiety levels and improved exploratory behavior (**Fig. 21B-C**). The second test conducted to examine anxiety-related behavior was the elevated plus maze. An elevated plus-shaped maze containing two dark and enclosed arms and two open and lit arms was used. Mice were placed in the center of the maze, tracked for 5 min and then returned to their home cage. Time spent in the open arms, the numbers of entries to the open arms, and latency to enter the open arms were measured. Since no significant difference was observed between male and female performance, the analysis was united

for both genders. As was observed, ED11 treatment did not result in a significant improvement in time in open arms and open arms entries (**Fig. 22A-B**). A trend toward statistically significant improvement was found when addressing latency to first open arm entry (**Fig. 22C**). Another measurement of anxiety-related behavior is done by the dark light choice test. The light–dark choice test consists of two compartments, a dark compartment and an illuminated compartment, connected by a small passage. Mice were placed in the light compartment to initiate a 5-min test session. The time spent in the dark compartment, the number of entries to the dark compartment, and the latency of entering the dark zone were measured. Time spent in the dark and number of entries to the dark compartment were not significantly different in any of the groups tested (Data not shown). However, latency to enter the dark zone is reduced in the vehicle-treated BACHD males compared to the wild-type. A possible interpretation of this data is that the vehicle-treated BACHD mice seek a dark and safe ground faster than the wild-type mice. This anxiety-related behavior is corrected by the treatment of ED11 (21.53±3.52 vs. 12.14±2.10, $P<0.05$) (**Fig. 23**)

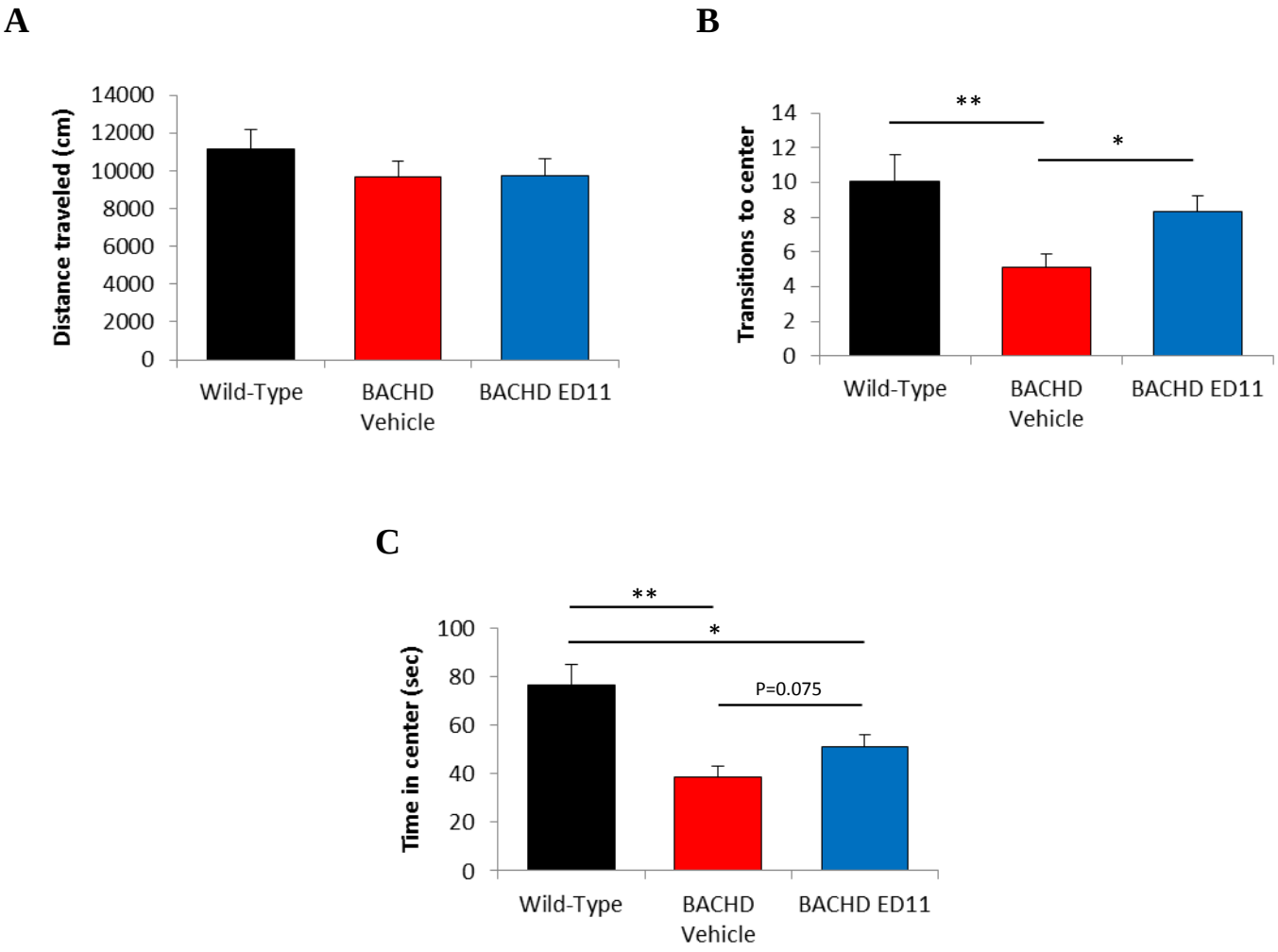

Figure 21: ED11 attenuated anxiety related behavior in open field test

Distance moved, time spent in center and transitions to center were measured in the open field test. **A.** Quantification of distance moved shows no difference between the groups. **B.** Vehicle treated BACHD show less exploratory activity as measured by no. of transitions to center. ED11 treatment attenuated this deficit. **C.** Time spent in the center is significantly less both in the vehicle treated BACHD mice and in the ED11 treated mice. Nonetheless, ED11 treatment shows a trend toward attenuation of the deficit (n=20-22).

P<0.05, **P<0.001, #P<0.05. One-way ANOVA followed by Tukey's post-hoc test. Data is presented as mean ± SEM.

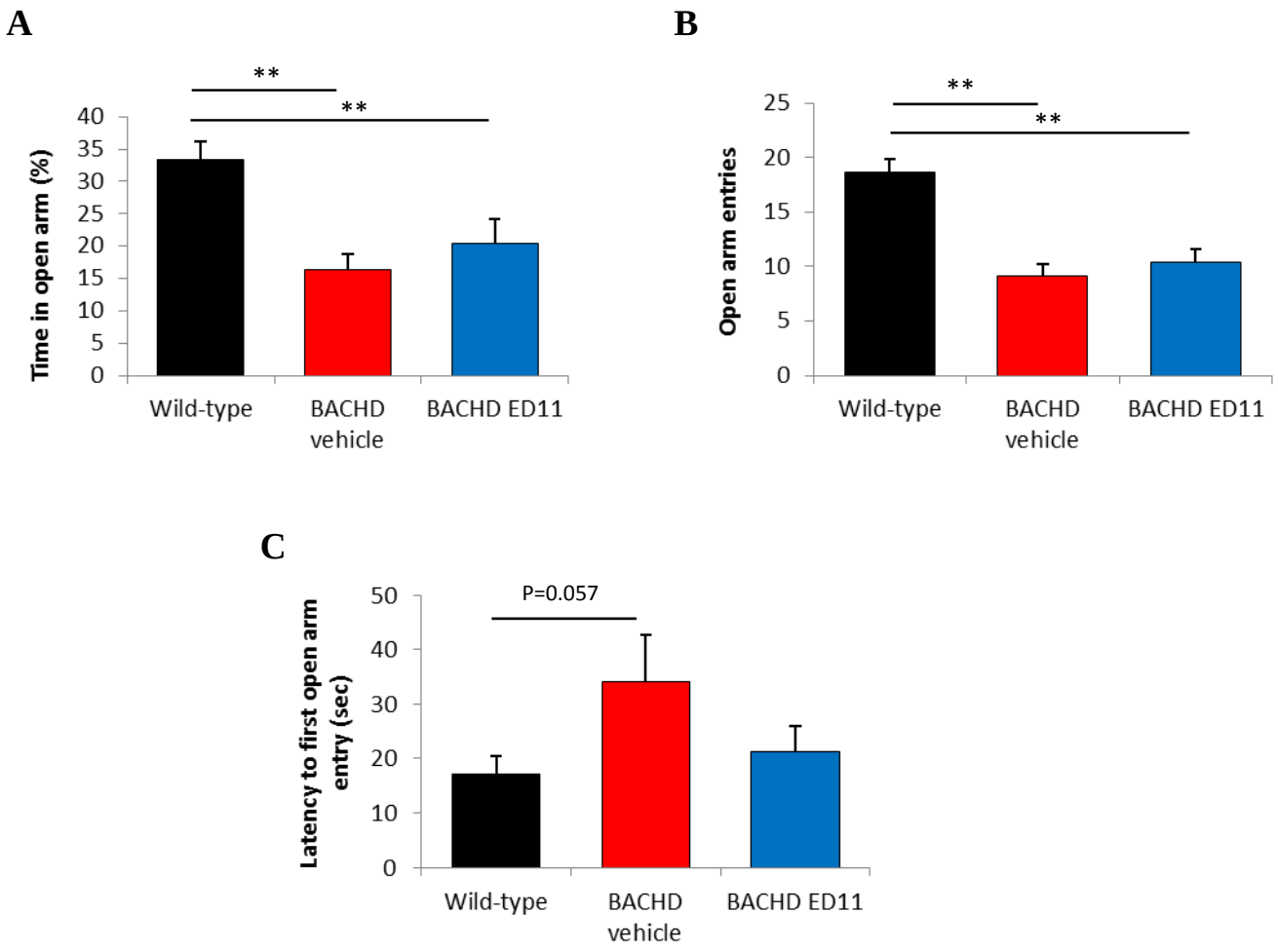

Figure 22: ED11 partly attenuated anxiety related behavior in the elevated plus maze

Time in open arms, open arms entries and latency to first open arm entry was recorded in the elevated plus maze test. **A-B.** Both treated and untreated BACHD mice spent significantly less time in the open arms and significantly made less open arm entries. **C.** While vehicle treated BACHD mice showed a trend toward higher latency to first open arm entry, ED11 treated mice did not differ significantly from the wild-type mice (n=20-22).

**P<0.001. One-way ANOVA followed by Tukey's post-hoc test. Data is presented as mean ± SEM.

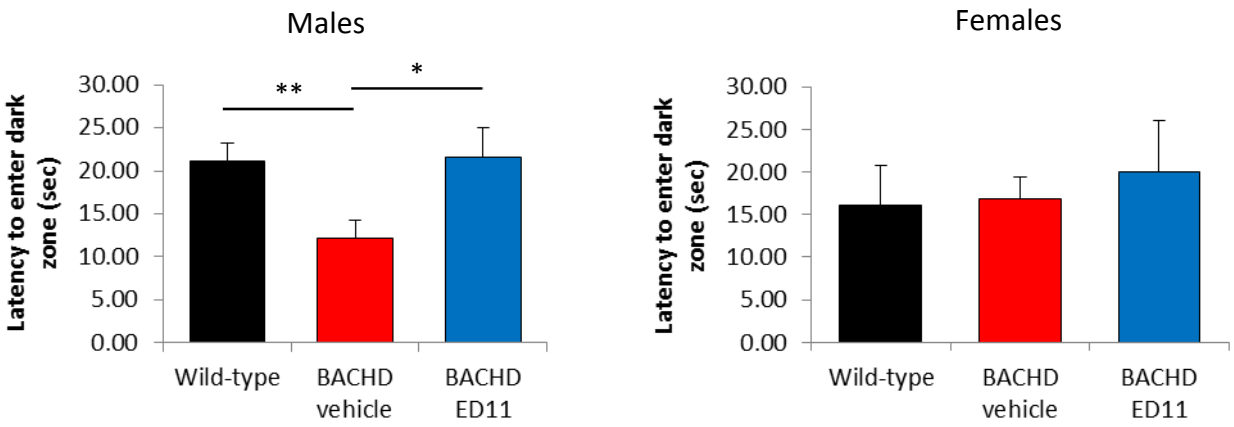

Figure 23: ED11 attenuated anxiety related behavior in the dark light choice test

Mice were placed in the light compartment and latency to enter the dark zone was measured. As was observed, latency to enter the dark zone is reduced in the vehicle treated BACHD males compared to the wild-type males. In contrary, the ED11 treated mice behavior is comparable to that of the wild-type mice (n=10-12).

*P<0.05, **P<0.001. One-way ANOVA followed by Tukey's post-hoc test. Data is presented as mean ± SEM.

5.4.3. The efficacy of ED11 treatment in-vivo in an advanced disease state

Following the demonstration of ED11 ability to provide protection from mutant Htt toxicity when the intervention is done at a very early disease state, it is important to evaluate the ability of ED11 to provide a beneficial effect in an advanced disease state. This is important in order to assess the motor and behavioral recovery rate after treatment. In addition, cognitive impairment in the BACHD mice begins at the age of 12 months, therefore examining the influence of ED11 on cognitive impairment required late intervention. To achieve this goal, treatment commenced at the age of 36 weeks. As was done in the early treatment paradigm, the mice were treated by a subcutaneously implanted mini-pump, injecting continuously at the rate of 4mg/kg/day. Three male treatment groups were tested – Wild type mice treated with vehicle (20% ddH20, 80% saline), BACHD mice treated with vehicle, and BACHD mice treated with ED11. Motor and behavioral performances were evaluated throughout this period. The experimental timeline is presented in the following diagram (**Fig. 24**).

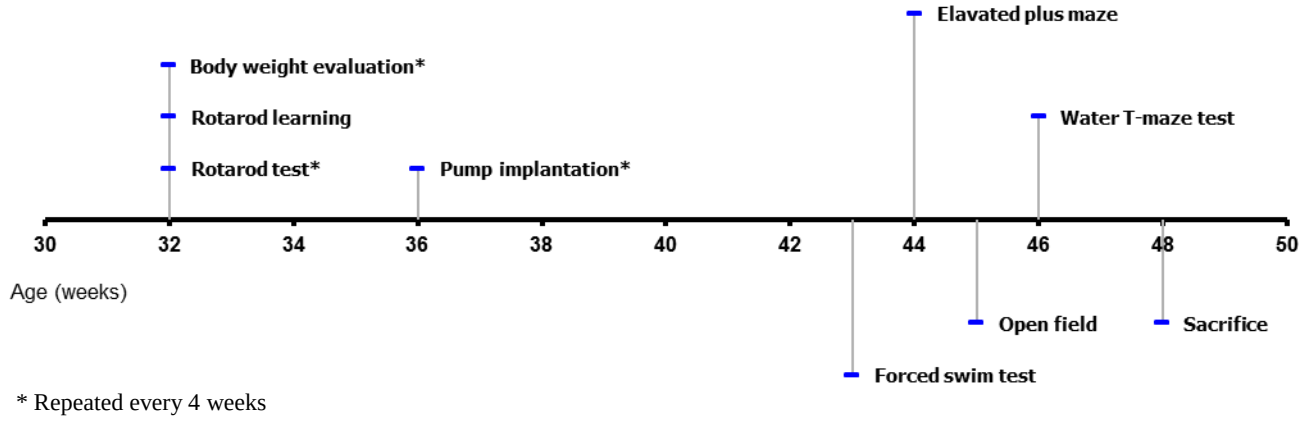

Figure 24: late treatment paradigm experimental time-line

5.4.3.1. Partial restoration of motor ability

In order to evaluate ED11 ability to influence the motor skills in an advanced disease state, the BACHD mice were divided into groups according to their baseline motor ability as was elaborated in the methods section. Treatment commenced at the age of 36 weeks, and the influence on motor performance was monitored for another 10 weeks, in a 2-week interval between tests. Measurements of latency to fall from the accelerating rod indicate that while the vehicle-treated performance remained confined to the same level throughout the testing period, the ED11 treated mice demonstrated a partial increase in Rotarod performance (**Fig. 25A**). This effect was statistically significant in relation to the BACHD mice pre-treatment state (63.98±12.16 vs. 101.20±20.53, P<0.01) (**Fig. 25B**). The results indicate ED11 was able to exert a restorative effect on the BACHD mice motor ability in a significant matter.

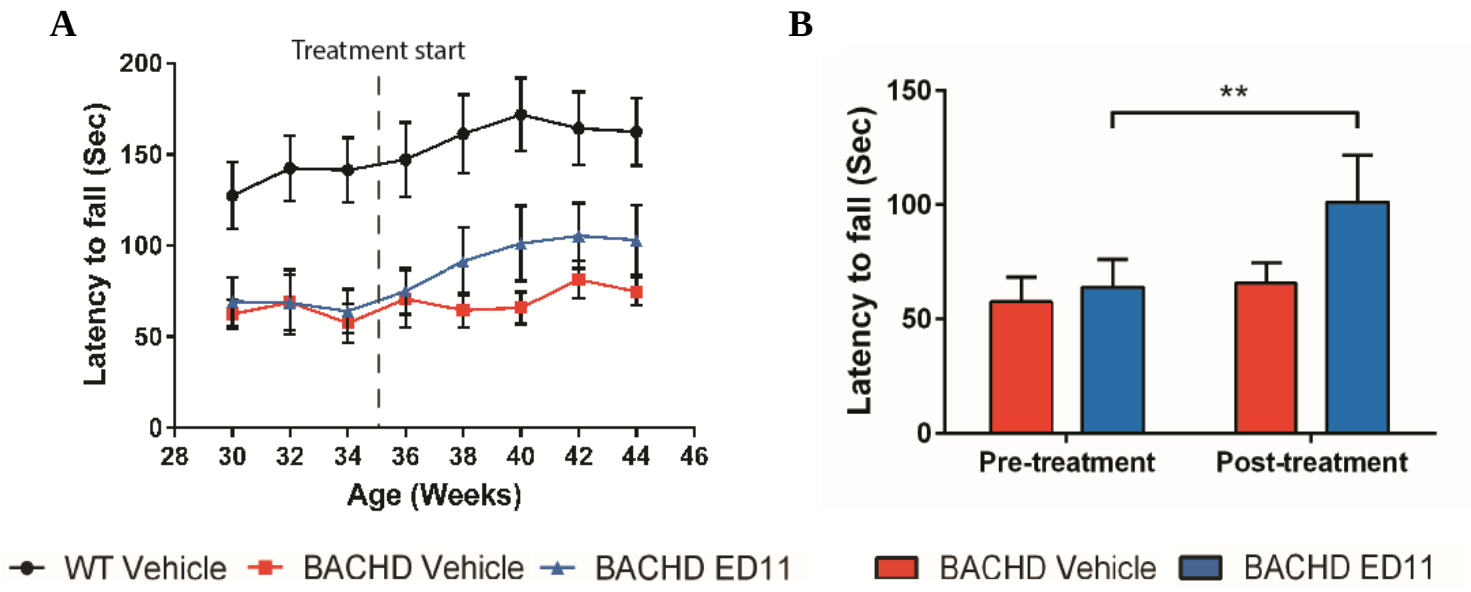

Figure 25: ED11 treatment partially restores motor function in progressive disease stage.

Determination of motor performance as measured by latency to fall from an accelerating rod. **A.** Rotarod test performed every two weeks. The time point of treatment initiation is indicated with a dashed line. **B.** The pre-treatment state was recorded at the age of 34 weeks, and post-treatment state was recorded at the age of 40 weeks, 5 weeks after treatment initiation. ED11 treatment resulted in a significant improvement in motor performance (n=9-11).

**P<0.01. Paired samples student's t-test. Data is presented as mean ± SEM.

5.4.3.2. Influence on depression-related behavior

To evaluate the effect of ED11 on the depression-related phenotype in symptomatic BACHD mice, they were tested using the FST at 11 months of age. As was observed, while vehicle-treated BACHD mice were found to be more immobile than their wild-type littermates (70.28±11.59 vs. 28.94±6.24, P<0.01), the immobility of ED11-treated mice was similar to wild-type animals, indicating a reversal of the depressive-like phenotype evidenced in the vehicle-treated BACHD mice (38.02±5.27, P<0.05) (**Fig. 26**). The effect of ED11 on the mobility state in the FST was not related to motor ability, as no correlation between motor performance in the rotarod test and time spent immobile in the FST was detected (Pearson correlation coefficient r = 0.12, P-value = 0.73, two-tailed Student's t-test).

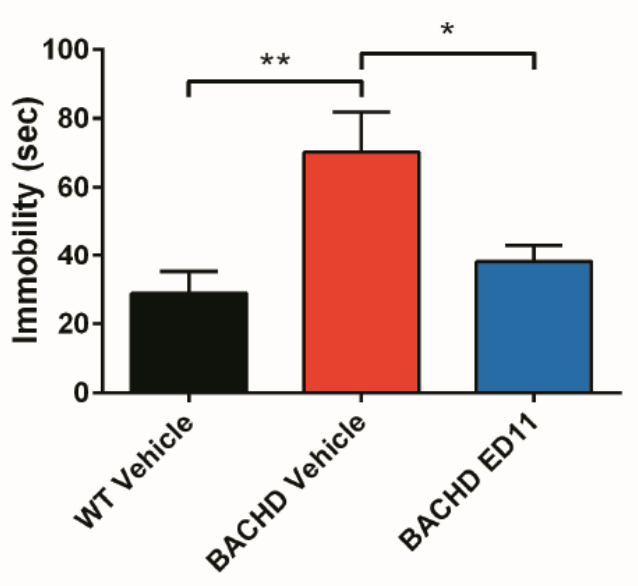

Figure 26: ED11 treatment attenuates depression-related behavior in a progressive disease stage.

The effect of ED11 on the depressive-like behavior as measured by time spent immobile in the FST. Time spent immobile in the vehicle treated BACHD was significantly higher than the wild-type group. This immobile state was normalized in the ED11-treated mice, indicating a reversal of the depressive-like phenotype (n=9-11).

*P<0.05, **P<0.01. One-way ANOVA followed by Tukey's post-hoc test. Data is presented as mean ± SEM.

5.4.3.3. Cognitive impairment alleviation

Deterioration of cognitive abilities is characteristic of HD and significantly impacts the lives of individuals with the disease. To address the possible effect of ED11 treatment on cognitive deficits also observed in the BACHD mice, we used the swimming T-maze test. On the first three days, the mice are subject to a learning period. In the learning period, a transparent platform is hidden at the end of the right arm. The mouse is placed at the stern of the T-maze 4 times a day and time to reach the hidden platform is recorded. During the 3-day learning period, all experimental groups learned to swim directly to the platform, as measured by a progressive decrease in the time to reach the target (**Fig. 27A and C**). On the fourth day, the strategy shifting ability was tested by relocating the hidden platform to the opposite arm. We found impairment in the strategy shifting ability of vehicle-treated BACHD mice, as their time to reach the hidden platform was longer than for wild-type mice (25.26±4.18s vs. 13.64±1.072s, $P<0.01$). In contrast, the performance of ED11-treated BACHD mice was comparable to their WT littermates (15.32±1.21s, $P<0.05$ compared to the vehicle-treated BACHD mice) (**Fig. 27B-C**), indicating a reversal of cognitive rigidity by ED11.

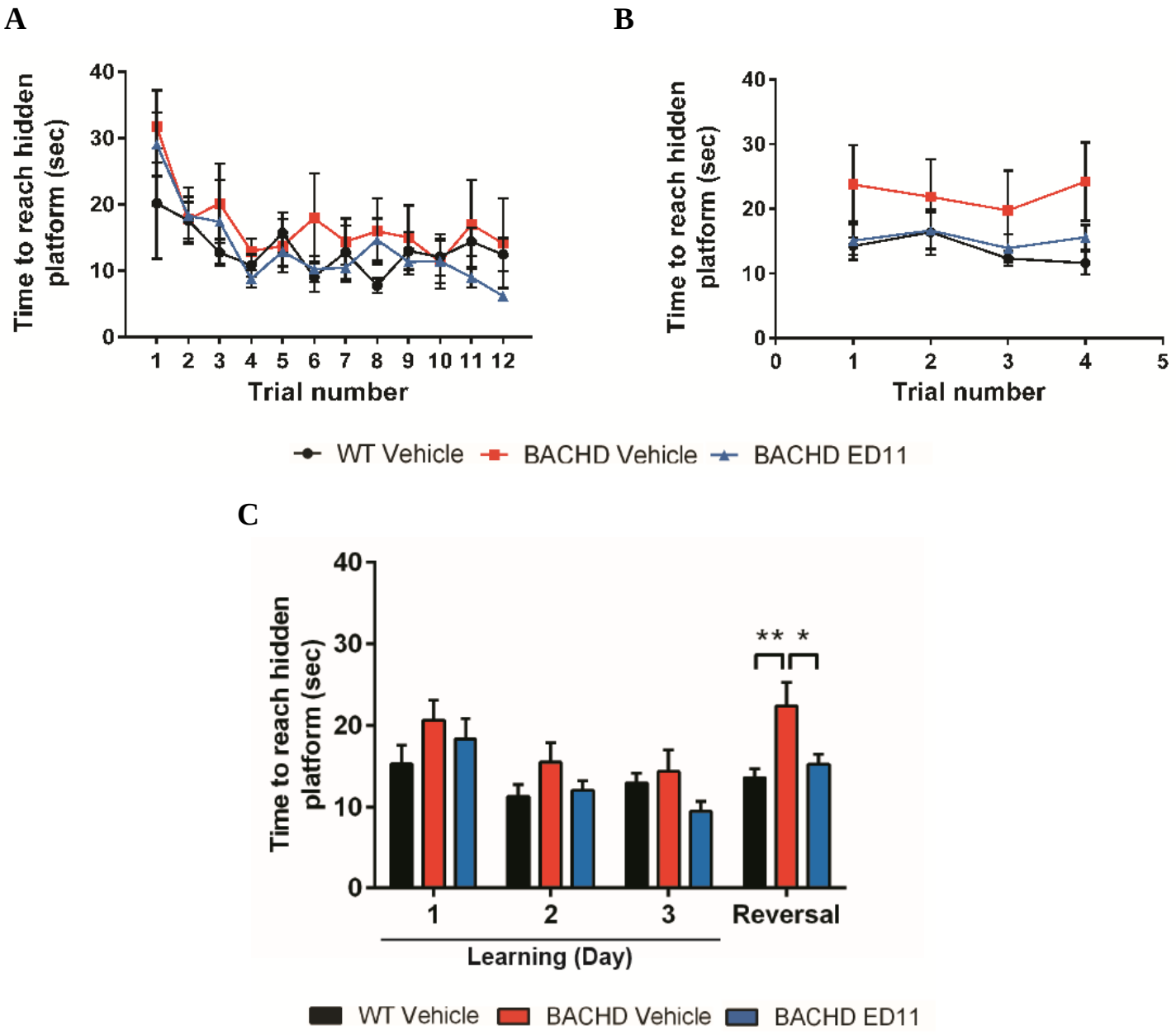

Figure 27: ED11 treatment reverses cognitive rigidity.

Strategy shifting ability was tested in the swimming T-maze test by recording the time to reach the hidden platform. **A.** During the 3-day learning phase, all experimental groups learned to swim directly to the platform. **B.** During strategy shifting tests on the fourth day, vehicle treated mice showed impaired performance compared to wild-type and ED11 treated BACHD mice. **C.** Daily averages of the time to reach the hidden platform reveals that in the reversal session, vehicle treated BACHD mice demonstrated cognitive rigidity, while ED11 treated BACHD mice performed at a similar level to the wild-type mice (n=9-11).

*P<0.05, **P<0.01. One-way ANOVA followed by Tukey's post-hoc test. Data is presented as mean ± SEM.

5.5. ED11 effect on neuropathology

After conducting efficacy studies in which protection from mutant Htt toxicity by the treatment with ED11 was evidenced, the effect of ED11 on neuropathology was evaluated. This was done by examining the effect on brain atrophy, neuronal degeneration, mutant Htt aggregation and fragmentation.

5.5.1. MRI assessment of brain atrophy

MRI volumetric measurements were performed at the age of 12 months to examine the possible effect of ED11 treatment on striatal, cortical and hippocampal atrophy. However, no significant reduction in the BACHD mice compared with WT mice has been detected (**Fig. 28**), precluding any evaluation of ED11-mediated effects on brain atrophy. This suggests that in these mice, the therapeutic intervention can be effective between the onset of HD-like behavioral phenotypes and irreversible brain atrophy.

5.5.2. Evaluation of the impact on neuronal degeneration

One of the mostly affected neuron populations in HD is the medium spiny projection neurons in the striatum. Therefore, the impact of ED11 on their level as a measure of neuronal degeneration was evaluated. To achieve this goal, 12 months old BACHD mice brain were immune-stained with antibodies against DARPP-32 levels, a marker for medium spiny projection neurons. In correlation with the brain MRI data, quantification of DARPP-32 levels showed that the BACHD mice did not show any reduction in DARPP-32 levels, precluding any evaluation of the impact of ED11 on striatal neuronal degeneration (**Fig. 29**).

A

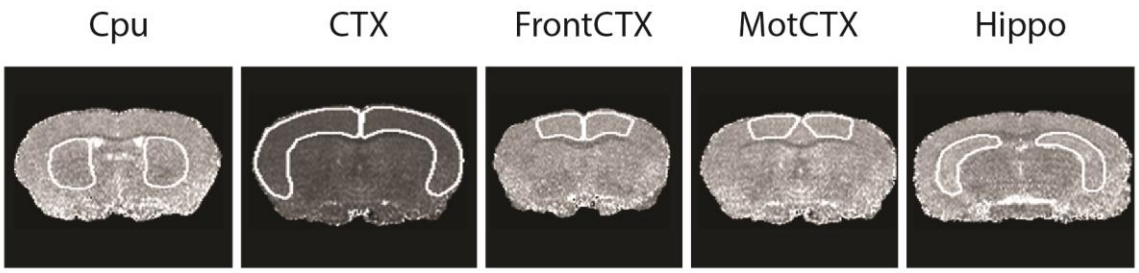

B

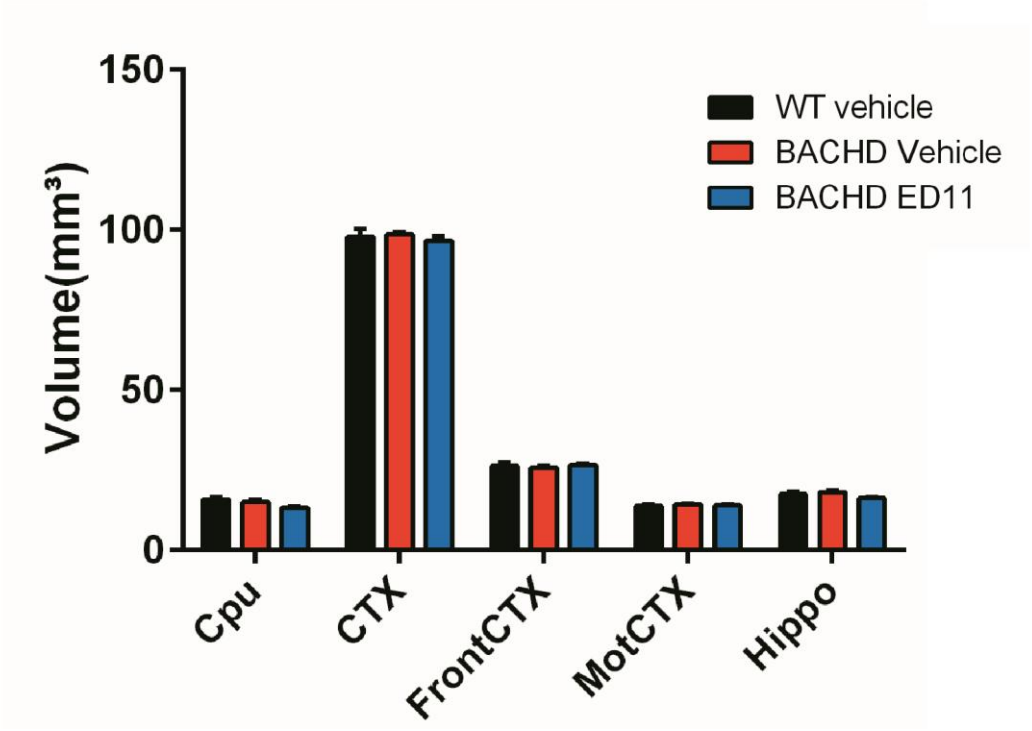

Figure 28: Evaluation of BACHD mice brain atrophy by MRI

A. Representative images obtained for volumetric analysis by MRI. A. Manual volumetric analysis for the caudate putamen (Cpu), total cortex (CTX), frontal cortex (FrontCTX) motor cortex (MotCTX) and hippocampus (Hippo). **B.** Comparison between wild-type, vehicle-treated BACHD and ED11 treated BACHD yielded no statistically significant volume differences in any of the zones tested (n=8). One-way ANOVA was followed by Tukey's post-hoc test. All data are expressed as mean ± S.E.M.

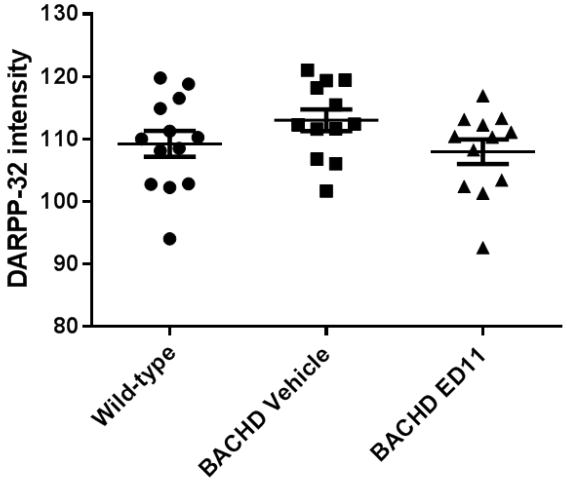

Figure 29: Evaluation of DARPP-32 levels in the BACHD mice striatum

Quantification of DARPP-32 levels in striatal brain sections demonstrates no significant difference between the groups in DARPP levels (n=11-12).

Data is presented as mean ± SEM including individual subject data.

5.5.3. Influence of ED11 treatment on aggregates formation

Aggregate formation is one of HD hallmarks. Therefore, evaluation of ED11 influence on aggregate formation was conducted. First, immunohistochemistry studies on mice brains were conducted. The S830 antibody was used, which in previous reports have been shown to stain aggregates in the BACHD mice[60]. When the BACHD cohort used in our study was tested, no increase in immunohistochemistry staining over the background staining that was also observed in wild-type mice was detected (**Fig. 30A-B**), both in the early treatment paradigm and the late treatment paradigm. To further clarify the influence of ED11 on mutant Htt aggregates, the filter trap assay method was used. Cortical protein lysates were vacuumed through a cellulose acetate membrane in order to trap the aggregates. The membrane was then stained with the 1C2 antibody, which is directed at the glutamine repeats of mutant Htt. It was observed that while BACHD brain lysates demonstrated a significant increase in signal intensity, indicating the abundance of mutant Htt aggregates, the ED11 treated mice demonstrated a mixed pattern, in which lowering of mHtt aggregates level was observed for some but not all the late treated mice (**Fig. 31A-B**).

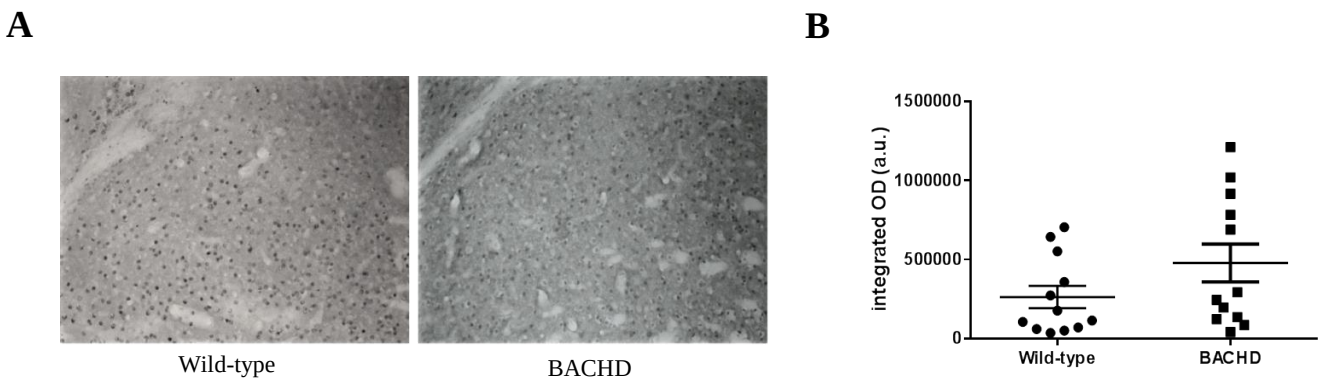

Figure 30: No specific mutant Htt aggregate staining by S830 antibody in BACHD striatum.

A. Brain sections from BACHD mice and their wild-type littermates were subjected to immunohistochemical staining with the S830 antibody after antigen retrieval according to published protocols[60]. **B.** Microscopic analysis, as well as densitometry quantification, revealed no specific mutant Htt aggregate staining in BACHD animals compared to wt. Magnification: 20x, striatum. Data is presented as mean ± SEM including individual subject data (n=12).

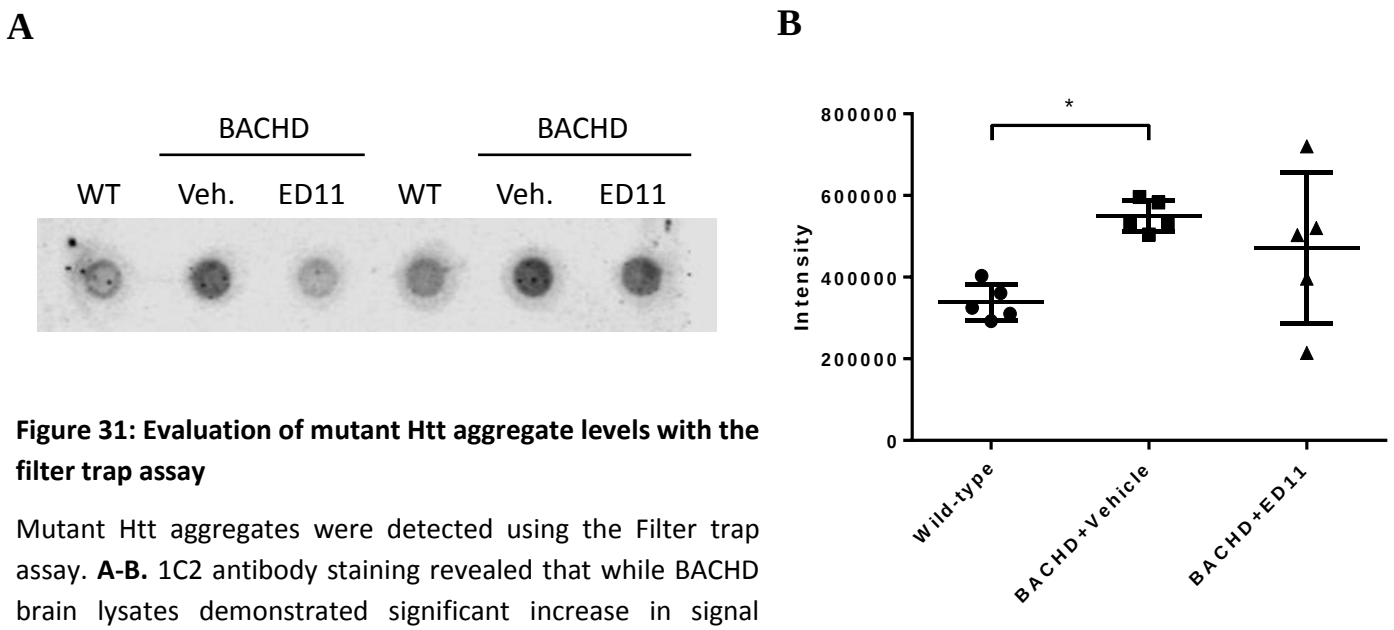

Figure 31: Evaluation of mutant Htt aggregate levels with the filter trap assay

Mutant Htt aggregates were detected using the Filter trap assay. **A-B.** 1C2 antibody staining revealed that while BACHD brain lysates demonstrated significant increase in signal intensity, indicating the abundance of mHtt aggregates (n=5), the ED11 treated mice demonstrated a mixed pattern.*P<0.05, one-way ANOVA followed by Tukey's post-hoc test. Data is presented as mean ± SEM.

5.5.4. Influence of ED11 on mutant Huntingtin fragmentation levels

An important issue to be addressed is the influence of ED11 on human mutant Htt fragmentation levels by caspase-6 in-vivo. Unfortunately, the analysis of Htt fragments in vivo, and in particular the 586aa fragment, is hampered by the fact that this fragment is of very low abundance in brain tissues[58,174]. Therefore, we were unable to detect a corresponding fragment in the 6 month old and 12 months old BACHD animals used in the current study (**Fig. 32**).

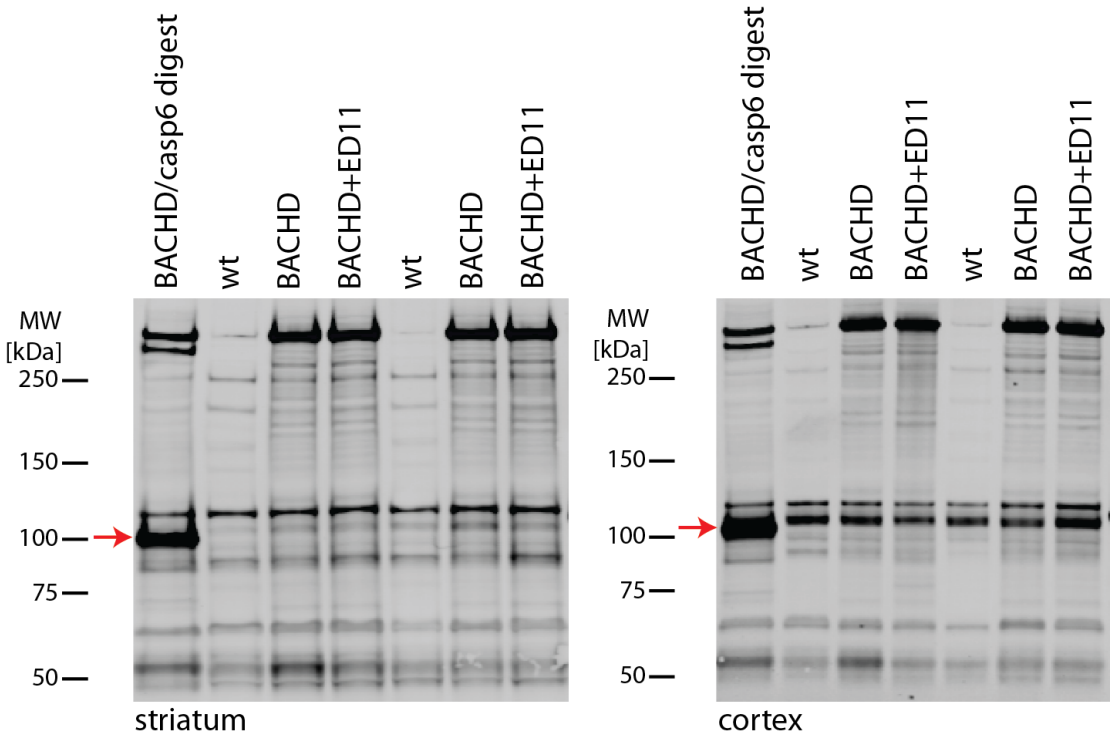

Figure 32: The mHtt-586 fragment is not detected in BACHD brain lysates.

Striatal and cortical lysates from BACHD mice with/without ED11 treatment and their wild-type littermates were subjected to Western blot analysis with the 1C2 antibody. As a control, BACHD lysates were digested with caspase-6 enzyme in vitro to generate the mHtt-586 fragment (red arrows). No bands corresponding in size to mHtt-586 and specific to BACHD animals were identified, indicating that the levels of this protein fragment are below detection level in the BACHD samples.

6. Discussion

6.1. Peptide concept and design

In this study, we addressed the potential of mutant Htt proteolysis regulation in HD therapy. The first goal was to design a peptide that would act as a modulator of caspase-6 activity. To this end, amino acids around the cleavage site of the native Htt protein were selected as the proposed inhibitor of the caspase-6 recognition site. While the use of a native caspase substrate sequence as an inhibitor of caspase activity has long been established, the method typically involves chemically attached chemical groups to increase caspase binding affinity. Due to the hydrophilic nature of these inhibitors, however, this group not only increases affinity to the caspase, but also leads to the lack of selectivity as well as the lack of blood-brain barrier penetration. These characteristics drove us to pursue a more subtle approach. Our approach might suffer a disadvantage in the form of the risk that a native peptide could be cleaved by natural proteolytic enzymes, thus causing the peptide to possess short in-vivo half-life properties. This aspect was taken into accounted when deciding on the method of drug administration to be used in this study. Nonetheless, any future development of ED11 as a therapeutic compound, will necessitate testing the pharmacokinetic properties of the peptide and potentially also modifying the composition of the peptide. To address the issue of cell and nuclear penetration, and the blood-brain barrier penetration, the TAT (48-60) sequence was utilized because it has been proven in the past that it facilitates efficient cellular and nuclear penetration as well as transportation through the blood-brain barrier, without causing apparent toxic effects[167-169]. The exact mechanism by which the CPP enables

cellular penetration is complex and still under investigation. While no FDA-approved drug contains this TAT sequence, the application of compounds conjugated to the TAT peptide in clinical trials is underway[179], indicating that the use of TAT peptides as CPP is likely to be feasible in clinical settings in the near future.

6.2. Caspase inhibition potency, selectivity, and safety considerations

To gain preliminary proof of concept for our approach, we tested whether ED11 can directly inhibit caspase-6 proteolysis of a luminescence-based activity probe in in-vitro enzymatic reaction study. Indeed, ED11 was shown to inhibit the reaction in a dose-dependent matter. Next, we have shown that the ED11 active site is dependent on the amino acids conserved for caspase-6 recognition. The replacement of amino acids within the recognition site succeeded in deactivating the effect of ED11. This is an important observation eliminating any contention that the effect of ED11 is mediated by allosteric inhibition mechanisms within the reaction. The fact that changing the caspase-6 active site recognition influences inhibition capability implies that ED11 operates by inhibiting the caspase-6 active site.

Selectivity properties of ED11 were first tested against caspase-3, since this cross-reactivity has been reported as a common feature of caspase-6 inhibitors[173]. The selectivity of ED11 for caspase-6 over caspase-3 was established by luminescence-based probe and protein proteolysis tests. This is the first time such selectivity is reported, and indeed, it is very encouraging given implications to safety considerations, since caspase-3 knockout is not compatible with life due to the vital role caspase-3 activity plays in normal physiologic processes[171].

After testing the general effect of ED11 on caspase-6 activity, it was also imperative to test the efficacy of ED11 inhibition on human Htt caspase-6 cleavage. A comparison was conducted between the pan-caspase inhibitor zVAD-FMK, a most potent synthetic inhibitor, and ED11 effect on human Htt cleavage. Calculated IC50 values indicated that ED11 inhibits human Htt cleavage by caspase-6 with high competency, comparable to that of the covalently binding synthetic inhibitor zVAD-FMK. This observation is significant to the therapeutic potential of compounds because it indicates that ED11 can prevent human Htt cleavage in relatively minor concentrations, a factor that may play into safety considerations by increasing therapeutic concentration window. Inhibition of human Htt cleavage was then assessed for caspases 1-10, for both further elucidation of ED11 selectivity and the evaluation of the overall effect of ED11 on human Htt caspase cleavage. This was feasible as following the recent discovery of Professor Michael Hayden's laboratory that Htt can be cleaved by caspases 1-10 in-vitro (unpublished data). We found that in addition to caspase-6, to a lesser degree, ED11 also inhibits the activity of caspase 1, 2, and 10 but increases caspase-5-mediated human Htt cleavage. For most of these caspases, the in-vivo relevance of their Htt cleavage processes, as well as their contribution to HD pathogenesis, remains unknown. Notwithstanding, the inhibition of caspase-2 mediated human Htt cleavage by ED11 may contribute to the preservation and improvement of in-vivo behavioral functionality, since the ablation of this enzyme has been associated with therapeutic benefits in YAC128 mice[180]. Data is limited regarding the safety of caspase-1, caspase-2, and caspase-10 inhibition, although it has been shown that caspase-1 knockout influences inflammatory processes[81] and caspase-2 knockout

influence reactions to chemotherapeutic drugs[82]. Future studies may further elucidate this cross-reactivity influence on drug safety.

6.3. Intra-cellular human mutant Huntingtin proteolysis regulation

A fundamental issue in therapeutic processes is the ability of a compound to penetrate cellular membranes. The TAT (48-60) sequence enables the ED11 peptide to transport through the cellular membrane, as shown by immunofluorescence using an antibody against the TAT sequence. We demonstrated ED11 safety in terms of influence on basal cell activity in that ED11 does not affect viability, proliferation, or cell cycle status in basal conditions. This aspect of caspase inhibition is considered essential since caspases usually play a role in normal cellular functions, and their inhibition may result in cellular dysfunction. The absence of influence on basal cellular properties may originate in the fact that ED11 mainly affects caspase-6. Caspase-6 is found to be active in a progressive manner primarily during two periods in life, the embryonic period and throughout the aging process. Therefore, the cell's homeostasis may remain unchanged in the presence of ED11 when devoid of meaningful cellular stress.

Next, ED11 was found to significantly reduce intracellular caspase-6 human Htt cleavage, indicating that the inhibitory effect of ED11 occurs in a cellular environment. The intra-cellular activity of ED11 suggests that it does not interact with other proteins in cells that deactivate its inhibition activity, enabling it to exert its action on the caspase-6 cleavage of Htt. Functional outcome of human mutant Htt cleavage was tested by measuring the viability of inducible human 145Q-mHtt expressing PC12 cells, after treatment with ED11. The preservation of cell function with ED11 demonstrates the link

between inhibiting mutant Htt cleavage and protecting against cell dysfunction. These findings correlate with earlier reports that linked mutant Htt caspase cleavage inhibition and the preservation of cellular viability and function[83].

In addition to the effect on cell function, we have measured the effect of ED11 treatment on caspase activity in the inducible human 145Q-mHtt expressing PC12 cells. According to the toxic fragments theory, human mutant Htt leads to the activation of toxic cellular pathways, which leads to activation of caspases and the subsequent additional instigation of toxic pathways. Measurements of caspase activity following ED11 treatment indicate that the treatment resulted in the normalization of caspase activity, suggesting that ED11 was able to break the vicious cycle described by the toxic fragment theory. Inhibition of human mutant Htt proteolysis may therefore provide additional benefit by preventing excess activation of other caspases.

6.4. Protection against human mutant Huntingtin toxicity in-vivo

The first step in evaluating in-vivo efficacy of ED11 treatment was to demonstrate blood-brain penetration ability. The dynamic and complex blood-brain barrier is formed by endothelial cells that deny the transportation of undesired substances from the blood circulation into the CNS. Blood-brain penetration, then, is important in testing the effect of therapeutic compounds on CNS-related pathologies. Using novel in-vivo fluorescence methods, we detected FITC tagged ED11 penetration into the brain parenchyma, a penetration ability that was not found when using ED11 that lacks the TAT sequence. This data correlates with data acquired in numerous other studies that employed both negative and positive control regarding compounds containing TAT sequences[167,181,182].

Since the data presented in this study is of qualitative nature rather than quantitative, future studies are required to further confirm these results. For example, by employing LC-MS/MS or proteomic methods.

BACHD mice were selected to evaluate the in-vivo potency of human mutant Htt proteolysis regulation. These mice express the full-length human mutant Htt and exhibit behavioral deficit that correlates with HD. Due to the inherent short half-life of peptides when administrated to living animals, we opted to use a continuous delivery method. Considering the need for the long-term treatment required by the chronic nature of HD, we used the subcutaneous injection mode of delivery for the compound. Alzet mini-pumps were thus injected subcutaneously, continuously delivering the tested substrate. The first paradigm tested was the early, pre-symptomatic treatment, which was conducted to establish the neuro-protective properties of ED11. In addition, pre-symptomatic treatment is relevant for HD because it is one of the few diseases that is detectable by genetic methods prior to its eruption, thereby enabling commencement of treatment prior to the onset of symptoms. Treatment with ED11 enabled the attenuation of body weight alteration in the BACHD mice. Although HD patients typically demonstrate a progressive decrease in body weight[175], the BACHD mice show an increase this parameter. This discrepancy is explained by the modulation of weight gain by human Htt and human mutant Htt in different tissues[148,149]. The fact that ED11 is able to prevent this excess body weight gain correlates with previous data obtained from studies conducted with caspase-6 knockout BACHD mice[60]. Since the corrected body weight may influence results of other tests in a dependent manner[183], we verified the independency between

body weight and other test results using sample matching by body weight and correlation analysis.

HD patients present motor learning skill deficiency, which is considered to be mediated by striatal dysfunction[176]. In our study, we have shown that the treatment with ED11 in BACHD mice caused marked preservation of motor learning skills in mice treated pre-symptomatically. In fact, we found that in five months of treatment, ED11 allowed for the preservation of motor function in BACHD mice at a level comparable to that of wild-type mice. The effect of long-term treatment was therefore continuous, influencing the chronic mutant Htt toxicity in an adequate manner. This observation suggests that the influence of ED11 in the BACHD mouse model is directed at an early process in disease pathogenesis, since it influenced the result of a variety of pathogenic mechanisms. For example, motor learning skill is perceived to be mediated by the basal ganglia. Therefore, the influence of ED11 treatment on this feature supports the argument that human mutant Htt proteolysis regulation maintains striatal function.

Long-term motor function deficit in HD is also considered to involve CNS dysfunction resulting from anatomic, metabolic, and synaptic mechanisms[184-187] as well as peripheral skeletal muscle tissue in both patients and mouse models of the disease[57].

Neuropsychiatric symptoms, such as obsessions, apathy, depressed mood, irritability, and anxiety also contribute to the functional decline of HD patients[177,178]. Depression-related behavior was tested in the BACHD mice using the FST test, which has been used for years as a gauging tool to evaluate depressive behaviors and test compounds with anti-depressant activity[188]. We found that ED11 treatment suppressed depressive-like activity

in the BACHD mice. This result can indicate that the influence of ED11 on human mutant Htt toxicity can help relieve the intensity of neuropsychiatric symptoms. The precise mechanism of depression is unclear and still under investigation, but the fact that ED11 influenced this feature helps support the notion that the influence on mutant Htt toxicity protects from the neuronal dysfunction associated with neuropsychiatric symptoms in HD. To assess anxiety-related behavior, we tested the effect of ED11 on BACHD performance in three stressful environments[189]: open-field, EPM, and dark-light choice. In the open-field and in the dark-light choice tests, non-treated BACHD behaved in a significantly more anxious manner compared to treated or wild-type mice. This effect was less significant in the EPM test. The influence on neuropsychiatric symptoms correlates with previous data, in which the prevention of mutant Htt proteolysis with either genetic mutation or caspase-6 knockout resulted in the attenuation of neuropsychiatric related symptoms[163,174].

6.5. HD treatment at an advanced state of disease

Since HD is a progressive disorder, it is imperative to understand the effect of treatment at a stage in which disease symptoms have already erupted. At this stage, the desired treatment effects would be the restoration of disabilities and/or protection from further deterioration. We therefore designed a post-symptomatic treatment paradigm to test the influence of treatment with ED11 on disease progression and determine the potential of recovery from disease manifestations.

ED11 treatment resulted in significant motor performance recovery compared to the pre-treatment stage. Our data correlates with previous data regarding the recovery potential of

motor functions in an HD mouse model that was engineered to conditionally discontinue mutant Htt expression. The inactivation of gene expression resulted in the recovery of motor ability even at advanced disease stages. Interestingly, motor function recovery in these mice also occurred in the presence of neuronal loss, suggesting that functional motor ability is conserved even after a significant loss of striatal neurons has taken place[190,191].

We found that not only can motor functions be improved at a progressive disease stage, but depressive-like behavior can also be reversed at this stage, as manifested by the fact that late-treated ED11 BACHD mice demonstrated lower depressive-like behavior in the FST. Cognitive deficits characterize early stages of HD, and symptoms worsen throughout the course of the disease. In particular, clinical investigation in HD patients has revealed impairment in shifting strategy cognitive tests[192]. Since the BACHD mouse model demonstrates this cognitive deficit at an advanced stage of the disease[154], we tested cognitive performance in late-treated BACHD mice. BACHD mice treated with ED11 scored higher on performance tests for strategy shifting ability, attesting to the role of protection from human mutant Htt toxicity in preserving cognitive function.

6.6. Neuropathology

Neuroimaging techniques have played an important role in characterizing structural and functional changes in the brain during both asymptomatic and symptomatic stages of the disease. Structural MRI has been shown to provide evidence on brain atrophy in numerous studies in HD patients as well as in HD mouse models [193,194]. We therefore used the MRI technique using to elucidate the impact of ED11 treatment on brain atrophy

of BACHD mice. We did not, however, observe any significant changes in vehicle-treated BACHD mice compared to wild-type animals at 12 months of age, suggesting that in these mice, a window for therapeutic intervention exists between the onset of HD-like behavioral phenotypes and irreversible brain atrophy. We were therefore unable to determine whether treatment with ED11 after brain atrophy is feasible.

Due to the absence of striatal, cortical, or hippocampal atrophy in our BACHD cohort, we were also unable to evaluate the effects of ED11 on the prevention of brain atrophy. We tested neuronal loss in HD as a measurement of DARPP-32, a dopamine and cyclic AMP-regulated neuronal phosphoprotein found on MSN, which is primarily affected in HD. No differences were recorded in DARPP-32 levels between BACHD and wild-type mice, hence no conclusions can be offered regarding the impact of ED11 on MSN degeneration.

Aggregation of mutant Htt protein fragment is a hallmark of HD. However, the question whether the aggregate formation is a protective or a harmful process is still debatable[195,196]. To detect the level of aggregation, we used both direct immunohistochemistry and filter trap assay. While no detection of aggregates was evident by immunohistochemistry, the filter trap assay did reveal aggregates in the BACHD mice. Treatment by ED11 resulted in a mixed pattern, as no significant variance was evident between the treated BACHD group and the wild-type or vehicle-treated group. Therefore, we were unable to determine the influence of ED11 on aggregate formation.

Finally, we set to examine the impact of ED11 on caspase-6 cleavage of human mutant Htt in-vivo. The analysis of human Htt fragments in-vivo, and in particular the 586aa fragment, is hampered by the low prevalence of this fragment in brain tissues[58,174]. Previous studies on this fragment have been performed in YAC128 mice, where a weak band corresponding to mHtt-586 was detected with antibody 1C2. Unfortunately, we were unable to detect a corresponding fragment in the BACHD mice used in the current study.

7. Conclusions

The research study presented here elucidated the potential of targeting mutant Htt proteolysis by caspase-6 as a therapeutic strategy for HD. This was done using a peptide based on Htt caspase-6 cleavage site that serves as an inhibitor of caspases-6 activity. The therapeutic potential of the peptide was evidenced by its ability to directly inhibit caspase-6 activity. Evidence was gathered that the peptide is specific and selective. The peptide proved to be competent in reducing Htt proteolysis in both the in-vitro enzymatic reaction studies and the intra-cellular environments. The Intra-cellular safety was established, and the potential of the peptide to protect cells from mutant Htt toxicity was demonstrated. In-vivo blood-brain barrier penetration was confirmed, and the alleviation of behavioral phenotype in HD mouse model was revealed in both early and late treatment paradigms. This alleviation appears to be unrelated to protection from brain atrophy or aggregate formation.

Our study demonstrates that the use of substrate-based peptides is a feasible concept in the inhibition of caspase-mediated protein cleavage for therapeutic purposes. Further studies are required to translate our findings from animal models to HD patients. In addition, our findings might be applicable to other neurodegenerative or neurological diseases where caspase-6 activity plays a part in the pathogenic process. We truly hope that in the future, data generated by this research study will help to ease the suffering of HD patients.

8. References

1. Ross CA, Tabrizi SJ. Huntington's disease: From molecular pathogenesis to clinical treatment. *Lancet Neurol*. 2011;10(1):83-98.

2. Dorsey ER, Beck CA, Darwin K, et al. Natural history of huntington disease. *JAMA Neurol*. 2013;70(12):1520-1530.

3. Rosenblatt A. Neuropsychiatry of huntington's disease. *Dialogues Clin Neurosci*. 2007;9(2):191-197.

4. Politis M, Pavese N, Tai YF, Tabrizi SJ, Barker RA, Piccini P. Hypothalamic involvement in huntington's disease: An in vivo PET study. *Brain*. 2008;131(Pt 11):2860-2869.

5. Quarrell O, O'Donovan KL, Bandmann O, Strong M. The prevalence of juvenile huntington's disease: A review of the literature and meta-analysis. *PLoS Curr*. 2012;4:e4f8606b742ef3.

6. Reiner A, Albin RL, Anderson KD, D'Amato CJ, Penney JB, Young AB. Differential loss of striatal projection neurons in huntington disease. *Proc Natl Acad Sci U S A*. 1988;85(15):5733-5737.

7. Ferrante RJ, Gutekunst CA, Persichetti F, et al. Heterogeneous topographic and cellular distribution of huntingtin expression in the normal human neostriatum. *J Neurosci*. 1997;17(9):3052-3063.

8. Ferrante RJ, Kowall NW, Beal MF, Martin JB, Bird ED, Richardson EP,Jr. Morphologic and histochemical characteristics of a spared subset of striatal neurons in huntington's disease. *J Neuropathol Exp Neurol*. 1987;46(1):12-27.

9. Kassubek J, Juengling FD, Kioschies T, et al. Topography of cerebral atrophy in early huntington's disease: A voxel based morphometric MRI study. *J Neurol Neurosurg Psychiatry*. 2004;75(2):213-220.

10. Sieradzan KA, Mann DM. The selective vulnerability of nerve cells in huntington's disease. *Neuropathol Appl Neurobiol*. 2001;27(1):1-21.

11. Rosas HD, Koroshetz WJ, Chen YI, et al. Evidence for more widespread cerebral pathology in early HD: An MRI-based morphometric analysis. *Neurology*. 2003;60(10):1615-1620.

12. Rosas HD, Hevelone ND, Zaleta AK, Greve DN, Salat DH, Fischl B. Regional cortical thinning in preclinical huntington disease and its relationship to cognition. *Neurology*. 2005;65(5):745-747.

13. Rosas HD, Tuch DS, Hevelone ND, et al. Diffusion tensor imaging in presymptomatic and early huntington's disease: Selective white matter pathology and its relationship to clinical measures. *Mov Disord*. 2006;21(9):1317-1325.

14. Wolf RC, Thomann PA, Thomann AK, et al. Brain structure in preclinical huntington's disease: A multi-method approach. *Neurodegener Dis*. 2013;12(1):13-22.

15. Andre R, Scahill RI, Haider S, Tabrizi SJ. Biomarker development for huntington's disease. *Drug Discov Today*. 2014;19(7):972-979.

16. MacDonald ME, Ambrose CM, Duyao MP, et al. A novel gene containing a trinucleotide repeat that is expanded and unstable on huntington's disease chromosomes. *Cell*. 1993;72(6):971-983.

17. Zuccato C, Valenza M, Cattaneo E. Molecular mechanisms and potential therapeutical targets in huntington's disease. *Physiol Rev*. 2010;90(3):905-981.

18. Godin JD, Colombo K, Molina-Calavita M, et al. Huntingtin is required for mitotic spindle orientation and mammalian neurogenesis. *Neuron*. 2010;67(3):392-406.

19. Albin RL, Young AB, Penney JB, et al. Abnormalities of striatal projection neurons and N-methyl-D-aspartate receptors in presymptomatic huntington's disease. *N Engl J Med*. 1990;322(18):1293-1298.

20. Arrasate M, Mitra S, Schweitzer ES, Segal MR, Finkbeiner S. Inclusion body formation reduces levels of mutant huntingtin and the risk of neuronal death. *Nature*. 2004;431(7010):805-810.

21. Miller J, Arrasate M, Shaby BA, Mitra S, Masliah E, Finkbeiner S. Quantitative relationships between huntingtin levels, polyglutamine length, inclusion body formation, and neuronal death provide novel insight into huntington's disease molecular pathogenesis. *J Neurosci*. 2010;30(31):10541-10550.

22. Dunah AW, Jeong H, Griffin A, et al. Sp1 and TAFII130 transcriptional activity disrupted in early huntington's disease. *Science*. 2002;296(5576):2238-2243.

23. Stack EC, Dedeoglu A, Smith KM, et al. Neuroprotective effects of synaptic modulation in huntington's disease R6/2 mice. *The Journal of Neuroscience*. 2007;27(47):12908-12915.

24. Tang T, Slow E, Lupu V, et al. Disturbed Ca2+ signaling and apoptosis of medium spiny neurons in huntington's disease. *Proceedings of the National Academy of Sciences of the United States of America*. 2005;102(7):2602-2607.

25. Leavitt BR, van Raamsdonk JM, Shehadeh J, et al. Wild-type huntingtin protects neurons from excitotoxicity. *J Neurochem*. 2006;96(4):1121-1129.

26. Cattaneo E, Zuccato C, Tartari M. Normal huntingtin function: An alternative approach to huntington's disease. *Nat Rev Neurosci*. 2005;6(12):919-930.

27. Thornberry NA, Rano TA, Peterson EP, et al. A combinatorial approach defines specificities of members of the caspase family and granzyme B. functional relationships established for key mediators of apoptosis. *J Biol Chem*. 1997;272(29):17907-17911.

28. Wei Y, Fox T, Chambers SP, et al. The structures of caspases-1, -3, -7 and -8 reveal the basis for substrate and inhibitor selectivity. *Chem Biol*. 2000;7(6):423-432.

29. Talanian RV, Quinlan C, Trautz S, et al. Substrate specificities of caspase family proteases. *Journal of Biological Chemistry*. 1997;272(15):9677-9682.

30. McIlwain DR, Berger T, Mak TW. Caspase functions in cell death and disease. *Cold Spring Harbor Perspectives in Biology*. 2013;5(4).

31. Goldberg YP, Nicholson DW, Rasper DM, et al. Cleavage of huntingtin by apopain, a proapoptotic cysteine protease, is modulated by the polyglutamine tract. *Nat Genet*. 1996;13(4):442-449.

32. Wellington CL, Hayden MR. Caspases and neurodegeneration: On the cutting edge of new therapeutic approaches. *Clin Genet*. 2000;57(1):1-10.

33. Hackam AS, Hodgson JG, Singaraja R, et al. Evidence for both the nucleus and cytoplasm as subcellular sites of pathogenesis in huntington's disease in cell culture and in transgenic mice expressing mutant huntingtin. *Philos Trans R Soc Lond B Biol Sci*. 1999;354(1386):1047-1055.

34. Li SH, Li XJ. Aggregation of N-terminal huntingtin is dependent on the length of its glutamine repeats. *Hum Mol Genet*. 1998;7(5):777-782.

35. Wheeler VC, Gutekunst CA, Vrbanac V, et al. Early phenotypes that presage late-onset neurodegenerative disease allow testing of modifiers in hdh CAG knock-in mice. *Hum Mol Genet*. 2002;11(6):633-640.

36. Ratovitski T, Nakamura M, D'Ambola J, et al. N-terminal proteolysis of full-length mutant huntingtin in an inducible PC12 cell model of huntington's disease. *Cell Cycle*. 2007;6(23):2970-2981.

37. Wellington CL, Ellerby LM, Leavitt BR, Roy S, Nicholson DW, Hayden MR. Huntingtin proteolysis in huntington disease. *Clinical Neuroscience Research*. 2003;3(3):129-139.

38. Hackam AS, Singaraja R, Zhang T, Gan L, Hayden MR. In vitro evidence for both the nucleus and cytoplasm as subcellular sites of pathogenesis in huntington's disease. *Hum Mol Genet*. 1999;8(1):25-33.

39. Li SH, Lam S, Cheng AL, Li XJ. Intranuclear huntingtin increases the expression of caspase-1 and induces apoptosis. *Hum Mol Genet*. 2000;9(19):2859-2867.

40. Sanchez I, Xu CJ, Juo P, Kakizaka A, Blenis J, Yuan J. Caspase-8 is required for cell death induced by expanded polyglutamine repeats. *Neuron*. 1999;22(3):623-633.

41. Wellington CL, Ellerby LM, Hackam AS, et al. Caspase cleavage of gene products associated with triplet expansion disorders generates truncated fragments containing the polyglutamine tract. *J Biol Chem*. 1998;273(15):9158-9167.

42. Graham RK, Deng Y, Carroll J, et al. Cleavage at the 586 amino acid caspase-6 site in mutant huntingtin influences caspase-6 activation in vivo. *J Neurosci*. 2010;30(45):15019-15029.

43. Wellington CL, Singaraja R, Ellerby L, et al. Inhibiting caspase cleavage of huntingtin reduces toxicity and aggregate formation in neuronal and nonneuronal cells. *Journal of Biological Chemistry*. 2000;275(26):19831-19838.

44. Fernandes-Alnemri T, Litwack G, Alnemri ES. Mch2, a new member of the apoptotic ced-3/ice cysteine protease gene family. *Cancer Res*. 1995;55(13):2737-2742.

45. Crawford ED, Wells JA. Caspase substrates and cellular remodeling. *Annu Rev Biochem*. 2011;80:1055-1087.

46. Takahashi A, Alnemri ES, Lazebnik YA, et al. Cleavage of lamin A by Mch2 alpha but not CPP32: Multiple interleukin 1 beta-converting enzyme-related proteases with distinct substrate recognition properties are active in apoptosis. *Proc Natl Acad Sci U S A*. 1996;93(16):8395-8400.

47. Mintzer R, Ramaswamy S, Shah K, et al. A whole cell assay to measure caspase-6 activity by detecting cleavage of lamin A/C. *PLoS One*. 2012;7(1):e30376.

48. Galande S, Dickinson LA, Mian IS, Sikorska M, Kohwi-Shigematsu T. SATB1 cleavage by caspase 6 disrupts PDZ domain-mediated dimerization, causing detachment from chromatin early in T-cell apoptosis. *Mol Cell Biol*. 2001;21(16):5591-5604.

49. Pellegrini L, Passer BJ, Tabaton M, Ganjei JK, D'Adamio L. Alternative, non-secretase processing of alzheimer's beta-amyloid precursor protein during apoptosis by caspase-6 and -8. *J Biol Chem*. 1999;274(30):21011-21016.

50. van de Craen M, de Jonghe C, van den Brande I, et al. Identification of caspases that cleave presenilin-1 and presenilin-2. five presenilin-1 (PS1) mutations do not alter the sensitivity of PS1 to caspases. *FEBS Lett*. 1999;445(1):149-154.

51. Robert G, Puissant A, Dufies M, et al. The caspase 6 derived N-terminal fragment of DJ-1 promotes apoptosis via increased ROS production. *Cell Death Differ*. 2012;19(11):1769-1778.

52. Cho JH, Lee PY, Son WC, et al. Identification of the novel substrates for caspase-6 in apoptosis using proteomic approaches. *BMB Rep*. 2013;46(12):588-593.

53. Inoue S, Browne G, Melino G, Cohen GM. Ordering of caspases in cells undergoing apoptosis by the intrinsic pathway. *Cell Death Differ*. 2009;16(7):1053-1061.

54. Allsopp TE, McLuckie J, Kerr LE, Macleod M, Sharkey J, Kelly JS. Caspase 6 activity initiates caspase 3 activation in cerebellar granule cell apoptosis. *Cell Death Differ*. 2000;7(10):984-993.

55. Cowling V, Downward J. Caspase-6 is the direct activator of caspase-8 in the cytochrome c-induced apoptosis pathway: Absolute requirement for removal of caspase-6 prodomain. *Cell Death Differ*. 2002;9(10):1046-1056.

56. Warby SC, Doty CN, Graham RK, et al. Activated caspase-6 and caspase-6-cleaved fragments of huntingtin specifically colocalize in the nucleus. *Hum Mol Genet*. 2008;17(15):2390-2404.

57. Ehrnhoefer DE, Skotte NH, Ladha S, et al. p53 increases caspase-6 expression and activation in muscle tissue expressing mutant huntingtin. *Hum Mol Genet*. 2013.

58. Graham RK, Deng Y, Slow EJ, et al. Cleavage at the caspase-6 site is required for neuronal dysfunction and degeneration due to mutant huntingtin. *Cell*. 2006;125(6):1179-1191.

59. Tebbenkamp ATN, Green C, Xu G, et al. Transgenic mice expressing caspase-6-derived N-terminal fragments of mutant huntingtin develop neurologic abnormalities with predominant cytoplasmic inclusion pathology composed largely of a smaller proteolytic derivative. *Hum Mol Genet*. 2011;20(14):2770-2782.

60. Gafni J, Papanikolaou T, DeGiacomo F, et al. Caspase-6 activity in a BACHD mouse modulates steady-state levels of mutant huntingtin protein but is not necessary for production of a 586 amino acid proteolytic fragment. *J Neurosci*. 2012;32(22):7454-7465.

61. Landles C, Weiss A, Franklin S, Howland D, Bates G. Caspase-6 does not contribute to the proteolysis of mutant huntingtin in the HdhQ150 knock-in mouse model of huntington's disease. *PLoS Curr*. 2012:10.1371/4fd085bfc9973.

62. Yuan J, Shaham S, Ledoux S, Ellis HM, Horvitz HR. The C. elegans cell death gene ced-3 encodes a protein similar to mammalian interleukin-1 beta-converting enzyme. *Cell*. 1993;75(4):641-652.

63. Bai L, Wang S. Targeting apoptosis pathways for new cancer therapeutics. *Annu Rev Med*. 2014;65:139-155.

64. LeBlanc AC. Caspase-6 as a novel early target in the treatment of alzheimer's disease. *Eur J Neurosci*. 2013;37(12):2005-2018.

65. Akpan N, Troy CM. Caspase inhibitors: Prospective therapies for stroke. *The Neuroscientist*. 2013;19(2):129-136.

66. Akpan N, Serrano-Saiz E, Zacharia BE, et al. Intranasal delivery of caspase-9 inhibitor reduces caspase-6-dependent axon/neuron loss and improves neurological function after stroke. *The Journal of Neuroscience*. 2011;31(24):8894-8904.

67. Narkilahti S, Pitkanen A. Caspase 6 expression in the rat hippocampus during epileptogenesis and epilepsy. *Neuroscience*. 2005;131(4):887-897.

68. Berta T, Park C, Xu Z, et al. Extracellular caspase-6 drives murine inflammatory pain via microglial TNF-Î± secretion. *J Clin Invest*. 2014;124(3):1173-1186.

69. Henshall DC, Skradski SL, Meller R, et al. Expression and differential processing of caspases 6 and 7 in relation to specific epileptiform EEG patterns following limbic seizures. *Neurobiol Dis*. 2002;10(2):71-87.

70. Khadija S, Veluthakal R, Sidarala V, Kowluru A. Glucotoxic and diabetic conditions induce caspase 6-mediated degradation of nuclear lamin A in human islets, rodent islets and INS-1 832/13 cells. *Apoptosis*. 2014;19(12):1691-1701.

71. Harjai M, Bogra J, Kohli M, Pant AB. Is suppression of apoptosis a new therapeutic target in sepsis? *Anaesth Intensive Care*. 2013;41(2):175-183.

72. Yang B, Ye D, Wang Y. Caspase-3 as a therapeutic target for heart failure. *Expert Opin Ther Targets*. 2013;17(3):255-263.

73. Edwards NL, So A. Emerging therapies for gout. *Rheum Dis Clin North Am*. 2014;40(2):375-387.

74. Olsson M, Zhivotovsky B. Caspases and cancer. *Cell Death Differ*. 2011;18(9):1441-1449.

75. Foveau B, Van Der Kraak L, Beauchemin N, Albrecht S, LeBlanc AC. Inflammation-induced tumorigenesis in mouse colon is caspase-6 independent. *PLoS One*. 2014;9(12):e114270.

76. Licht V, Noack K, Schlott B, et al. Caspase-3 and caspase-6 cleave STAT1 in leukemic cells. *Oncotarget*. 2014;5(8):2305-2317.

77. Vegran F, Boidot R. Survivin-3B promotes chemoresistance and immune escape by inhibiting caspase-8 and -6 in cancer cells. *Oncoimmunology*. 2013;2(11):e26328.

78. Kuida K, Zheng TS, Na S, et al. Decreased apoptosis in the brain and premature lethality in CPP32-deficient mice. *Nature*. 1996;384(6607):368-372.

79. Varfolomeev EE, Schuchmann M, Luria V, et al. Targeted disruption of the mouse caspase 8 gene ablates cell death induction by the TNF receptors, fas/Apo1, and DR3 and is lethal prenatally. *Immunity*. 1998;9(2):267-276.

80. Hakem R, Hakem A, Duncan GS, et al. Differential requirement for caspase 9 in apoptotic pathways in vivo. *Cell*. 1998;94(3):339-352.

81. Li P, Allen H, Banerjee S, et al. Mice deficient in IL-1 beta-converting enzyme are defective in production of mature IL-1 beta and resistant to endotoxic shock. *Cell*. 1995;80(3):401-411.

82. Bergeron L, Perez GI, Macdonald G, et al. Defects in regulation of apoptosis in caspase-2-deficient mice. *Genes Dev*. 1998;12(9):1304-1314.

83. Uribe V, Wong BKY, Graham RK, et al. Rescue from excitotoxicity and axonal degeneration accompanied by age-dependent behavioral and neuroanatomical alterations in caspase-6-deficient mice. *Hum Mol Genetic*. 2012;21(9):1954-1967.

84. Nikolaev A, McLaughlin T, O'Leary DD, Tessier-Lavigne M. APP binds DR6 to trigger axon pruning and neuron death via distinct caspases. *Nature*. 2009;457(7232):981-989.

85. Albrecht S, Bourdeau M, Bennett D, Mufson EJ, Bhattacharjee M, LeBlanc AC. Activation of caspase-6 in aging and mild cognitive impairment. *Am J Pathol*. 2007;170(4):1200-1209.

86. Guo H, Albrecht S, Bourdeau M, Petzke T, Bergeron C, LeBlanc AC. Active caspase-6 and caspase-6-cleaved tau in neuropil threads, neuritic plaques, and neurofibrillary tangles of alzheimer's disease. *Am J Pathol*. 2004;165(2):523-531.

87. Ekert PG, Silke J, Vaux DL. Caspase inhibitors. *Cell Death Differ*. 1999;6(11):1081-1086.

88. Thornberry NA, Peterson EP, Zhao JJ, Howard AD, Griffin PR, Chapman KT. Inactivation of interleukin-1 beta converting enzyme by peptide (acyloxy)methyl ketones. *Biochemistry*. 1994;33(13):3934-3940.

89. Berger AB, Sexton KB, Bogyo M. Commonly used caspase inhibitors designed based on substrate specificity profiles lack selectivity. *Cell Res*. 2006;16(12):961-963.

90. Chauvier D, Ankri S, Charriaut-Marlangue C, Casimir R, Jacotot E. Broad-spectrum caspase inhibitors: From myth to reality? *Cell Death Differ*. 2006;14(2):387-391.

91. Garcia-Calvo M, Peterson EP, Leiting B, Ruel R, Nicholson DW, Thornberry NA. Inhibition of human caspases by peptide-based and macromolecular inhibitors. *J Biol Chem*. 1998;273(49):32608-32613.

92. Brasnjevic I, Steinbusch HW, Schmitz C, Martinez-Martinez P, European NanoBioPharmaceutics Research Initiative. Delivery of peptide and protein drugs over the blood-brain barrier. *Prog Neurobiol*. 2009;87(4):212-251.

93. Wiessner C, Sauer D, Alaimo D, Allegrini PR. Protective effect of a caspase inhibitor in models for cerebral ischemia in vitro and in vivo. *Cell Mol Biol (Noisy-le-grand)*. 2000;46(1):53-62.

94. Graczyk PP. Caspase inhibitors as anti-inflammatory and antiapoptotic agents. *Prog Med Chem*. 2002;39:1-72.

95. Fischer U, Schulze-Osthoff K. Apoptosis-based therapies and drug targets. *Cell Death Differ*. 2005;12 Suppl 1:942-961.

96. Van Noorden CJ. The history of Z-VAD-FMK, a tool for understanding the significance of caspase inhibition. *Acta Histochem*. 2001;103(3):241-251.

97. Fiorucci S, Antonelli E, Tocchetti P, Morelli A. Treatment of portal hypertension with NCX-1000, a liver-specific NO donor. A review of its current status. *Cardiovasc Drug Rev*. 2004;22(2):135-146.

98. Pockros PJ, Schiff ER, Shiffman ML, et al. Oral IDN-6556, an antiapoptotic caspase inhibitor, may lower aminotransferase activity in patients with chronic hepatitis C. *Hepatology*. 2007;46(2):324-329.

99. Linton SD, Aja T, Armstrong RA, et al. First-in-class pan-caspase inhibitor developed for the treatment of liver disease. *J Med Chem*. 2005;48(22):6779-6782.

100. MacKenzie SH, Schipper JL, Clark AC. The potential for caspases in drug discovery. *Curr Opin Drug Discov Devel*. 2010;13(5):568-576.

101. Levy DI, Sucher NJ, Lipton SA. Redox modulation of NMDA receptor-mediated toxicity in mammalian central neurons. *Neurosci Lett*. 1990;110(3):291-296.

102. Koh JY, Choi DW. Vulnerability of cultured cortical neurons to damage by excitotoxins: Differential susceptibility of neurons containing NADPH-diaphorase. *J Neurosci*. 1988;8(6):2153-2163.

103. May PC, Gray PN. L-homocysteic acid as an alternative cytotoxin for studying glutamate-induced cellular degeneration of huntington's disease and normal skin fibroblasts. *Life Sci*. 1985;37(16):1483-1489.

104. Gray PN, May PC, Mundy L, Elkins J. L-glutamate toxicity in huntington's disease fibroblasts. *Biochem Biophys Res Commun*. 1980;95(2):707-714.

105. Mandavilli BS, Boldogh I, Van Houten B. 3-nitropropionic acid-induced hydrogen peroxide, mitochondrial DNA damage, and cell death are attenuated by bcl-2 overexpression in PC12 cells. *Brain Res Mol Brain Res*. 2005;133(2):215-223.

106. Lunkes A, Mandel JL. A cellular model that recapitulates major pathogenic steps of huntington's disease. *Hum Mol Genet*. 1998;7(9):1355-1361.

107. Peters PJ, Ning K, Palacios F, et al. Arfaptin 2 regulates the aggregation of mutant huntingtin protein. *Nat Cell Biol*. 2002;4(3):240-245.

108. Wang GH, Mitsui K, Kotliarova S, et al. Caspase activation during apoptotic cell death induced by expanded polyglutamine in N2a cells. *Neuroreport*. 1999;10(12):2435-2438.

109. Sun Y, Savanenin A, Reddy PH, Liu YF. Polyglutamine-expanded huntingtin promotes sensitization of N-methyl-D-aspartate receptors via post-synaptic density 95. *J Biol Chem*. 2001;276(27):24713-24718.

110. Ferreira IL, Nascimento MV, Ribeiro M, et al. Mitochondrial-dependent apoptosis in huntington's disease human cybrids. *Exp Neurol*. 2010;222(2):243-255.

111. Giuliano P, De Cristofaro T, Affaitati A, et al. DNA damage induced by polyglutamine-expanded proteins. *Hum Mol Genet*. 2003;12(18):2301-2309.

112. Li SH, Cheng AL, Li H, Li XJ. Cellular defects and altered gene expression in PC12 cells stably expressing mutant huntingtin. *J Neurosci*. 1999;19(13):5159-5172.

113. DiFiglia M. Huntingtin fragments that aggregate go their separate ways. *Mol Cell*. 2002;10(2):224-225.

114. Colby DW, Chu Y, Cassady JP, et al. Potent inhibition of huntingtin aggregation and cytotoxicity by a disulfide bond-free single-domain intracellular antibody. *Proc Natl Acad Sci U S A*. 2004;101(51):17616-17621.

115. Kim M, Lee H, LaForet G, et al. Mutant huntingtin expression in clonal striatal cells: Dissociation of inclusion formation and neuronal survival by caspase inhibition. *The Journal of Neuroscience*. 1999;19(3):964-973.

116. Oliveira JM, Chen S, Almeida S, et al. Mitochondrial-dependent Ca2+ handling in huntington's disease striatal cells: Effect of histone deacetylase inhibitors. *J Neurosci*. 2006;26(43):11174-11186.

117. Soldati C, Bithell A, Conforti P, Cattaneo E, Buckley NJ. Rescue of gene expression by modified REST decoy oligonucleotides in a cellular model of huntington's disease. *J Neurochem*. 2011;116(3):415-425.

118. Igarashi S, Morita H, Bennett KM, et al. Inducible PC12 cell model of huntington's disease shows toxicity and decreased histone acetylation. *Neuroreport*. 2003;14(4):565-568.

119. Liang Y, Jiang H, Ratovitski T, et al. ATF3 plays a protective role against toxicity by N-terminal fragment of mutant huntingtin in stable PC12 cell line. *Brain Res*. 2009;1286:221-229.

120. An MC, Zhang N, Scott G, et al. Genetic correction of huntington's disease phenotypes in induced pluripotent stem cells. *Cell Stem Cell*. 2012;11(2):253-263.

121. HD iPSC Consortium. Induced pluripotent stem cells from patients with huntington's disease show CAG-repeat-expansion-associated phenotypes. *Cell Stem Cell*. 2012;11(2):264-278.

122. Chae JI, Kim DW, Lee N, et al. Quantitative proteomic analysis of induced pluripotent stem cells derived from a human huntington's disease patient. *Biochem J*. 2012;446(3):359-371.

123. Mattis VB, Tom C, Akimov S, et al. HD iPSC-derived neural progenitors accumulate in culture and are susceptible to BDNF withdrawal due to glutamate toxicity. *Hum Mol Genet*. 2015;24(11):3257-3271.

124. Beal MF, Ferrante RJ, Swartz KJ, Kowall NW. Chronic quinolinic acid lesions in rats closely resemble huntington's disease. *J Neurosci*. 1991;11(6):1649-1659.

125. McGeer EG, McGeer PL. Duplication of biochemical changes of huntington's chorea by intrastriatal injections of glutamic and kainic acids. *Nature*. 1976;263(5577):517-519.

126. Brouillet E, Hantraye P. Effects of chronic MPTP and 3-nitropropionic acid in nonhuman primates. *Curr Opin Neurol*. 1995;8(6):469-473.

127. Beal MF, Kowall NW, Ellison DW, Mazurek MF, Swartz KJ, Martin JB. Replication of the neurochemical characteristics of huntington's disease by quinolinic acid. *Nature*. 1986;321(6066):168-171.

128. Mehrotra A, Kanwal A, Banerjee SK, Sandhir R. Mitochondrial modulators in experimental huntington's disease: Reversal of mitochondrial dysfunctions and cognitive deficits. *Neurobiol Aging*. 2015;36(6):2186-2200.

129. Kumar A, Chaudhary T, Mishra J. Minocycline modulates neuroprotective effect of hesperidin against quinolinic acid induced huntington's disease like symptoms in rats: Behavioral, biochemical, cellular and histological evidences. *Eur J Pharmacol*. 2013;720(1-3):16-28.

130. Kalonia H, Mishra J, Kumar A. Targeting neuro-inflammatory cytokines and oxidative stress by minocycline attenuates quinolinic-acid-induced huntington's disease-like symptoms in rats. *Neurotox Res*. 2012;22(4):310-320.

131. Shetty S, Hariharan A, Shirole T, Jagtap AG. Neuroprotective potential of escitalopram against behavioral, mitochondrial and oxidative dysfunction induced by 3-nitropropionic acid. *Ann Neurosci*. 2015;22(1):11-18.

132. Sanberg PR, Lehmann J, Fibiger HC. Impaired learning and memory after kainic acid lesions of the striatum: A behavioral model of huntington's disease. *Brain Res*. 1978;149(2):546-551.

133. Menalled LB, Chesselet MF. Mouse models of huntington's disease. *Trends Pharmacol Sci*. 2002;23(1):32-39.

134. Jackson GR, Salecker I, Dong X, et al. Polyglutamine-expanded human huntingtin transgenes induce degeneration of drosophila photoreceptor neurons. *Neuron*. 1998;21(3):633-642.

135. Yang SH, Cheng PH, Banta H, et al. Towards a transgenic model of huntington's disease in a non-human primate. *Nature*. 2008;453(7197):921-924.

136. Mangiarini L, Sathasivam K, Seller M, et al. Exon 1 of the HD gene with an expanded CAG repeat is sufficient to cause a progressive neurological phenotype in transgenic mice. *Cell*. 1996;87(3):493-506.

137. Tang B, Seredenina T, Coppola G, et al. Gene expression profiling of R6/2 transgenic mice with different CAG repeat lengths reveals genes associated with disease onset and progression in huntington's disease. *Neurobiol Dis*. 2011;42(3):459-467.

138. Rattray I, Smith E, Gale R, Matsumoto K, Bates GP, Modo M. Correlations of behavioral deficits with brain pathology assessed through longitudinal MRI and histopathology in the R6/2 mouse model of HD. *PLoS One*. 2013;8(4):e60012.

139. Hering T, Birth N, Taanman JW, Orth M. Selective striatal mtDNA depletion in end-stage huntington's disease R6/2 mice. *Exp Neurol*. 2015;266:22-29.

140. Magnusson-Lind A, Davidsson M, Silajdzic E, et al. Skeletal muscle atrophy in R6/2 mice - altered circulating skeletal muscle markers and gene expression profile changes. *J Huntingtons Dis*. 2014;3(1):13-24.

141. Zhang Y, Ona VO, Li M, et al. Sequential activation of individual caspases, and of alterations in bcl-2 proapoptotic signals in a mouse model of huntington's disease. *J Neurochem*. 2003;87(5):1184-1192.

142. Schilling G, Becher MW, Sharp AH, et al. Intranuclear inclusions and neuritic aggregates in transgenic mice expressing a mutant N-terminal fragment of huntingtin. *Hum Mol Genet*. 1999;8(3):397-407.

143. Waldron-Roby E, Ratovitski T, Wang X, et al. Transgenic mouse model expressing the caspase 6 fragment of mutant huntingtin. *J Neurosci*. 2012;32(1):183-193.

144. Slow EJ, van Raamsdonk J, Rogers D, et al. Selective striatal neuronal loss in a YAC128 mouse model of huntington disease. *Hum Mol Genet*. 2003;12(13):1555-1567.

145. Gray M, Shirasaki DI, Cepeda C, et al. Full-length human mutant huntingtin with a stable polyglutamine repeat can elicit progressive and selective neuropathogenesis in BACHD mice. *J Neurosci*. 2008;28(24):6182-6195.

146. Spampanato J, Gu X, Yang XW, Mody I. Progressive synaptic pathology of motor cortical neurons in a BAC transgenic mouse model of huntington's disease. *Neuroscience*. 2008;157(3):606-620.

147. Andre VM, Fisher YE, Levine MS. Altered balance of activity in the striatal direct and indirect pathways in mouse models of huntington's disease. *Front Syst Neurosci*. 2011;5:46.

148. Van Raamsdonk JM, Gibson WT, Pearson J, et al. Body weight is modulated by levels of full-length huntingtin. *Hum Mol Genet*. 2006;15(9):1513-1523.

149. Pouladi MA, Xie Y, Skotte NH, et al. Full-length huntingtin levels modulate body weight by influencing insulin-like growth factor 1 expression. *Hum Mol Genet*. 2010;19(8):1528-1538.

150. Hult S, Soylu R, Bjorklund T, et al. Mutant huntingtin causes metabolic imbalance by disruption of hypothalamic neurocircuits. *Cell Metab*. 2011;13(4):428-439.

151. Kudo T, Schroeder A, Loh DH, et al. Dysfunctions in circadian behavior and physiology in mouse models of huntington's disease. *Exp Neurol*. 2011;228(1):80-90.

152. Menalled L, El-Khodor BF, Patry M, et al. Systematic behavioral evaluation of huntington's disease transgenic and knock-in mouse models. *Neurobiol Dis*. 2009;35(3):319-336.

153. Lundh SH, Soylu R, Petersen A. Expression of mutant huntingtin in leptin receptor-expressing neurons does not control the metabolic and psychiatric phenotype of the BACHD mouse. *PLoS One*. 2012;7(12):e51168.

154. Abada YS, Schreiber R, Ellenbroek B. Motor, emotional and cognitive deficits in adult BACHD mice: A model for huntington's disease. *Behav Brain Res*. 2013;238:243-251.

155. Pouladi MA, Stanek LM, Xie Y, et al. Marked differences in neurochemistry and aggregates despite similar behavioural and neuropathological features of huntington disease in the full-length BACHD and YAC128 mice. *Hum Mol Genet*. 2012;21(10):2219-2232.

156. Hult Lundh S, Nilsson N, Soylu R, Kirik D, Petersen A. Hypothalamic expression of mutant huntingtin contributes to the development of depressive-like behavior in the BAC transgenic mouse model of huntington's disease. *Hum Mol Genet*. 2013;22(17):3485-3497.

157. Baldo B, Cheong RY, Petersen A. Effects of deletion of mutant huntingtin in steroidogenic factor 1 neurons on the psychiatric and metabolic phenotype in the BACHD mouse model of huntington disease. *PLoS One*. 2014;9(10):e107691.

158. Doria JG, de Souza JM, Andrade JN, et al. The mGluR5 positive allosteric modulator, CDPPB, ameliorates pathology and phenotypic signs of a mouse model of huntington's disease. *Neurobiol Dis*. 2015;73:163-173.

159. Kalchman MA, Koide HB, McCutcheon K, et al. HIP1, a human homologue of S. cerevisiae Sla2p, interacts with membrane-associated huntingtin in the brain. *Nat Genet*. 1997;16(1):44-53.

160. Ehrnhoefer DE, Skotte NH, Savill J, et al. A quantitative method for the specific assessment of caspase-6 activity in cell culture. *PLoS One*. 2011;6(11):e27680.

161. Koffie RM, Farrar CT, Saidi L, William CM, Hyman BT, Spires-Jones TL. Nanoparticles enhance brain delivery of blood–brain barrier-impermeable probes for in vivo optical and magnetic resonance imaging. *Proc Natl Acad Sci U S A*. 2011;108(46):18837-18842.

162. Jung JC, Mehta AD, Aksay E, Stepnoski R, Schnitzer MJ. In vivo mammalian brain imaging using one- and two-photon fluorescence microendoscopy. *J Neurophysiol*. 2004;92(5):3121-3133.

163. Pouladi MA, Graham RK, Karasinska JM, et al. Prevention of depressive behaviour in the YAC128 mouse model of huntington disease by mutation at residue 586 of huntingtin. *Brain*. 2009;132(4):919-932.

164. Bourin M, Hascoët M. The mouse light/dark box test. *Eur J Pharmacol*. 2003;463(1–3):55-65.

165. Marco S, Giralt A, Petrovic MM, et al. Suppressing aberrant GluN3A expression rescues synaptic and behavioral impairments in huntington's disease models. *Nat Med*. 2013;19(8):1030-1038.

166. Timmer JC, Salvesen GS. Caspase substrates. *Cell Death Differ*. 2007;14(1):66-72.

167. Schwarze SR, Ho A, Vocero-Akbani A, Dowdy SF. In vivo protein transduction: Delivery of a biologically active protein into the mouse. *Science*. 1999;285(5433):1569-1572.

168. Hällbrink M, Florén A, Elmquist A, Pooga M, Bartfai T, Langel Ü. Cargo delivery kinetics of cell-penetrating peptides. *Biochim Biophys Acta*. 2001;1515(2):101-109.

169. Thorén PEG, Persson D, Isakson P, Goksör M, Önfelt A, Nordén B. Uptake of analogs of penetratin, tat(48–60) and oligoarginine in live cells. *Biochem Biophys Res Commun*. 2003;307(1):100-107.

170. D'Amelio M, Cavallucci V, Cecconi F. Neuronal caspase-3 signaling: Not only cell death. *Cell Death Differ*. 2010;17(7):1104-1114.

171. Degterev A, Boyce M, Yuan J. A decade of caspases. *Oncogene*. 2003;22(53):8543-8567.

172. Chéreau D, Kodandapani L, Tomaselli KJ, Spada AP, Wu JC. Structural and functional analysis of caspase active sites. *Biochemistry*. 2003;42(14):4151-4160.

173. Leyva MJ, DeGiacomo F, Kaltenbach LS, et al. Identification and evaluation of small molecule pan-caspase inhibitors in huntington's disease models. *Chem Biol*. 2010;17(11):1189-1200.

174. Wong BK, Ehrnhoefer DE, Graham RK, et al. Partial rescue of some features of huntington disease in the genetic absence of caspase-6 in YAC128 mice. *Neurobiol Dis*. 2015;76:24-36.

175. Aziz NA, van der Burg JM, Landwehrmeyer GB, et al. Weight loss in huntington disease increases with higher CAG repeat number. *Neurology*. 2008;71(19):1506-1513.

176. Heindel WC, Butters N, Salmon DP. Impaired learning of a motor skill in patients with huntington's disease. *Behav Neurosci*. 1988;102(1):141-147.

177. Thompson JC, Snowden JS, Craufurd D, Neary D. Behavior in huntington's disease: Dissociating cognition-based and mood-based changes. *J Neuropsychiatry Clin Neurosci*. 2002;14(1):37-43.

178. Dale M, van Duijn E. Anxiety in huntington's disease. *J Neuropsychiatry Clin Neurosci*. 2015:appineuropsych14100265.

179. Rizzuti M, Nizzardo M, Zanetta C, Ramirez A, Corti S. Therapeutic applications of the cell-penetrating HIV-1 tat peptide. *Drug Discov Today*. 2015;20(1):76-85.

180. Carroll J, Southwell A, Graham R, et al. Mice lacking caspase-2 are protected from behavioral changes, but not pathology, in the YAC128 model of huntington disease. *Molecular Neurodegeneration*. 2011;6(1):59.

181. Jeong HJ, Kim DW, Kim MJ, et al. Protective effects of transduced tat-DJ-1 protein against oxidative stress and ischemic brain injury. *Exp Mol Med*. 2012;44(10):586-593.

182. Goswami D, Vitorino HA, Alta RY, et al. Deferasirox-TAT(47-57) peptide conjugate as a water soluble, bifunctional iron chelator with potential use in neuromedicine. *Biometals*. 2015.

183. Kudwa AE, Menalled LB, Oakeshott S, et al. Increased body weight of the BAC HD transgenic mouse model of huntington's disease accounts for some but not all of the observed HD-like motor deficits. *PLoS Curr*. 2013;5:10.1371/currents.hd.0ab4f3645aff523c56ecc8ccbe41a198.

184. Kim D, Jeon J, Cheong E, et al. Neuroanatomical visualization of the impaired striatal connectivity in huntington's disease mouse model. *Mol Neurobiol*. 2015.

185. Schwab LC, Garas SN, Drouin-Ouellet J, Mason SL, Stott SR, Barker RA. Dopamine and huntington's disease. *Expert Rev Neurother*. 2015;15(4):445-458.

186. Wolf RC, Thomann PA, Sambataro F, et al. Abnormal cerebellar volume and corticocerebellar dysfunction in early manifest huntington's disease. *J Neurol*. 2015;262(4):859-869.

187. Sepers MD, Raymond LA. Mechanisms of synaptic dysfunction and excitotoxicity in huntington's disease. *Drug Discov Today*. 2014;19(7):990-996.

188. Abelaira HM, Reus GZ, Quevedo J. Animal models as tools to study the pathophysiology of depression. *Rev Bras Psiquiatr*. 2013;35 Suppl 2:S112-20.

189. Sestakova N, Puzserova A, Kluknavsky M, Bernatova I. Determination of motor activity and anxiety-related behaviour in rodents: Methodological aspects and role of nitric oxide. *Interdiscip Toxicol*. 2013;6(3):126-135.

190. Yamamoto A, Lucas JJ, Hen R. Reversal of neuropathology and motor dysfunction in a conditional model of huntington's disease. *Cell*. 2000;101(1):57-66.

191. Diaz-Hernandez M, Torres-Peraza J, Salvatori-Abarca A, et al. Full motor recovery despite striatal neuron loss and formation of irreversible amyloid-like inclusions in a conditional mouse model of huntington's disease. *J Neurosci*. 2005;25(42):9773-9781.

192. Lawrence AD, Sahakian BJ, Hodges JR, Rosser AE, Lange KW, Robbins TW. Executive and mnemonic functions in early huntington's disease. *Brain*. 1996;119 (Pt 5)(Pt 5):1633-1645.

193. Georgiou-Karistianis N, Scahill R, Tabrizi SJ, Squitieri F, Aylward E. Structural MRI in huntington's disease and recommendations for its potential use in clinical trials. *Neurosci Biobehav Rev*. 2013;37(3):480-490.

194. Sawiak SJ, Wood NI, Carpenter TA, Morton AJ. Huntington's disease mouse models online: High-resolution MRI images with stereotaxic templates for computational neuroanatomy. *PLoS One*. 2012;7(12):e53361.

195. Cajavec B, Bernard S, Herzel H. Aggregation in huntington's disease: Insights through modelling. *Genome Inform*. 2005;16(1):262-271.

196. Swart C, Haylett W, Kinnear C, Johnson G, Bardien S, Loos B. Neurodegenerative disorders: Dysregulation of a carefully maintained balance? *Exp Gerontol*. 2014;58:279-291.

9. Appendix

9.1. Peer reviewed publication

Human Molecular Genetics, 2015, Vol. 24, No. 9 2604–2614

doi: 10.1093/hmg/ddv023
Advance Access Publication Date: 23 January 2015
Original Article

ORIGINAL ARTICLE

A Huntingtin-based peptide inhibitor of caspase-6 provides protection from mutant Huntingtin-induced motor and behavioral deficits

Israel Aharony[1], Dagmar E. Ehrnhoefer[2], Adi Shruster[1], Xiaofan Qiu[2], Sonia Franciosi[2], Michael R. Hayden[2] and Daniel Offen[1,*]

[1]Neuroscience Laboratory, Felsenstein Medical Research Center, Sackler Faculty of Medicine, Tel-Aviv University, Israel and [2]Centre for Molecular Medicine and Therapeutics, Department of Medical Genetics, University of British Columbia, Vancouver, BC, Canada

*To whom correspondence should be addressed at: Felsenstein Medical Research Center, Rabin Medical Center, Petah Tikva 49100, Israel. Tel: +972 39376130; Fax: +972 39376130; Email: danioffen@gmail.com

Abstract

Over the past decade, increasing evidence has implied a significant connection between caspase-6 activity and the pathogenesis of Huntington's disease (HD). Consequently, inhibiting caspase-6 activity was suggested as a promising therapeutic strategy to reduce mutant Huntingtin toxicity, and to provide protection from mutant Huntingtin-induced motor and behavioral deficits. Here, we describe a novel caspase-6 inhibitor peptide based on the huntingtin caspase-6 cleavage site, fused with a cell-penetrating sequence. The peptide reduces mutant Huntingtin proteolysis by caspase-6, and protects cells from mutant Huntingtin toxicity. Continuous subcutaneous administration of the peptide protected pre-symptomatic BACHD mice from motor deficits and behavioral abnormalities. Moreover, administration of the peptide in an advanced disease state resulted in the partial recovery of motor performance, and an alleviation of depression-related behavior and cognitive deficits. Our findings reveal the potential of substrate-based caspase inhibition as a therapeutic strategy, and present a promising agent for the treatment of HD.

Introduction

Huntington's disease (HD) is a fatal neurodegenerative disease with autosomal dominant inheritance. It is characterized by progressive motor, cognitive and psychiatric symptoms. The average age of HD onset is 40, and death occurs after ~10–15 years. Currently, no disease-modifying treatment is available (1).

The protein responsible for the pathogenesis of HD is Huntingtin (Htt), and the mutated form of Htt carries >35 glutamine repeats in its N-terminus. Htt is a substrate for caspase cleavage and can be cleaved by caspase-3 at Asp513 and Asp552, caspase-2 at Asp552 and caspase-6 at Asp586 (2,3). Caspase cleavage of mHtt precedes neurodegeneration and generates N-terminal fragments that aggregate in the cytoplasm and nucleus of neurons (3). Caspase-6 in particular serves an important role in HD pathogenesis: its activation is an early pathogenic event in HD mutation carriers, and the level of activation is directly correlated with CAG repeat length and inversely correlated with age of onset (4). In addition, activated caspase-6 and cleaved fragments of Htt are found in the nuclei of striatal neurons after the initiation of cellular stress, which correlates with increased toxicity (5). Recent evidence shows that caspase-6 activity induced by mHtt is not restricted to the central nervous system (CNS), but can be found in muscle tissue from HD patients and in HD mouse models (6), suggesting that caspase-6 might be involved in central as well as peripheral features of HD.

Received: November 15, 2014. **Revised and Accepted:** January 21, 2015

The importance of mHtt proteolysis at Asp586 was revealed in a mouse model genetically engineered to express Caspase-6 Resistant (C6R) mHtt. Mice expressing C6R mHtt do not develop striatal neurodegeneration and are protected from motor deficits and the depressive phenotype seen in HD mouse models. Furthermore, these mice are protected from neurotoxicity induced by multiple stressors including NMDA, quinolinic acid and staurosporine, demonstrating the protective effects of C6R mHtt expression (7,8). In a complementary study, transgenic mice expressing the 586 amino acid N-terminal fragment of mHtt demonstrated severe neurologic abnormalities and aggregate formation (9). These observations imply that inhibition of mHtt proteolysis by caspase-6 would both reduce the load of toxic N-terminal fragments and maintain the neuroprotective function of wild-type (WT) Htt. Therefore, specific inhibition of caspase-6 was suggested as a disease-modifying therapeutic strategy.

Here, we describe a novel peptide inhibitor based on the Htt caspase-6 cleavage site (amino acids 550–560). This inhibitor is expected to compete with Htt for the caspase-6 active site, and thus reduce Htt cleavage. To facilitate cell penetration, we utilized the HIV-1 TAT-derived peptide. TAT (amino acids 48–60) is known to enable efficient cellular and nuclear penetration, as well as transportation through the blood–brain barrier (BBB) without causing apparent toxic effects (10–12). These considerations led to the peptide sequence GRKKRRQRRRPPQSSEIVLDGTDN (Supplementary material, Fig. S1), designated as ED11.

Results

ED11 inhibits caspase-6 activity

To assess the ability of ED11 to directly inhibit caspase-6, cleavage of Z-VEID-aminoluciferin was monitored. We found that Z-VEID-aminoluciferin cleavage by caspase-6 was reduced by ED11 in a dose-dependent matter, while a control peptide containing the TAT (48–60) sequence alone did not affect the reaction (Fig. 1A). Replacement of amino acids at positions Ile4 or Asp7 within the caspase recognition site of ED11 eliminated the ability of ED11 to inhibit caspase-6 (Fig. 1B), indicating that these amino acids are crucial for ED11's effectiveness.

To test the ability of ED11 to interfere with caspase-6 cleavage of mHtt, striatal extracts from BACHD mice were incubated with caspase-6 in the presence of ED11. In this experiment, the addition of 10 μM ED11 abolished proteolysis of the human mHtt transgene by caspase-6 (Fig. 1C). To determine IC_{50} values for the inhibition of caspase-6 by ED11, a FRET-based Htt cleavage assay was used. This assay measures Htt cleavage using FRET between an N-terminal Htt antibody and a neo-epitope antibody directed against the 586 cleavage site (5). The IC_{50} value determined for ED11 was 12.12 nM, whereas the IC_{50} for the commercial pan-caspase inhibitor Z-VAD-FMK was determined as 4.62 nM (Fig. 1D).

Due to the structural similarity of active sites among the caspase family, small molecule caspase-6 inhibitors frequently demonstrate cross-reactivity with other caspases. This is evident especially with caspase-3, which is the most abundant caspase in adult rodent brain (13–15). Therefore, we examined the specificity of ED11 to caspase-6 over caspase-3, using Z-VEID-aminoluciferin as a substrate and the synthetic pan-caspase inhibitor Z-VAD-FMK as a control. When monitoring the influence on caspase-6 activity, we observed that both ED11 and Z-VAD-FMK inhibited the proteolytic process to a similar extent. However, when caspase-3 was used in the experiment, no influence of ED11 on Z-VEID-aminoluciferin cleavage was recorded, whereas Z-VAD-FMK still strongly inhibited the luminescent signal (Fig. 1E). To confirm these findings, caspase-3 was incubated with HEK293 cell lysate, and the cleavage of PARP and Spectrin, two endogenous caspase-3 targets, was quantified by western blot. We observed that Z-VAD-FMK inhibited caspase-3-mediated cleavage of PARP and Spectrin, as expected, whereas ED11 did not influence the reaction, indicating that its influence on caspase-3 is insignificant (Fig. 1F and G). To test the inhibitory effect of ED11 on a wider range of caspases, we tested Htt protein cleavage by caspases 1–10 and the effect of ED11 on fragment generation. We have demonstrated recently that these caspases can cleave Htt at different sites (16). After incubation of the different caspases with Huntingtin, western blot staining by BKP1 antibody demonstrated that the inhibitory effect of ED11 was most pronounced for the generation of the 586 fragment by caspase-6. A lesser effect of the inhibitor was found on caspase-1 and -10-mediated generation of the 513 fragment and caspase-2-mediated generation of the 552 fragment (Supplementary material, Fig. S2).

ED11 protects cells from 145Q-mHtt-induced toxicity

To confirm the ability of ED11 to penetrate cellular membranes, different concentrations of ED11 were incubated with mouse embryonic fibroblast (MEF) cells. Staining with an anti-TAT antibody demonstrated the dose-dependent accumulation of ED11 inside the cells (Fig. 2A). We furthermore confirmed that ED11 does not affect cell viability, proliferation or cell cycle status in a basal state (Supplementary material, Fig. S3).

To evaluate the ability of ED11 to reduce intracellular Htt cleavage by caspase-6, we co-transfected HEK293 cells with caspase-6 and the N-terminal 1212 amino acids of 15Q-Htt and added ED11 to the medium. Htt 586 fragment levels were quantified 24 h after transfection using anti-Htt (mab2166) and anti-Htt586 neo-epitope antibodies. Treatment with ED11 resulted in a significant reduction of the 586 fragment resulting from caspase-6 cleavage (Fig. 2B and C), whereas no effect on the auto-activation of caspase-6 was observed. The cell-permeable pan-caspase inhibitor Q-VD-OPh, however, inhibited both caspase-6 auto-activation and Htt cleavage (Fig. 2B). These findings suggest that ED11 is able to block the intracellular cleavage of Htt by caspase-6.

To evaluate ED11's ability to protect cells from mHtt toxicity, PC12 cells harboring an inducible 145Q-mHtt-expressing vector were placed under chronic serum deprivation stress and induced to express mHtt for 72 h. Cell viability measurements showed that while 145Q-mHtt expression gradually decreases viability, treatment with ED11 resulted in the preservation of cell viability (Fig. 2D). Measuring LDH release revealed that ED11 treatment attenuated cell death that was evident after 72 h of 145Q-mHtt expression in untreated cells (Fig. 2E). Next, we evaluated caspase activity levels in 145Q-mHtt-expressing cells with a FAM-VEID-FMK caspase-6 activity reporter. Whereas the induction of 145Q-mHtt significantly increased caspase activity in vehicle-treated cells, ED11-treated cells maintained baseline levels of caspase activation (Fig. 2F and G), confirming that the peptide is able to inhibit caspase-6 intracellularly.

Pre-symptomatic ED11 treatment protects BACHD mice from motor and behavioral deficits

To evaluate the ability of ED11 to penetrate the BBB, we labeled ED11 with a fluorescein isothiocyanate (FITC) tag at the C-terminus. Then, we monitored the extravasation of labeled

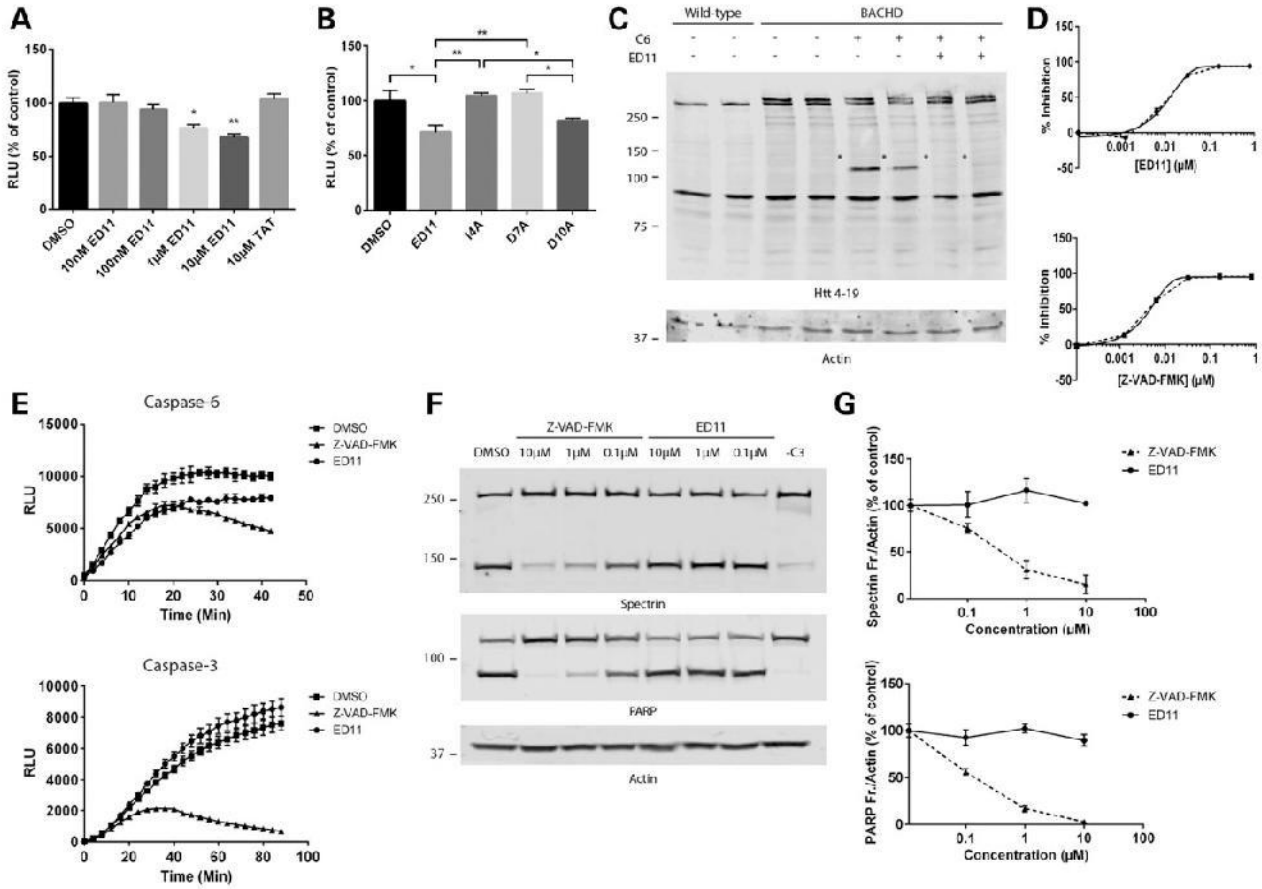

Figure 1. ED11 potently and selectively inhibits caspase-6 proteolytic activity. (**A**) Cleavage of Z-VEID-aminoluciferin by caspase-6 was quantified by light emission ($n = 3$). (**B**) Influence of alanine substitution of the indicated amino acids within ED11 on the inhibition of caspase-6 was evaluated. The peptides were administrated at a concentration of 10 μM each. (**C**) Western blots of BACHD striatal lysates incubated with caspase-6 and labeled with mab2166 antibody (*caspase-6-generated fragments). (**D**) FRET assay to monitor Htt cleavage by caspase-6 for the determination of ED11 and Z-VAD-FMK IC50 values. (**E**) Effect of ED11 and Z-VAD-FMK on the cleavage of Z-VEID-aminoluciferin by caspase-6 or caspase-3 ($n = 3$). (**F**) Western blots of HEK293 cell lysates incubated with caspase-3 in the presence of ED11 or Z-VAD-FMK and stained with anti-Spectrin and anti-PARP antibodies. (**G**) Quantification of caspase-3 generated Spectrin and PARP fragments as a function of ED11 and Z-VAD-FMK concentrations ($n = 2$). $^*P < 0.05$, $^{**}P < 0.01$ one-way ANOVA followed by Tukey's *post hoc* test. All data are expressed as mean ± SEM.

ED11 into the brain parenchyma. While FITC-conjugated albumin and ED11 lacking the cell-penetrating sequence TAT (48–60) remained inside the blood vessels, FITC-conjugated TAT and ED11 can be seen in the brain parenchyma (Fig. 3A).

To evaluate the ability of ED11 to protect from mHtt toxicity *in vivo*, the full-length 97Q-mHtt transgenic BACHD mouse model was used. ED11 treatment was commenced at the age of 5 weeks with a subcutaneously implanted Alzet mini-pump, which infused the peptide continuously for 28 days at a dose of 4 mg/kg/day. The pump was replaced every 28 days for the duration of the experiment. Since mHtt expression causes a metabolic imbalance manifested by an excessive body weight gain in BACHD mice (17), animals were weighed regularly throughout the study. Notably, treatment with ED11 attenuated the excess body weight gain in BACHD mice (Fig. 3B).

Mice were tested for motor performance 4 weeks after treatment initiation by measuring the latency to fall on an accelerating rotarod. During the training session, BACHD mice treated with ED11 demonstrated higher motor learning capabilities than the vehicle-treated BACHD mice (Fig. 3C). Long-term motor performance was monitored starting at the age of 9 weeks, and was evaluated monthly. Male BACHD mice treated with ED11 showed preserved motor performance compared with WT mice. The same trend was detected in the female group, which did not show a significant motor impairment in our cohort (Fig. 3D). Since body weight differences were observed, it was important to verify that the effect of ED11 on motor performance was not weight-dependent. To this end, we matched male subjects with the same body weight and compared their rotarod performance. The results showed that the beneficial effect of ED11 cannot be attributed to the lower body weight of the ED11-treated mice (Fig. 3E).

To evaluate the influence of ED11 on the depressive-like behavior of the BACHD mice, the forced swim test (FST) was conducted at 5 months of age. ED11-treated mice did not exhibit the increased immobility observed in the vehicle-treated BACHD mice (Fig. 3F), indicating that ED11 protects against this depression-related phenotype. No correlation was found between motor performance in the rotarod test and time spent immobile in the FST (Pearson correlation coefficient $r = 0.057$, P-value = 0.83, two-tailed Student's t-test), confirming that the protective effect of ED11 was not directly related to motor ability.

To assess the effect of ED11 on basal locomotor activity, exploratory activity and anxiety-related behavior the open field test were examined at 22 weeks of age. In this test, no significant differences in total distance traveled were observed between the

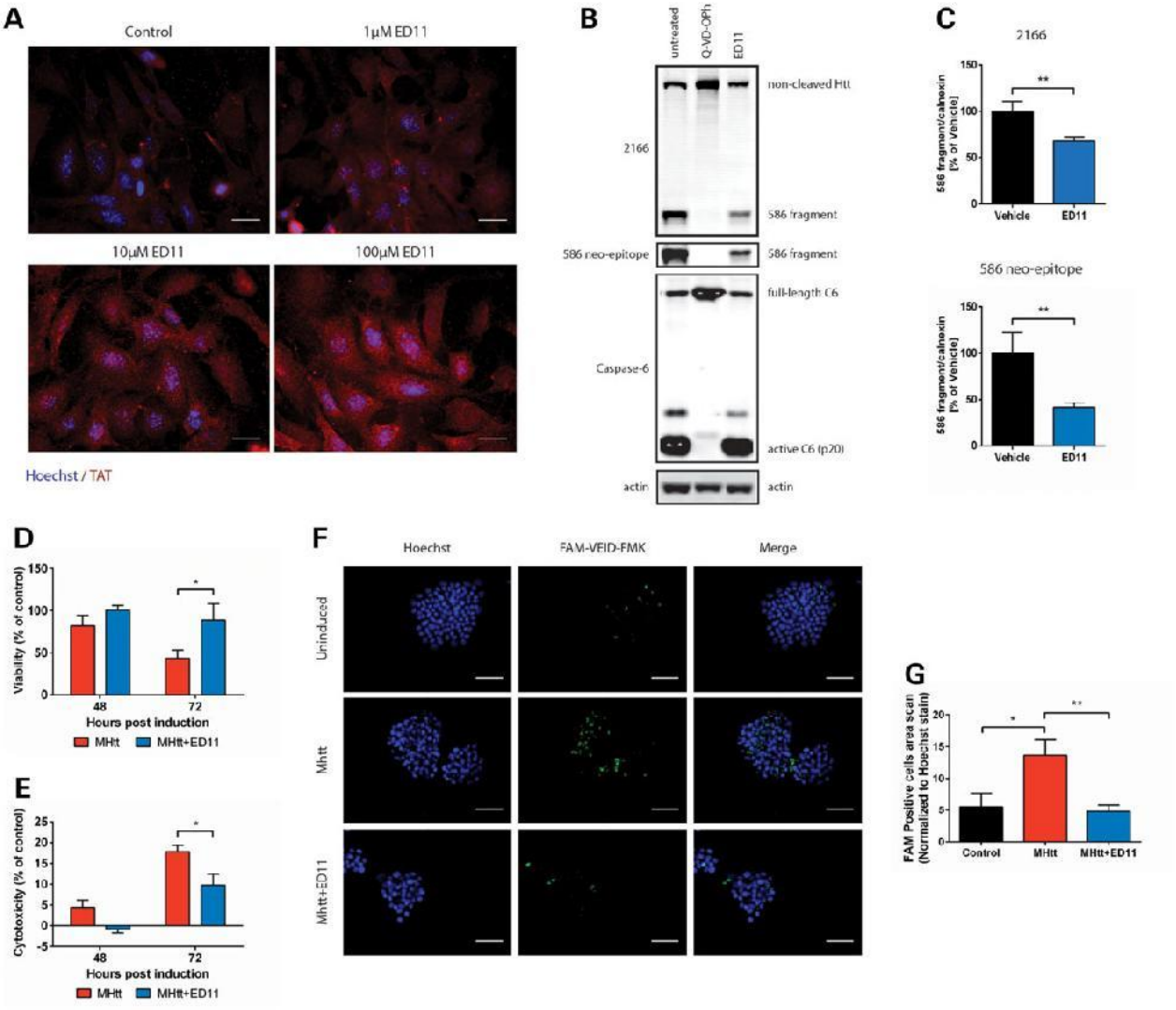

Figure 2. ED11 penetrates the cell membrane, inhibits caspase-6 activity intracellularly and protects cells from mHtt-induced toxicity. (**A**) Representative images of MEF cells incubated with the indicated concentrations of ED11 and labeled with anti-TAT antibody. (**B**) Western blots of HEK293 cells co-transfected with caspase-6 and Htt, and stained with mab2166 and 586 neo-epitope antibodies. (**C**) Quantification of the Htt fragment generated by caspase-6 that was detected by mab2166 and 586 neo-epitope antibodies ($n = 4–8$). (**D**) Viability measurement of 145Q-mHtt-expressing, serum-deprived PC12 cells by Alamar blue viability assay ($n = 5$). (**E**) Cell death measurement of 145Q-mHtt-expressing, serum-deprived PC12 cells by LDH release assay ($n = 5$). (**F**) Caspase activity measurement of 145Q-mHtt-expressing, serum-deprived PC12 cells by incubation with FAM-VEID-FMK. (**G**) Quantification of caspase activity-dependent FAM-VEID-FMK fluorescence signal normalized to Hoechst nuclear staining ($n = 7$). Scale bars indicate 50 μM. $^*P < 0.05$, $^{**}P < 0.01$ one-way ANOVA followed by Tukey's *post hoc* test. All data are expressed as mean ± SEM.

treatment groups, indicating that basal locomotor activity was unchanged (Fig. 3G). Exploratory activity and anxiety-related behavior were measured by quantification of the time spent in the center and number of transitions to the center. Whereas BACHD mice show decreased exploratory and increased anxiety-related behavior, the ED11-treated mice showed more transitions to the center and a trend toward increased time spent in the center compared with vehicle-treated BACHD mice, indicating lower anxiety levels and improved exploratory behavior (Fig. 3H and I).

In agreement with published data, where mHtt-586 fragments were only detectable in 13- to 15-month-old BACHD animals (18), the levels of this fragment were below detection in our 6-month-old cohorts (data not shown). Similarly, mHtt aggregation cannot be detected at this age in BACHD mice (19,20), precluding an assessment of ED11-mediated effects on this readout.

Post-symptomatic ED11 treatment partially restores motor ability in BACHD mice and protects from behavioral and cognitive deficits

To evaluate whether treatment with ED11 is also effective in a more advanced disease state, we treated BACHD mice at the age of 36 weeks, when HD-related phenotypes are already more pronounced. For motor evaluation, BACHD mice were trained on the accelerating rotarod at the age of 30 weeks and assigned to treatment groups according to a similar baseline motor performance. Treatment with ED11 or vehicle was started at 36 weeks of age. While the performance of vehicle-treated BACHD mice remained at the same level throughout the testing period, ED11-treated mice demonstrated an increase in rotarod performance, indicating that ED11 was able to exert a restorative effect in these mice (Fig. 4A). This effect was

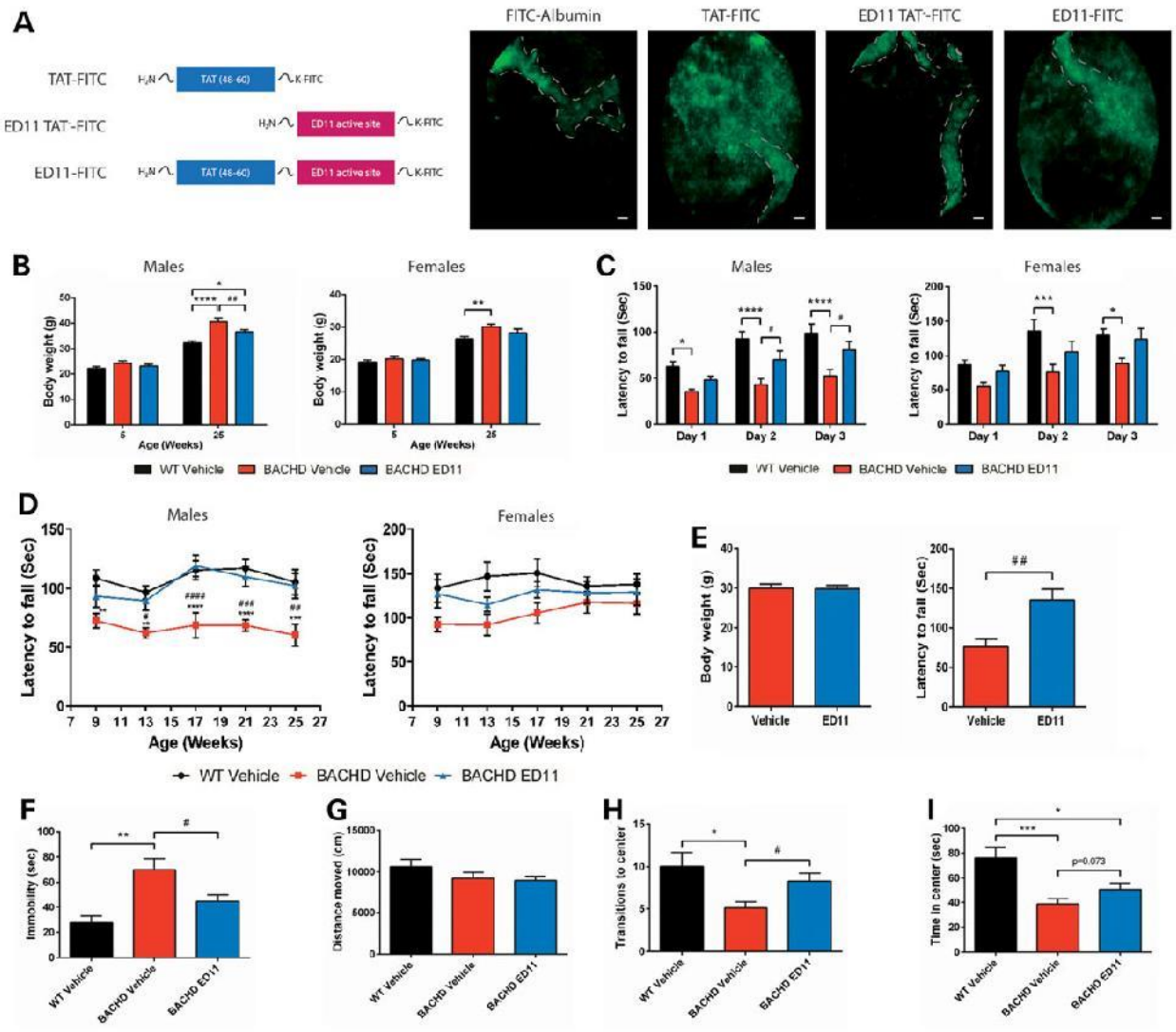

Figure 3. ED11 penetrates the CNS and protects BACHD mice from motor and behavioral deficits. (**A**) *In vivo* fluorescence tracking of the indicated peptides, 40 min after IV injection. The estimated blood vessel pattern is marked with a dashed line. (**B–F**) BACHD mice were treated with ED11 starting from the age of 5 weeks and the indicated parameters were tested. (B) Body weight measurements of pre- and post-treatment animals ($n = 10–11$ per sex). (C) Rotarod training performance was measured by latency to fall from an accelerating rod 3 weeks after treatment commencement for 3 consecutive days, average of three trials per day. (D) Long-term rotarod performance was measured by latency to fall from an accelerating rod every 4 weeks. (E) Body weight matching for the ED11 and vehicle-treated mice and their corresponding rotarod performance ($n = 6$). (F) Depressive-like behavior as measured by time spent immobile in the FST ($n = 20–22$). (**G–I**) Distance moved, time spent in center and transitions to center in the open field test ($n = 20–22$). Scale bars indicate 20 μM. Asterisk indicates statistical difference from the WT-vehicle group, whereas hash indicates statistical difference from the BACHD ED11 group. $^{*}P < 0.05$, $^{**}P < 0.01$, $^{***}P < 0.001$, $^{****}P < 0.0001$. $^{\#}P < 0.05$, $^{\#\#}P < 0.01$, $^{\#\#\#}P < 0.001$, $^{\#\#\#\#}P < 0.0001$. (B–D) Two-way ANOVA followed by Tukey's *post hoc* test. (E) Two-tailed unpaired Student's *t*-test. (F–I) One-way ANOVA followed by Tukey's *post hoc* test. All data are expressed as mean ± SEM.

statistically significant in relation to the pretreatment state of BACHD mice (Fig. 4B).

To evaluate the effect of ED11 on the depression-related phenotype in symptomatic BACHD mice, mice were tested using the FST at 11 months of age. While vehicle-treated BACHD mice were found to be more immobile than their WT littermates, the immobility of ED11-treated mice was similar to WT animals, indicating a reversal of the depressive-like phenotype (Fig. 4C). The effect of ED11 on the mobility state in the FST is not related to motor ability, as no correlation between motor performance in the rotarod test and time spent immobile in the FST was detected (Pearson correlation coefficient $r = 0.12$, P-value = 0.73, two-tailed Student's t-test).

To address the possible effect of ED11 treatment on cognitive deficits observed in the BACHD mice, we used the swimming T-maze test. During the 3-day learning period, all experimental groups learned to swim directly to the platform, as measured by a progressive decrease in the time to reach the target (Fig. 4D and F). On the fourth day, the strategy shifting ability was tested by relocating the hidden platform to the opposite arm. We found impairment in the strategy shifting ability of vehicle-treated BACHD mice, as their time to reach the hidden platform was longer than for WT mice. In contrast, the performance of ED11-treated BACHD mice was comparable to their WT littermates (Fig. 4E and F), indicating a reversal of cognitive rigidity by ED11.

MRI volumetric measurements were performed at the age of 12 months to examine the possible effect of ED11 treatment on striatal, cortical and hippocampal atrophy. However, we did not detect significant reduction in the BACHD mice compared with

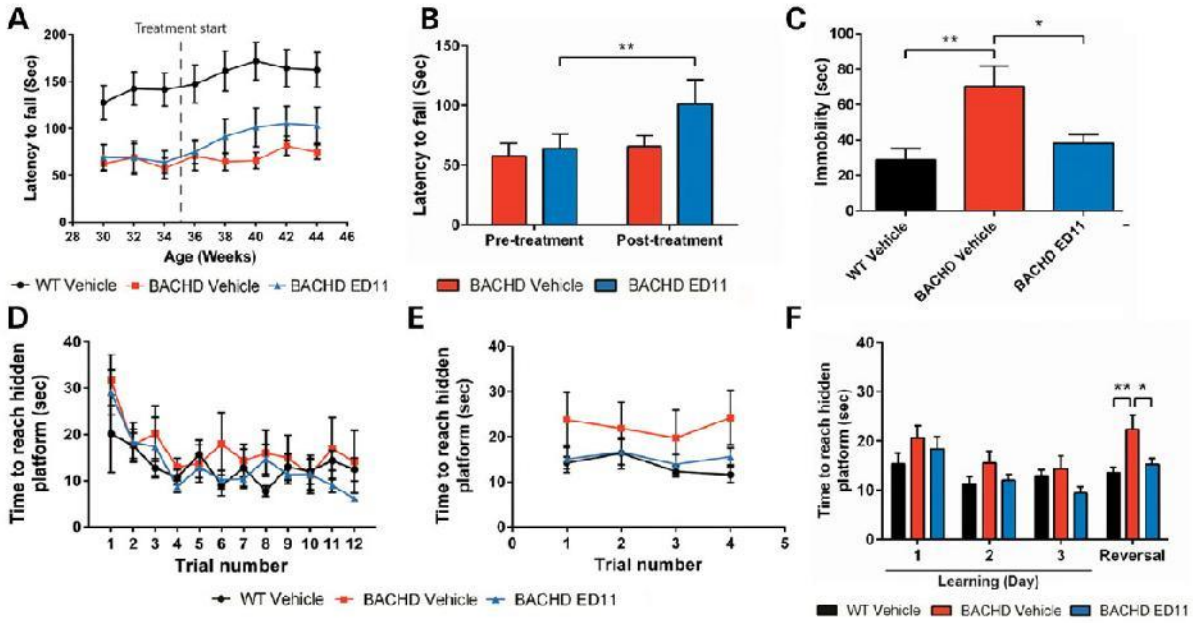

Figure 4. ED11 treatment partially restores motor ability and reverses behavioral and cognitive deficits in progressive disease stage BACHD mice. (**A**) Determination of rotarod performance in an advanced disease state with the rotarod test. The time point of treatment initiation is indicated with a dashed line. (**B**) Motor performance in the rotarod test was measured at different time points. The pretreatment state was recorded at the age of 34 weeks, and post-treatment values were recorded at the age of 40 weeks, 5 weeks after treatment initiation. (**C**) The effect of ED11 on the depressive-like behavior as measured by time spent immobile in the FST. (**D**) Time to reach the hidden platform in the learning phase of the swimming T-maze test for 3 consecutive days, four trials per day. (**E**) Time to reach hidden platform in the strategy shifting phase of the swimming T-maze test, four trials a day following the learning phase. (**F**) Daily averages of the time to reach the hidden platform. $^{*}P < 0.05$, $^{**}P < 0.01$. (B) Paired samples Student's *t*-test. (C and F) One-way ANOVA followed by Tukey's *post hoc* test. All data are expressed as mean ± SEM.

WT mice (Supplementary material, Fig. S4), precluding any evaluation of ED11-mediated effects on brain atrophy.

Discussion

In our study, we used a peptide encompassing the human Htt sequence around amino acid Asp586 to compete for caspase-6 activity and inhibit the proteolysis of Htt. We show that the peptide inhibits Htt cleavage, rescues a cell culture model from mHtt toxicity and significantly reduces the motor deficits and behavioral abnormalities in BACHD mice. Moreover, treatment in an advanced disease state resulted in partial recovery of motor performance, an alleviation of the depressive-like behavior and cognitive deficits.

Subsequent to the discovery of Htt as a substrate for caspase cleavage, it was shown that caspase-6 activation plays a major pathogenic role in human HD patients and in HD models. However, the importance of caspase-6 in mHtt pathogenesis has recently been challenged in studies that crossed caspase-6-deficient mice and HD mouse models (18,21). These reports have demonstrated the continued presence of 586 amino acid mHtt fragments in the absence of caspase-6, suggesting that additional proteases are involved in mHtt fragmentation at this site. Nonetheless, caspase-6 deficiency provided significant beneficial effects including a decrease of full-length mHtt and mHtt fragments and a significant reduction in aggregate formation. Furthermore, body weight levels and motor deficits were attenuated.

In contrast to the genetic ablation of caspase-6, compound-based inhibition of caspase-6 activity in adulthood may be more efficient in providing protection from mHtt toxicity *in vivo*. Caspase-6 knockout mice demonstrate alterations in striatum and cortex (22), regions that are specifically affected in HD. Furthermore, caspase-6 is important in neurodevelopment, as it is profoundly involved in axonal pruning during development (23). Its absence may lead to a compensatory upregulation of other members of the caspase family, a scenario that has been described for caspase-$3^{-/-}$ mice (24). Our approach to use an Htt-derived peptide as a sink for excessive caspase-6 activity, on the other hand, should also trap other proteases that can recognize and cleave at amino acid 586. It is a target-independent approach to prevent mHtt proteolysis and thus has significant advantages over both caspase-6 ablation and classical caspase inhibitors, which are nonspecific, lack sufficient cell and brain permeability and could cause nonspecific toxic effects when added at concentrations required to inhibit intracellular caspases (25–27). Interestingly, our *in vitro* Htt cleavage experiment demonstrates that ED11 may profoundly alter caspase cleavage patterns of this protein. We recently found that Htt can be cleaved by caspases 1–10 *in vitro*, and we now show that ED11 inhibits caspase-1, -2 and -10 as well as increases caspase-5-mediated Htt cleavage. For most of these caspases, the *in vivo* relevance of their Htt cleavage processes as well as their contribution to HD pathogenesis remains unknown. However, the inhibition of caspase-2-mediated Htt cleavage by ED11 may contribute to the preservation and improvement of the *in vivo* behavioral function, since the ablation of this enzyme has been associated with therapeutic benefits in YAC128 mice in a previous study (28).

The ability of ED11 to reverse HD-like phenotypes in post-symptomatic BACHD mice is likely due to the restoration of neuronal function prior to the occurrence of neuronal death. We did not observe any significant changes by MRI in vehicle-treated BACHD mice compared with WT animals at 12 months of age, suggesting that in these mice, a window for therapeutic intervention exists between the onset of HD-like behavioral phenotypes and irreversible brain atrophy. In patients, treatment should similarly be most effective prior to neuronal loss and with the

availability of an accurate genetic prediction could even be envisaged pre-symptomatically.

Due to the absence of striatal, cortical or hippocampal atrophy in our BACHD cohort, we were however unable to evaluate the effects of ED11 on the prevention of brain atrophy. These neuroanatomical endpoints will have to be analyzed in a more long-term study, which will furthermore determine whether ED11 treatment is likely to provide the long-lasting therapeutic benefits that are necessary to successfully treat a chronic illness like HD.

Our study demonstrates that the use of substrate-based peptides is a feasible concept for inhibition of caspase-mediated protein cleavage for therapeutic purposes. In view of its potency and selectivity, we suggest ED11 as a treatment for HD. Further studies should be performed to translate our findings from animal models to HD patients. In addition, our findings might be applicable in other neurodegenerative or neurological diseases where caspase-6 activity plays a part in the pathogenic process.

Materials and Methods

Peptide synthesis and dissolvent

ED11 (GRKKRRQRRRPPQSSEIVLDGTDN), TAT-only (GRKKRRQRRR PPQ), ED11-FITC (GRKKRRQRRRPPQSSEIVLDGTDNK-FITC), ED11-No TAT-FITC (SSEIVLDGTDNK-FITC), TAT-FITC (YGRKKRRK-FITC), I4A (GRKKRRQRRRPPQSSEAVLDGTDN), D7A (GRKKRRQRRR PPQSSEIVLAGTDN) and D10A (GRKKRRQRRRPPQSSEIVLDGTAN) were synthesized by China-Peptides Ltd (Shanghai, China) with a purification level at over 95%. For the purified caspase activity assays, peptides were dissolved in DMSO. For the cell culture involved experiments, peptides were initially dissolved in cell culture grade H_2O and further diluted by phosphate-buffered saline (PBS) to the desired concentrations. For *in vivo* studies, peptides were initially dissolved in cell culture grade H_2O and further diluted by 0.9% saline.

Luminescent caspase inhibition assays

To determine caspase inhibition by ED11, the Caspase-Glo® 6 assay (Promega, Fitchburg, WI, USA) was carried out according to the manufacturer's instructions. Briefly, 0.1 U/ml of purified caspase-6 (Enzo Life Sciences, Farmingdale, NY, USA) or caspase-3 (Abcam, Cambridge, UK) was incubated with 5 μM Z-VEID-aminoluciferin in the presence of 5 μM ED11 or DMSO as a vehicle control, and the luminescent signal of released aminoluciferin was detected using a Synergy HT multi-mode micro-plate reader (Bio-Tek, Winooski, VT, USA).

Protein caspase cleavage assays

For brain lysate preparation, FVB/N BACHD mice and their WT littermates were euthanized by decapitation. Striata were dissected, suspended in a lysis buffer (200 mM HEPES, 150 mM NaCl, 1 mM Na_3VO_4, 5 mM EDTA, 1% NP-40, 0.5% DOC and 50 mM NaF) with protease inhibitors (Roche), homogenized with a dounce homogenizer and placed for 1 h on ice. Tissue debris was removed by centrifugation at 20 000*g* for 15 min at 4°C. Protein concentration was determined by the BCA method (Pierce). About 50 μg of lysate proteins were exposed to 100 U/ml of purified active human caspase-6 for 45 min at 37°C in the presence of 10 μM ED11 or DMSO as a vehicle control. Lysates were subsequently loaded on 7.5% SDS–PAGE gels and transferred to 0.45 μM nitrocellulose membranes. The membranes were probed with rabbit anti-Htt 4–19 (1 : 1000, CHDI) and mouse anti-β-actin (1 : 10 000, Sigma). The secondary antibodies used were IRDye 800CW Goat anti-rabbit IgG and IRDye 680RD Goat anti-Mouse IgG (Licor Ltd), respectively. The fluorescent signal was read using the Odyssey imaging system (Li-Cor Biosciences, Nebraska, NE, USA).

FRET assay for caspase-6 activity

The N-terminal 1212 amino acids of Htt with 15Q and the 4c mutations (D513A, D552A, D530A and D589A) (5) were transiently transfected and overexpressed in COS-7 cells. Cells were lysed in SDP buffer (50 mM Tris pH 8, 150 mM NaCl, 1% Igepal and 1× Roche complete protease inhibitor) and cleared lysates were used as a substrate for the activity assay. Caspase-6 enzyme (Bio-Mol GmbH, Hamburg, Germany) was diluted to 0.125 U/μl in FRET buffer (10 mM HEPES pH 7.4, 100 mM NaCl, 0.05% gelatin, 0.1% CHAPS and 2 mM DTT) and mixed with different concentrations of ED11 at a final volume of 22 μl in a white 384-well plate. Samples were incubated for 1 h at room temperature, and then 28 μl of a mixture of COS-7 lysate containing Htt protein (90 ng/μl), Tb-labeled BKP1 antibody (36 ng/ml) and D2-labeled monoclonal 586 neo-epitope antibody (360 ng/ml) (5) in FRET buffer were added. The plate was incubated at 37°C for 6 h, and then stored for an additional 18 h at 4°C. Plates were measured with a Xenon lamp Victor Plate Reader (Perkin Elmer, Waltham, MA, USA) after excitation at 340 nm (time delay 50 ms and window 200 ms). The signal measured at 615 nm resulted from the emission of the Terbium-labeled antibody and was used for normalization of potential signal artifacts. The cleaved Htt-specific signal at 665 nm resulted from the emission of the D2-labeled neo-epitope antibody after time-delayed excitation by the Terbium. Caspase-6 activity was measured by the amount of cleaved Htt generated and represented by the 665/615 nm ratio.

PARP cleavage by caspase-3

HEK293 cells were lysed in MCB buffer (50 mM HEPES pH 7.4, 100 mM NaCl, 1% Igepal, 1 mM EDTA, 10% glycerol, Roche complete protease inhibitors), and DTT was added to 10 mM after the protein concentration was measured in cleared lysates. Caspase-3 enzyme (50 U) was mixed with ED11 or Z-VAD-FMK in MCB buffer supplemented with 10 mM DTT at a total volume of 5 μl and incubated at room temperature for 1 h. Then, 40 μg of HEK lysate (adjusted to 2 μg/μl) were added and the samples were incubated at 37°C for 1 h. SDS–PAGE loading dye was added, samples were denatured and run on a 3–8% Tris-acetate SDS–PAGE gel (Invitrogen, Carlsbad, CA, USA). After transfer to PVDF membranes, the blots were probed with Spectrin (Enzo), PARP (Cell Signaling Technology, Beverly MA, USA) and actin (Millipore, Billerica, MA, USA) antibodies in the Li-Cor system.

Cleavage of Htt by caspases 1–10

COS7 cells were transiently transfected with the 3949-15Q-HTT construct (5) using the Xtreme gene 9 transfection reagent (Roche Applied Science, Quebec, Canada), according to the manufacturer's protocol.

Twenty-four hours post-transfection, cells were harvested and lysed. Fifty units of purified active human caspase-1 through 10 each (Enzo Life Sciences) were mixed with 10 μM ED11 in caspase buffer (100 mM HEPES pH 7.4, 200 mM NaCl, 0.2% CHAPS, 2 mM EDTA, 20% glycerol and 10 mM DTT) and incubated for 30 min at room temperature. About 40 μg of total protein from cell lysates were added, and the reaction was incubated for 1 h

at 37°C. A HTT 15Q fragment truncated at amino acid 586 was overexpressed in COS7 cells and used as a size control on the western blot. SDS–PAGE loading dye was added, and samples were denatured and run on a 10% Tris-Glycine SDS–PAGE gel. After transfer to PVDF membranes, the blots were probed with the polyclonal antibody BKP1(29) directed against amino acids 1–17 of Htt. Membranes were scanned and quantified using the Li-Cor system.

TAT antibody staining in MEFs

MEFs derived from FVB/N WT mice (30) were treated with different amounts of ED11 in the media for 16 h. Cells were washed with PBS, fixed with 4% paraformaldehyde in PBS for 30 min at room temperature and processed for immunofluorescence with an anti-TAT antibody (Abcam), Alexa-488-labeled secondary antibody (Invitrogen) and Hoechst nuclear counterstaining.

Htt–caspase-6 co-transfection

COS-7 cells were transiently co-transfected with equal amounts of FLAG-tagged human caspase-6 and the N-terminal 1212 amino acids of Htt with 15Q (5) using the X-treme Gene reagent (Roche, Basel, Switzerland) according to manufacturer's instructions. One hour after transfection, ED11 peptide was added to the growth medium. Cells were harvested in the medium 24 h after transfection and the presence of cleaved Htt was assessed by western blotting using the Htt antibody 2166 (Millipore) or the neo-epitope antibody against Htt cleaved at amino acid 586 (5). Signals were normalized to calnexin as a loading control.

Cell culture

Human neuroblastoma cells, SH-SY5Y cells (ATCC), were grown on tissue culture plates (Greiner, Frickenhausen, Germany) in Dulbecco's Modified Eagle's Medium (DMEM), supplemented with 10% fetal calf serum (FCS), 1% L-glutamine and 1% SPN antibiotics (Biological Industries, Beit Haemek, Israel). Inducible 145Q-MHtt-expressing PC12 cells were obtained from CHDI (by Coriell Institute). Cells were grown in suspension in 75 cm^3 culture flasks (Corning, Corning, NY, USA) in DMEM, supplemented with 15% Horse serum, 2.5% FCS, 0.1 mg/ml of G418 (Gibco, Paisley, UK), 0.1 mg/ml of Zeocin (Invitrogen), 1% L-glutamine and 1% SPN antibiotics (Biological Industries). Both cell types were incubated at 37°C in a humidified atmosphere with 5% CO_2, and passaged twice a week. For cell proliferation and cell cycle analysis, SH-SY5Y cells were pre-incubated with 25 µM ED11 for 1 h. Then, 10 µM 5-bromo-2-deoxyuridine (BrdU) was added for 2 h. The medium was discarded and cells were fixed with 70% ethanol. DNA denaturation was conducted with 1.5 M HCl exposure for 30 min. FITC-conjugated anti-BrdU antibody was used to mark incorporated BrdU, and DNA staining was performed using propidium iodide. A total of 15 000 cells per sample were read using a FACS-Calibur flow cytometer, and cell cycle analysis was conducted after doublet discrimination.

Mutant Huntingtin-induced toxicity

To induce mHtt expression, inducible 145Q-mHtt-expressing PC12 cells were incubated with 25 µM ponasterone A (PA, Invitrogen) for the indicated time periods, in the presence of 25 µM ED11 or vehicle as a control. For viability assessment, the medium was depleted and washed twice with PBS, and Alamar blue dye (AbD serotec, Kidlington, UK, 1/10 in culture medium) was added to the cells, as instructed by the manufacturer. Fluorescence was monitored with a 530–560 nm excitation and a 590 nm emission wavelength, and viability was calculated as a percentage of the untreated control. LDH release was measured with the LDH Cytotoxicity Detection Kit (Clontech, Mountain View, CA, USA), following the manufacturer's instructions. Briefly, PC12 cells were grown on six-well plate at a density of 7×10^5 cells/ml, and samples were taken at the indicated time points. Subsequently, samples were centrifuged, transferred to a 96-well plate and incubated with the reaction mixture for 30 min in the dark. The plate was read at 492 and 690 nm as a reference in the Synergy HT multi-mode micro-plate reader, and calculations were done with reference to a non-induced control. For FLICA caspase-6 assay (ICT, USA), cells were adjusted to 1.5×10^6 cells/ml and were incubated with FAM-VEID-FMK for 1 h at 37°C as described. Hoechst stain was used as nucleus counterstaining. The images were recorded with a fluorescence microscope (Olympus, Tokyo, Japan) and image analysis was performed using the Image-J software.

Animal studies

All animal-related procedures were approved by the Tel-Aviv University Committee of Animal Use for Research and Education, under protocols M-13-024, M-13-061 and M-13-110. BACHD mice were obtained from Jackson Laboratory (Bar Harbor, ME, USA). The mice were placed under 12 h light/dark conditions and housed in individually ventilated cages with *ad libitum* access to food and water.

Assessment of BBB penetration

To assess ED11's ability to penetrate the BBB and enter the brain parenchyma, a modified *in vivo* brain delivery detection method was used. A previously reported two photon-based brain delivery detection method (31) was adjusted to an endoscopic microscopy probe-based method (32) to enable deep brain detection. FVB/N mice ($n = 2$) were injected IV with one of the following compounds: FITC-conjugated albumin, a marker of intact blood vessels (10 mg in 200 µl of saline), FITC-conjugated TAT, as a positive control for extravasation from the blood vessels, FITC-conjugated ED11 lacking the TAT cell-penetrating sequence (50 mg/kg) and FITC-conjugated ED11 (50 mg/kg). Twenty minutes after compound injection, the mice were anesthetized with a mixture of ketamine (100 mg/kg) and xylazine (8 mg/kg). The mice were then placed in a stereotaxic device, and a 0.3 mm fluorescence detection probe was inserted into the central caudate–putamen. Coordinates with respect to the bregma used were: anterior-posterior +0.5, medial-lateral +2, dorsal-ventral −2.7. Forty minutes after compound injection, fluorescence was monitored using a 488 nm excitation laser.

ED11 *in vivo* efficacy trials

To evaluate ED11's ability to provide protection from mHtt toxicity *in vivo*, the HD mouse model BACHD (19) and their FVB/N WT littermates were used. Mice were assigned to different groups according to littermates to minimize inherent variability. Mice were housed in mixed genotype and treatment cages, and the researcher was blinded with regard to mouse genotype and treatment throughout all of the behavioral tests. The tested compounds were Vehicle, which was consisted of sterile water (20%) and normal saline (80%) only, or ED11 dissolved in an equal vehicle solution. Delivery of the tested compound was done by a subcutaneously implanted mini-pump alzet model

1004 (DURECT, Cupertino, CA, USA) according to the manufacturer's instructions. The pumps infused continuously for 28 days, at a dose of 4 mg/kg/day. Replacement with freshly prepared pumps was conducted every 28 days until the completion of the experiment.

Rotarod test

Motor coordination and strength were assessed using the accelerating rotarod according to an adapted, previously reported, protocol (19). During the training period, mice were placed on an accelerating rod (0–21 rpm in 4 min), and latency to fall from the rod was recorded. The mice were tested three times per day with a 2-h intertrial rest for 3 consecutive days. For the rotarod test, mice were placed on the accelerating rod (0–21 rpm in 4 min) for three consecutive trials with a 5-min intertrial rest, and average score was taken for analysis.

For emotional and cognitive evaluation, mice were tested in the following behavioral tasks, separated by a minimum of 1-week interval between each task.

Forced swim test

The FST was conducted as previously described (8) with minor modifications. The mice were placed in a 15 cm diameter 40 cm height cylinder, filled with water (23–25°C) to a depth of 20 cm. Animal behavior was recorded by a side camera for 6 min. For mobility analysis, the animal mobility state in the last 4 min was evaluated using the Noldus Ethovision (Wageningen, The Netherlands) video-tracking software

Open field test

For the open field test, an unfamiliar open field (50 × 50 cm) was used. Mice were placed in one corner of the arena and their behavior was recorded for 20 min and scored with the Ethovision video-tracking system. Total distance traveled, total time spent in the center and the number of entries to the center were measured.

Light dark choice test

The light dark choice test was conducted as previously described (33). The arena consisted of two compartments: a dark compartment (14 × 27 × 26 cm) and a compartment illuminated by 1050 lux (30 × 27 × 26 cm), connected by a small passage. Mice were placed in the light compartment to initiate a 5-min test session. The time spent in the dark compartment, the number of entries to the dark compartment and the latency of entering the dark zone were measured. The indices collected in these tests were quantified using the Ethovision video-tracking system.

Swimming T-maze strategy shift test

The swimming T-maze strategy shifting test was conducted as previously described (34). The apparatus consisted of three arms (9 × 50 cm each) filled with water to a depth of 15 cm. On the first 3 days, the mice were subjected to a learning period. In the learning period, a transparent platform was hidden at the end of the right arm. The mouse was placed at the stern of the T-maze four times a day with a 45-min interval between trials. On the fourth day, the strategy shift paradigm was initiated, as the platform was relocated to the left arm, and the mice were placed at the stern four times with a 45-min interval between trials. The time taken for the mice to reach hidden platform was recorded and analyzed using the Ethovision video-tracking system.

MRI protocols and analysis

MRI scanning and analysis was performed by BioImage (Haifa, Israel). MRI was performed with a 7 T MRI scanner (Bruker, Billerica, MA, USA) with a 30 cm bore and a gradient strength of up to 400 mT/m, using a quadrature head coil. The mice were anesthetized with 1–2% isoflurane and oxygen, and were maintained at 37°C. Animal breathing was monitored with a breathing sensor. T_2-weighted imaging was performed with the following parameters: multi-slice multi-echo sequence, repetition time 2000 ms, 10 different echo times (ms):10, 20, 30, 40, 50, 60, 70, 80, 90, 100 and spatial resolution: 0.07 × 0.07 × 0.8 mm^3. For image analysis, T_2-relaxation maps were calculated using BioImage software written in Matlab (Mathworks©), using least-squares algorithm. For volumetric analysis, the images were rotated and cropped, and the regions of interest were outlined manually. A trained operator manually segmented the caudate–putamen, cortex, frontal cortex, motor cortex and hippocampus to evaluate volume changes.

Statistical analysis

Statistical analysis was performed using GraphPad prism version 6.0. Statistical significance for differences between two groups was evaluated by Student's unpaired *t*-test. When three groups were addressed, statistical evaluation was made by one-way ANOVA followed by Tukey's multiple comparison *post hoc* test. When addressing time point-dependent alterations, two-way ANOVA with Tukey's multiple comparison *post hoc* test was used. Data are presented as mean ± SEM, and the level of $P < 0.05$ was accepted as statistically significant.

Supplementary Material

Supplementary Material is available at *HMG* online.

Acknowledgements

We thank Yael Zilberstein from the Sackler Cellular and Molecular Imaging Center at Tel-Aviv University for her dedicated help with the *in vivo* fluorescence imaging.

Conflict of Interest statement. D.O. and I.A. are registered as co-inventors in the patent filed for the caspase-6 peptide inhibitor ED11. M.R.H. is an employee of Teva Pharmaceuticals. Teva did not have any influence on the design of the study or the analysis and interpretation of data.

Funding

This work was supported by the Israel Ministry of Science and Technology, the Colton foundation and Teva Pharmaceutical Industries Ltd under the Israeli National Network of Excellence in Neuroscience (NNE) established by Teva. M.R.H. is a Killam Professor, holds a Canada Research Chair in Human Genetics and received funding from the Canadian Institutes of Health Research (grant MOP 84438).

References

1. Ross, C.A. and Tabrizi, S.J. (2011) Huntington's disease: from molecular pathogenesis to clinical treatment. *Lancet Neurol.*, **10**, 83–98.

2. Goldberg, Y.P., Nicholson, D.W., Rasper, D.M., Kalchman, M. A., Koide, H.B., Graham, R.K., Bromm, M., Kazemi-Esfarjani, P., Thornberry, N.A., Vaillancourt, J.P. *et al.* (1996) Cleavage of huntingtin by apopain, a proapoptotic cysteine protease, is modulated by the polyglutamine tract. *Nat. Genet.*, **13**, 442–449.
3. Wellington, C.L., Ellerby, L.M., Gutekunst, C.A., Rogers, D., Warby, S., Graham, R.K., Loubser, O., van Raamsdonk, J., Singaraja, R. and Yang, Y.Z. (2002) Caspase cleavage of mutant huntingtin precedes neurodegeneration in Huntington's disease. *J. Neurosci.*, **22**, 7862–7872.
4. Graham, R.K., Deng, Y., Carroll, J., Vaid, K., Cowan, C., Pouladi, M.A., Metzler, M., Bissada, N., Wang, L., Faull, R.L.M. *et al.* (2010) Cleavage at the 586 amino acid caspase-6 site in mutant huntingtin influences caspase-6 activation in vivo. *J. Neurosci.*, **30**, 15019–15029.
5. Warby, S.C., Doty, C.N., Graham, R.K., Carroll, J.B., Yang, Y., Singaraja, R.R., Overall, C.M. and Hayden, M.R. (2008) Activated caspase-6 and caspase-6-cleaved fragments of huntingtin specifically colocalize in the nucleus. *Hum. Mol. Genet.*, **17**, 2390–2404.
6. Ehrnhoefer, D.E., Skotte, N.H., Ladha, S., Nguyen, Y.T.N., Qiu, X., Deng, Y., Huynh, K.T., Engemann, S., Nielsen, S.M., Becanovic, K. *et al.* (2014) p53 increases caspase-6 expression and activation in muscle tissue expressing mutant huntingtin. *Hum. Mol. Genet.*, **23**, 717–729.
7. Graham, R.K., Deng, Y., Slow, E.J., Haigh, B., Bissada, N., Lu, G., Pearson, J., Shehadeh, J., Bertram, L., Murphy, Z. *et al.* (2006) Cleavage at the caspase-6 site is required for neuronal dysfunction and degeneration due to mutant huntingtin. *Cell*, **125**, 1179–1191.
8. Pouladi, M.A., Graham, R.K., Karasinska, J.M., Xie, Y., Santos, R. D., Petersén, Å and Hayden, M.R. (2009) Prevention of depressive behaviour in the YAC128 mouse model of Huntington disease by mutation at residue 586 of huntingtin. *Brain*, **132**, 919–932.
9. Tebbenkamp, A.T.N., Green, C., Xu, G., Denovan-Wright, E.M., Rising, A.C., Fromholt, S.E., Brown, H.H., Swing, D., Mandel, R.J., Tessarollo, L. *et al.* (2011) Transgenic mice expressing caspase-6-derived N-terminal fragments of mutant huntingtin develop neurologic abnormalities with predominant cytoplasmic inclusion pathology composed largely of a smaller proteolytic derivative. *Hum. Mol. Genet.*, **20**, 2770–2782.
10. Schwarze, S.R., Ho, A., Vocero-Akbani, A. and Dowdy, S.F. (1999) In vivo protein transduction: delivery of a biologically active protein into the mouse. *Science*, **285**, 1569–1572.
11. Hällbrink, M., Florén, A., Elmquist, A., Pooga, M., Bartfai, T. and Langel, Ü. (2001) Cargo delivery kinetics of cell-penetrating peptides. *Biochim. Biophys. Acta*, **1515**, 101–109.
12. Thorén, P.E.G., Persson, D., Isakson, P., Goksör, M., Önfelt, A. and Nordén, B. (2003) Uptake of analogs of penetratin, TAT (48–60) and oligoarginine in live cells. *Biochem. Biophys. Res. Commun.*, **307**, 100–107.
13. Chéreau, D., Kodandapani, L., Tomaselli, K.J., Spada, A.P. and Wu, J.C. (2003) Structural and functional analysis of caspase active sites. *Biochemistry*, **42**, 4151–4160.
14. Leyva, M.J., DeGiacomo, F., Kaltenbach, L.S., Holcomb, J., Zhang, N., Gafni, J., Park, H., Lo, D.C., Salvesen, G.S., Ellerby, L.M. *et al.* (2010) Identification and evaluation of small molecule pan-caspase inhibitors in Huntington's disease models. *Chem. Biol.*, **17**, 1189–1200.
15. Le, D.A., Wu, Y., Huang, Z., Matsushita, K., Plesnila, N., Augustinack, J.C., Hyman, B.T., Yuan, J., Kuida, K., Flavell, R.A. *et al.* (2002) Caspase activation and neuroprotection in caspase-3-deficient mice after in vivo cerebral ischemia and in vitro oxygen glucose deprivation. *Proc. Natl. Acad. Sci. USA*, **99**, 15188–15193.
16. Wong, B.K.Y., Ehrnhoefer, D.E., Graham, R.K., Martin, D.D.O., Ladha, S., Uribe, V., Stanek, L.M., Franciosi, S., Qiu, X., Deng, Y. *et al.* Partial rescue of some features of Huntington disease in the genetic absence of caspase-6 in YAC128 mice. *Neurobiol. Dis.*, doi:10.1016/j.nbd.2014.12.030.
17. Hult, S., Soylu, R., Björklund, T., Belgardt, B., Mauer, J., Brüning, J., Kirik, D. and Petersén, Å. (2011) Mutant huntingtin causes metabolic imbalance by disruption of hypothalamic neurocircuits. *Cell Metab.*, **13**, 428–439.
18. Gafni, J., Papanikolaou, T., DeGiacomo, F., Holcomb, J., Chen, S., Menalled, L., Kudwa, A., Fitzpatrick, J., Miller, S. and Ramboz, S. (2012) Caspase-6 activity in a BACHD mouse modulates steady-state levels of mutant huntingtin protein but is not necessary for production of a 586 amino acid proteolytic fragment. *J. Neurosci.*, **32**, 7454–7465.
19. Gray, M., Shirasaki, D.I., Cepeda, C., André, V.M., Wilburn, B., Lu, X., Tao, J., Yamazaki, I., Li, S., Sun, Y.E. *et al.* (2008) Full-length human mutant huntingtin with a stable polyglutamine repeat can elicit progressive and selective neuropathogenesis in BACHD mice. *J. Neurosci.*, **28**, 6182–6195.
20. Pouladi, M.A., Stanek, L.M., Xie, Y., Franciosi, S., Southwell, A. L., Deng, Y., Butland, S., Zhang, W., Cheng, S.H., Shihabuddin, L.S. *et al.* (2012) Marked differences in neurochemistry and aggregates despite similar behavioural and neuropathological features of Huntington disease in the full-length BACHD and YAC128 mice. *Hum. Mol. Genet.*, **21**, 2219–2232.
21. Landles, C., Weiss, A., Franklin, S., Howland, D. and Bates, G. (2012) Caspase-6 does not contribute to the proteolysis of mutant huntingtin in the HdhQ150 knock-in mouse model of Huntington's disease. *PLoS Curr.*, doi:10.1371/4fd085bfc9973.
22. Uribe, V., Wong, B.K.Y., Graham, R.K., Cusack, C.L., Skotte, N. H., Pouladi, M.A., Xie, Y., Feinberg, K., Ou, Y., Ouyang, Y. *et al.* (2012) Rescue from excitotoxicity and axonal degeneration accompanied by age-dependent behavioral and neuroanatomical alterations in caspase-6-deficient mice. *Hum. Mol. Genet.*, **21**, 1954–1967.
23. Nikolaev, A., McLaughlin, T., O'Leary, D.D.M. and Tessier-Lavigne, M. (2009) APP binds DR6 to trigger axon pruning and neuron death via distinct caspases. *Nature*, **457**, 981–989.
24. Houde, C., Banks, K.G., Coulombe, N., Rasper, D., Grimm, E., Roy, S., Simpson, E.M. and Nicholson, D.W. (2004) Caspase-7 expanded function and intrinsic expression level underlies strain-specific brain phenotype of caspase-3-null mice. *J. Neurosci.*, **24**, 9977–9984.
25. Berger, A.B., Sexton, K.B. and Bogyo, M. (2006) Commonly used caspase inhibitors designed based on substrate specificity profiles lack selectivity. *Cell Res.*, **16**, 961–963.
26. Chauvier, D., Ankri, S., Charriaut-Marlangue, C., Casimir, R. and Jacotot, E. (2006) Broad-spectrum caspase inhibitors: from myth to reality? *Cell Death Differ.*, **14**, 387–391.
27. Pereira, N.A. and Song, Z. (2008) Some commonly used caspase substrates and inhibitors lack the specificity required to monitor individual caspase activity. *Biochem. Biophys. Res. Commun.*, **377**, 873–877.
28. Carroll, J., Southwell, A., Graham, R., Lerch, J., Ehrnhoefer, D., Cao, L., Zhang, W., Deng, Y., Bissada, N., Henkelman, R. *et al.* (2011) Mice lacking caspase-2 are protected from behavioral changes, but not pathology, in the YAC128 model of Huntington disease. *Mol. Neurodegener.*, **6**, 59.
29. Kalchman, M.A., Koide, H.B., McCutcheon, K., Graham, R. K., Nichol, K., Nishiyama, K., Kazemi-Esfarjani, P., Lynn,

F.C., Wellington, C., Metzler, M. *et al.* (1997) HIP1, a human homologue of S. *cerevisiae* Sla2p, interacts with membrane-associated huntingtin in the brain. *Nat. Genet.*, **16**, 44–53.
30. Ehrnhoefer, D.E., Skotte, N.H., Savill, J., Nguyen, Y.T., Ladha, S., Cao, L.P., Dullaghan, E. and Hayden, M.R. (2011) A quantitative method for the specific assessment of caspase-6 activity in cell culture. *PLoS ONE*, **6**, e27680.
31. Koffie, R.M., Farrar, C.T., Saidi, L., William, C.M., Hyman, B.T. and Spires-Jones, T.L. (2011) Nanoparticles enhance brain delivery of blood–brain barrier-impermeable probes for in vivo optical and magnetic resonance imaging. *Proc. Natl. Acad. Sci. USA*, **108**, 18837–18842.
32. Jung, J.C., Mehta, A.D., Aksay, E., Stepnoski, R. and Schnitzer, M.J. (2004) In vivo mammalian brain imaging using one- and two-photon fluorescence microendoscopy. *J. Neurophysiol.*, **92**, 3121–3133.
33. Bourin, M. and Hascoët, M. (2003) The mouse light/dark box test. *Eur. J. Pharmacol.*, **463**, 55–65.
34. Marco, S., Giralt, A., Petrovic, M.M., Pouladi, M.A., Martinez-Turrillas, R., Martinez-Hernandez, J., Kaltenbach, L.S., Torres-Peraza, J., Graham, R.K., Watanabe, M. *et al.* (2013) Suppressing aberrant GluN3A expression rescues synaptic and behavioral impairments in Huntington's disease models. *Nat. Med.*, **19**, 1030–1038.